

AUG 30 1966

DEUT T60 0101

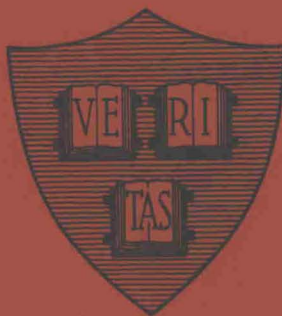
Office of Naval Research

---

Contract Nonr-1866 (10)

NR-017-308

PRESSURE DEPENDENCE OF THE HALL CONSTANT  
OF THE ALKALI METALS



By

Thomas Frederick Deutsch

July 1, 1960

Technical Report HP-6

---

Gordon McKay Laboratory of Applied Science  
Harvard University  
Cambridge, Massachusetts

Office of Naval Research

Contract Nonr-1866(10)

NR-017-308

Pressure Dependence of the Hall Constant  
of the Alkali Metals

by

Thomas Frederick Deutsch

July 1, 1960

The research reported in this document was made possible through support extended the Division of Engineering and Applied Physics, Harvard University, by the Office of Naval Research, under Contract Nonr-1866(10). Reproduction in whole or in part is permitted for any purpose of the United States Government.

Technical Report HP-6

Gordon McKay Laboratory of Applied Science

Harvard University

Cambridge, Massachusetts

## TABLE OF CONTENTS

	<u>Page</u>
Table of Contents	i
List of Figures	iii
List of Tables	v
Abstract	vi
I. Introduction	1
A. The Fermi Surface in Metals	1
B. Experimental Techniques for Obtaining the Fermi Surface	4
C. The Fermi Surface in the Alkalis - Experimental Evidence	7
D. The Fermi Surface as a Function of Pressure	13
References	17
II. Experimental Techniques	20
A. Electrical	20
1. The measurement problem.	20
2. The choice of an ac or dc method.	20
3. Description of the dc measuring system.	21
4. Spurious voltages.	24
B. High Pressure Apparatus	27
C. Sample Preparation	28
D. Measurements as a Function of Temperature	32
References	34
III. Experimental Results	35
A. The Hall Voltage and $n^*$ vs. Pressure	35
B. Hall Voltage and $n^*$ vs. Temperature	39
C. Absolute Values of $n^*$	40
References	41

IV. Discussion	42
A. Expressions for $n^*$	42
B. Calculation of the Warping Parameters	44
C. Dependence of $n^*$ on Pressure	46
D. The Scattering Time	50
E. Conclusions	61
References	62
Appendix	63
Acknowledgments	66

## LIST OF FIGURES

<u>Figure No.</u>		<u>After Page</u>
1-1	The Hall Effect	16
2-1	Hall Voltage Measuring Circuit	22
2-2	Galvanometer Amplifier	22
2-3	Schematic Diagram of 15,000 kg/cm <sup>2</sup> High Pressure Apparatus	28
2-4	Beryllium-Copper Bomb	28
2-5	Beryllium-Copper Bomb - Sealing Detail	28
2-6	Sample Holder and Sample	30
2-7	Low Temperature Measurement Apparatus	32
3-1	Hall Voltage vs. Magnetic Field ac Measurements	36
3-2	Normalized Hall Voltage vs. Pressure - Lithium	36
3-3	Normalized Hall Voltage vs. Pressure - Sodium	36
3-4	Normalized Hall Voltage vs. Pressure - Potassium	36
3-5	Decrease of $V_H$ in 10,000 kg/cm <sup>2</sup> vs. Sample Thickness. dc Measurements	36
3-6	Normalized Resistance R, vs. Pressure - Potassium	38
3-7	Normalized Hall Voltage vs. Pressure - Rubidium	38
3-8	Normalized Resistance R, vs. Pressure - Rubidium	38
3-9	Normalized Hall Voltage vs. Pressure - Cesium	38
3-10	$n^*$ vs. Pressure - Lithium	40

HP6

<u>Figure No.</u>		<u>After Page</u>
3-11	$n^*$ vs. Pressure - Sodium	40
3-12	$n^*$ vs. Pressure - Potassium	40
3-13	$n^*$ vs. Pressure - Rubidium	40
3-14	$n^*$ vs. Pressure - Cesium	40
3-15	$n^*$ vs. Temperature - Lithium	40
3-16	Hall Voltage vs. Sample Thickness <sup>-1</sup> - Lithium	40
3-17	Hall Voltage vs. Sample Thickness <sup>-1</sup> - Sodium	40
3-18	Hall Voltage vs. Sample Thickness <sup>-1</sup> - Potassium	40
4-1	$n^*$ vs. $A_1$	48
4-2	Cross Section, in 001 plane, of Brillouin Zones for B.C.C. Metal	56
4-3	$F(\theta)$ vs. $\theta$ for Potassium and Lithium	56

## LIST OF TABLES

<u>Table No.</u>		<u>After Page</u>
1-1	Properties of the Alkali Metals	8
2-1	The Ettingshausen, Nernst, and Righi-Leduc Effects	26
3-1	Hall Voltages of Four Alkali Metals at Room and Liquid Nitrogen Temperatures	40
3-2	Hall Constants for Lithium, Sodium, and Potassium	40
4-1	Warping Parameters for the Alkali Metals Computed from Data of F. Ham	46
4-2	Warping Parameters of Alkali Metals at Two Pressures, computed from Data of F. Ham	46
4-3	Velocity of Sound in Potassium	56
4-4	Scattering Functions for K <sub>2</sub> and Li using Bailyn's values of $u^3$ (JS) <sup>2</sup>	58
4-5	Scattering functions for k in 110 direction	60
4-6	Scattering functions for k in 100 direction	
4-7	Scattering functions for k in 111 direction	60
4-8	I(k) for Various Conditions	60

Abstract

Recent band structure calculations by Ham indicate how the Fermi surface of the alkali metals, which is expected to be nearly spherical under normal conditions, may change when the lattice constant is decreased through hydrostatic pressure. Since direct measurement of the distortion of the Fermi surface is difficult, we have tried to study its magnitude by measuring the Hall voltage in the alkalis as a function of hydrostatic pressure up to  $15,000 \text{ kg/cm}^2$ . In each case the Hall voltage decreases with increasing pressure, the size of the decrease ranging from 2 percent in  $15,000 \text{ kg/cm}^2$  for lithium to 37 percent in  $15,000 \text{ kg/cm}^2$  for cesium before compressibility corrections are applied.

The Hall constant,  $R$ , can be written as  $1/Necn^*$  where  $n^*$  is a factor of the order of unity which expresses the deviation from the free electron value of the Hall constant. The data, with all explicit volume dependence removed, are expressed in the form of curves of  $n^*$  vs. pressure. In all of the alkalis except cesium,  $n^*$  decreases monotonically with increasing pressure; the decreases range from 5 percent in  $15,000 \text{ kg/cm}^2$  for lithium to 8 percent in  $15,000 \text{ kg/cm}^2$  for rubidium. In the case of cesium  $n^*$  passes through a minimum at  $5000 \text{ kg/cm}^2$  and rises to a value of 1.2 at  $15,000 \text{ kg/cm}^2$ .

The change of  $n^*$  between room and liquid nitrogen temperatures was also measured. In all of the alkalis except lithium the change is less than 3 percent. In lithium  $n^*$  decreases by about 25 percent between room and liquid nitrogen temperature.

The warping of a nearly spherical Fermi surface is described by Kubic harmonics and the effect of the warping on  $n^*$  considered. Increases in the warping parameters increase  $n^*$ ; since the band structure calculations indicate that increasing pressure increases the warping parameters, the data cannot be explained on the basis of anisotropic Fermi surfaces alone. If anisotropic scattering times as well as warped Fermi surfaces are considered, then increases of the warping parameters can cause decreases in  $n^*$ .

The pressure results are explained in a semi-quantitative manner using a scattering time that varies by a factor of three over the Fermi surface. By contrast, the warping of the Fermi surface is small; with the exception of cesium, the electron wave vector at the Fermi surface deviates from the free electron value by less than 10 percent.

An approximate expression for  $\tau(\vec{k})$  is derived and the factors contributing to the anisotropy in  $\tau$  are considered. The most important factors are the anisotropy of the velocity of sound and the dependence of the size of the phonon wave vector used in umklapp processes upon the initial electron state. A crude calculation shows that with appropriate forms for the electron-phonon scattering matrix element, the latter factor alone can give a scattering time that varies by nearly 70 percent over the Fermi surface.

Pressure Dependence of the Hall Constant  
of the Alkali Metals

by

Thomas Frederick Deutsch

Gordon McKay Laboratory of Applied Science

Division of Engineering and Applied Physics

Harvard University

Cambridge, Massachusetts

I. Introduction

A. The Fermi Surface in Metals

Considerable work has recently been done in an effort to learn more about the Fermi surface in metals, both theoretically and experimentally. In a one electron picture, the Fermi surface is a surface of constant electron energy in  $k$  space, where  $k$  is the reduced momentum; the value of the energy on this surface is the Fermi energy,  $E_F$ , defined by  $f(E_F) = \frac{1}{2}$  where  $f(E)$  is the Fermi-Dirac distribution function. It may also be thought of as the surface separating regions of  $k$  space where the electron states are occupied from those that are empty. Although the concept of the Fermi surface grew out of a one electron picture, recently theoretical work has been done to show that it has some justification even in a many electron picture [ 1]. The possible topologies of the Fermi surface in metals have been discussed by many authors. A good review of the subject has recently been given by Ziman [ 2].

Although band structure calculations have been performed for many metals, especially the alkalis, relatively few of these are sufficiently detailed to allow a deduction of the shape of the Fermi surface. Generally, the energy has been computed only at certain symmetry points in the Brillouin zone; to obtain the Fermi surface, curves of electron energy vs.  $k$  for several

directions in the reciprocal lattice are needed. Recent calculations on the band structure of the alkali metals by Ham [3] are of importance for several reasons. First, they provide curves of  $E$  vs.  $k$  for the three principal directions and allow the deduction of an approximate shape for the Fermi surface. Second, they are made for the entire alkali series, (lithium, sodium, potassium, rubidium, and cesium), using the same method in each case and should give a qualitative picture of the change in the shape of the Fermi surface as one progresses through the series. Third, they have been carried out for several values of lattice constant and so provide a guide as to how the Fermi surface should change under pressure.

The work of Ham used a variational technique developed by Kohn and Rostoker [4]. They used a potential that had only a radial dependence within a sphere inscribed in the atomic polyhedron and was constant outside the sphere. The wave equation is solved in the actual atomic polyhedron and gives an  $E(\vec{k})$  which is not spherically symmetric. With this form of the potential, energy eigenvalues could be obtained using some geometrical structure constants, which depend only on the type of lattice, and the values of the logarithmic derivative of the solution of the radial wave equation at the boundary of the inscribed sphere. Ham [5,6] used the method of quantum defects to obtain the logarithmic derivatives needed; this made it unnecessary to assume a specific numerical potential. The use of the quantum defect method takes into account the polarization of the ion cores, relativistic effects, and exchange effects between the valence electrons and the ion cores. These effects are important in the heavy elements and a calculation which ignored them would probably be in error.

The accuracy of the Kohn-Rostoker technique used is limited by the realism of the assumed potential rather than by mathematical accuracy. Furthermore, the method is sufficiently tractable to make possible band structure calculations elaborate enough to indicate the shape of the Fermi surface. In the alkalis the size of the ion core is small, (about half the nearest neighbor distance in sodium) and consequently the Kohn-Rostoker potential may be fairly realistic.

Other band calculations have been carried out using explicit potentials; for example Heine [7] has computed the band structure of aluminum in a self-consistent manner using a method which takes approximate account of

the effects of correlation and exchange between the valence electrons and the ion core, and also among the valence electrons. This determination was checked with a combined theoretical-experimental one which used available experimental data, primarily from deHaas-van Alphen experiments, to supplement a simpler calculation [ 8] . The agreement between the two determinations of the behavior of  $E(\vec{k})$  away from the zone surface was used to justify the potential used in the more elaborate band structure calculation, even though the calculated shape of the surface at certain zone corners did not agree with the experimental results. Harrison [ 9] has obtained a different shape for the Fermi surface of aluminum using a similar theoretical-experimental approach; he was able to fit the experimental data with a model having fewer deviations from a free electron Fermi surface than Heine's. Harrison used the band calculations of Heine to modify the surface predicted by the free electron model and used data from deHass-van Alphen experiments to determine the details of the geometry.

Later work by Harrison has investigated the validity of a nearly free electron approach for determining the Fermi surface of the polyvalent metals [ 10] . The conduction electron wave functions are plane waves orthogonal to the wave functions of the core electrons (O.P.W.'s); the electron energy is proportional to  $k^2$  . Comparison of constant energy surfaces for aluminum calculated with one O.P.W. and with three or four O.P.W.'s shows that the latter show fewer sharp bends than the one O.P.W. surface, but are not greatly modified otherwise [ 11] .

While the use of plane waves or a nearly free electron picture to describe electrons moving in the periodic potential of the crystal lattice appears physically unrealistic, there seems to be theoretical justification for a one O.P.W. approach in terms of a pseudo-potential which cancels the lattice potential [ 12, 13] . This justification has not been worked out in detail.

Cohen and Heine have discussed the band structure of the alkali and noble metals in terms of a model which assumes that the wave function of an electron may be represented by one O.P.W. in the interior of the Brillouin

zone and by two O.P.W.'s near a zone face [14]. The energy,  $E(\vec{k})$ , is then spherically symmetric except near the zone boundaries and the  $E$  vs.  $\vec{k}$  curve is parabolic except near the zone face. In this picture the geometry of the band structure allows the warping of the Fermi surface to be expressed in terms of a distortion parameter which depends on the band gap at the zone face. This gap can be related to the observed atomic term values for the free atom and the distortion of the Fermi surface can be compared for the entire alkali series. The effective mass at the bottom of the conduction band,  $m^*$ , is also obtained from the distortion parameter and compared with the results of a quantum defect method calculation; both methods give the same trend for  $m^*$  in going through the series. The relationship Cohen and Heine derive depends upon having energy bands that are parabolic except near the zone faces; the description of the wave functions by 2 O.P.W.'s is one way, but not necessarily the only way, of justifying this energy dependence [15].

On the theoretical level techniques of band structure calculations have advanced to the point where predictions about the shape of the Fermi surface may be made, at least for some metals. The validity of the results depends upon whether the physical assumptions, primarily those about the potential, are correct; the correctness of the assumptions may be judged in part by the agreement with experimental determinations of the Fermi surface.

#### B. Experimental Techniques for Obtaining the Fermi Surface.

As the work of Heine and of Harrison on aluminum has pointed out, a purely theoretical determination of the Fermi surface is not always feasible and experimental information is badly needed. Chambers [16] and Pippard [17] have presented reviews of the techniques available. We shall summarize these methods and mention some more recent developments.

Measurements of the magnetic susceptibility of metal single crystals at low temperatures sometimes show oscillations which are periodic in  $H^{-1}$ , where  $H$  is the magnetic field. These oscillations constitute the de Haas-van Alphen effect. Their period gives the extremal area of a cross section through the Fermi surface with its normal along the direction of  $H$ . From measurements taken with different orientations of the crystal one can

attempt to construct the complete Fermi surface. Measurements of the temperature dependence of amplitude of the oscillations give an average effective mass for a cross section of the Fermi surface. Until fairly recently de Haas-van Alphen measurements had been done at low fields (15 kilogauss) and the effect was not seen in monovalent metals [18]. Lax has reviewed the information that these measurements have given for a number of metals, among them bismuth, arsenic, gallium, and zinc [19]. More recently Shoenberg has used pulsed fields of 160 kilogauss to make de Haas-van Alphen studies on copper, silver, and gold [20]. The results on copper are of special interest, because they confirm the picture, proposed by Pippard on the basis of anomalous skin effect data, of a Fermi surface which touches the zone boundaries.

The most complete anomalous skin effect measurement is the determination of the Fermi surface in copper by Pippard [21] mentioned above. Maxwell's equations predict that the surface impedance of a metal, defined as the real part of

$$Z = \left( \frac{4\pi E_x}{H_y} \right)_{z=0} \quad (I-1)$$

where E and H are the electric and magnetic fields respectively, is proportional to  $\sigma^{-1/2}$ , where  $\sigma$  is the dc conductivity. At sufficiently low temperatures, the surface resistance is anomalous in that it is independent of  $\sigma$ . In this anomalous region the surface resistance can be related to an integral containing the radius of curvature of a cross section of the Fermi surface. From measurements of the anomalous skin effect for surfaces of different orientations, one can attempt to reconstruct the Fermi surface. The method requires carefully polished surfaces and very pure materials, the latter to satisfy the requirement that the mean free path of an electron be much larger than the skin depth.

The attenuation of ultrasonic waves in metal single crystals subject to a dc magnetic field which is perpendicular to the direction of propagation has been used to investigate the Fermi surface of copper [22]. At low temperatures the main contribution to the acoustic attenuation is electronic; a magnetic

field can cause electron orbits in real space to have the same diameter as wavelengths of sound. By measuring the location of the maxima and minima of attenuation as a function of magnetic field, an average radius of a cross section of the Fermi surface may be obtained. The detailed theory of this effect has been recently reviewed [23]. Further work on copper has confirmed many of the details of the Fermi surface proposed by Pippard on the basis of anomalous skin effect work and by Shoenberg on the basis of de Haas-van Alphen measurements [24].

Conventional cyclotron resonance techniques must be modified in order to study metals, since the radio frequency electric field cannot penetrate into the metal much further than the skin depth. Azbel and Kaner [25] have shown that a resonance effect can be obtained by using a dc. magnetic field parallel to the surface of the metal. Some of the electrons, which have circular orbits about an axis parallel to the field, come within a skin depth of the surface of the metal and can absorb rf. energy. If the frequency of the microwave energy is correct, a resonance can occur. This technique has been used to obtain effective masses in copper [26].

Magneto-resistance measurements on single crystals at low temperatures have been used to study the Fermi surface of copper [27]. The interpretation of the data requires an assumption that the scattering time is isotropic [i. e.,  $\tau(\vec{k}) = \tau(E)$ ]. The theory computes the dependence of the magneto-resistance coefficients upon parameters that express the warping or anisotropy of a spherical Fermi surface in terms of Kubic harmonics. The requirement that the scattering time be isotropic is important, since if it were not, the observed magneto-resistance could be attributed to a spherical Fermi surface with an anisotropic  $\tau$ , or to a combination of anisotropic Fermi surfaces and scattering times. The amount of warping is obtained by fitting the theoretical expressions to the measured value of the coefficients. The results indicate that the Fermi surface actually touches the zone face in the 111 direction, in agreement with other work on copper; the fact that touching occurs indicates that the description of the Fermi surface as a warped sphere is not an entirely appropriate one and the warping parameters obtained may not be accurate.

The field dependence of the magneto-resistance as a function of the orientation of a single crystal sample has been used by Russian workers to distinguish between open and closed electron orbits on the Fermi surface [ 28]. This method has been used to examine sodium and has led to the conclusion that the Fermi surface is closed.

These are the techniques used to determine the Fermi surface in metals. They require the use of single crystals and low temperatures and the results are difficult to interpret without some theoretical model of the Fermi surface. The alkali metals are relatively simple from the theoretical viewpoint, but are difficult for the experimenter to prepare and handle. In this case there is some information about the shape of the Fermi surface, which we expect to be nearly spherical, but unfortunately no direct experimental determination of the surface. There is, however, some indirect evidence as to the shape of the Fermi surface in the alkalis.

### C. The Fermi Surface in the Alkalis - Experimental Evidence

As we have mentioned above, the magneto-resistance data on single crystals can be used to make some deductions about the shape of the Fermi surface. In the case of the alkalis the available data are almost exclusively on polycrystals and do not give the magneto-resistance coefficients directly. The only single crystal work is a measurement on sodium, where the single crystal nature of the sample was inferred from anisotropy in the transverse magneto-resistance, but not verified by X-ray data [ 29] and the Russian work mentioned before [ 30] which gives no detailed information. García-Moliner has undertaken to analyze the polycrystal data, taken in the range 4-20° K, in an effort to obtain some information about the shape of the surface [ 31]. He assumes that the scattering time is isotropic at low temperatures and that the wave vector at the Fermi surface can be expressed in an expansion in Kubic harmonics:

$$k = K_0(E_k) + K_1(E_k) Y_4(\theta, \phi) \quad (I-2)$$

where  $Y_4(100) = 1$ ,  $Y_4(110) = -1/4$ ,  $Y_4(111) = -2/3$ . He defines the

parameters

$$A = (K'_1/K'_0) E_F \qquad A' = (K''_1/K''_0) E_F \qquad (I-3)$$

where the ' indicates the derivative with respect to the energy  $E_k$ , and  $E_F$  is the Fermi energy. Davis has calculated the transverse and longitudinal magneto-resistance for a Fermi surface of this type, assuming the current to be along a 100 axis [32]. García-Moliner uses these calculations to obtain an expression for the transverse magneto-resistance of a polycrystalline sample. Because Davis' calculations do not give the three magneto-resistance coefficients for single crystals directly, but rather those combinations of them which give the transverse and longitudinal magneto-resistance for current in the 100 direction, García-Moliner equates the calculated ratio of longitudinal to transverse (polycrystal) magneto-resistance to the experimentally observed value in order to get a relation between the three coefficients which allows him to use Davis' results. He also needs to assume a value for  $A'/A$ . With these assumptions he can calculate  $A$ , which expresses the warping of the Fermi surface, from the available data on polycrystals. His results are shown in Table 1-1, which tabulates a number of properties of the alkalis. The values for rubidium and cesium are uncertain, since the experimental information is inadequate for a reliable calculation. Because the anisotropy parameter  $A$  enters in the expression for the magneto-resistance as  $A^2$ , small differences in the anisotropy predicted by various band structure calculations cause large differences in the predicted magneto-resistance; this approach is used to suggest that the 1934 calculation of Jones and Zener gives the best fit to the experimental data for lithium [33]. Moliner gives the alkalis in order of increasing anisotropy as sodium, rubidium, potassium, cesium and lithium; although the relative order of the intermediate metals is not definite, the extremes of the series are well determined.

Since both sodium and lithium undergo martensitic transformations from the body centered cubic to the close packed hexagonal form in cooling to below hydrogen temperature, it is not clear that the low temperature magneto-resistance data on these metals are meaningful [34, 35]. Even if the approach used by García-Moliner gives a correct picture of the relative anisotropies of

HP6

Property	Li	Na	K	Rb	Cs
$R - \frac{\text{volt-cm}}{\text{amp. -gauss}} \times 10^{13}$	-17 <sup>[3]</sup>	-21 <sup>[1]</sup>	-42 <sup>[1]</sup>	-59.2 <sup>[2]</sup>	-78 <sup>[1]</sup>
$n^*$ - computed from R	.79	1.17	1.11	.94	.98
$\theta_D$ - Debye Temp. <sup>[4]</sup> in °K	430	160	99	59	43
Melting Temp. °C <sup>[5]</sup>	180	97.7	63.6	39.0	28.5
Elastic Constants					
$C_{11} \times 10^{-11}$ in dynes/cm <sup>2</sup>		.615 <sup>[6]</sup>	.416 <sup>[6]</sup>		
$C_{12} \times 10^{-11}$ "		.469	.333		
$C_{44} \times 10^{-11}$ "		.592	.263		
Anisotropy $\frac{2C_{44}}{C_{11} - C_{12}}$		8.11	6.34		
Linear contraction <sub>2</sub> in 15,000 kg/cm <sup>2</sup>	3.5% <sup>[7]</sup>	5.5% <sup>[7]</sup>	8.7% <sup>[7]</sup>	10.3% <sup>[8]</sup>	12.5% <sup>[8]</sup>
$A \times 10^2$ (from García-Moliner) <sup>[9]</sup>	12.7	1.7	8.8	8??	9??
$ r  \times 10^2$ (from expression (I-5))	5.3	.6	1.3	2.5?	1?

Table 1-1

Properties of the Alkali Metals

ReferencesTable 1-1

1. F. J. Studer and W. D. Williams, Phys. Rev. 47, 291 (1935).
2. E. Krautz, Z. Naturf. 5a, 13 (1950).
3. International Critical Tables VI, McGraw-Hill, New York, p. 416 (1929).
4. A. H. Wilson, Theory of Metals, Cambridge University Press, p. 143 (1953).
5. Charles Kittel, Introduction to Solid State Physics, 1st ed., Wiley, New York, p. 57 (1953).
6. American Institute of Physics Handbook, McGraw-Hill, New York, p. 3-81, (1957).
7. P. W. Bridgman, Proc. Amer. Acad. Arts Sci. 70, 93-95 (1935).  
Linear contractions are computed from the volume data.
8. P. W. Bridgman, Phys. Rev. 27, 68 (1926).
9. F. García-Moliner, Proc. Phys. Soc. LXXII, 996 (1958).

the alkalis, his choice of the expansion for the wave vector  $k$  overestimates the degree of warping. We expect that the Fermi surface will bulge towards the nearest zone face, which in the case of the alkalis lies in the 110 direction in the reciprocal lattice. However, an expansion in terms of fourth-order Kubic harmonics can only give bulging towards the 100 faces (if  $A$  is positive) or towards the 111 face (if  $A$  is negative). On the other hand, if sixth-order Kubic harmonics are included in the expansion, the desired bulging in the 110 direction can be obtained. Furthermore, it turns out that the effect of the  $Y_6$  terms on the magneto-resistance coefficients is more than ten times that of the  $Y_4$  terms. This has been shown by the work of Olson and Rodriguez who expanded the energy at the Fermi surface, rather than the wave vector, in Kubic harmonics [36]. They used

$$E = \frac{\hbar^2 k_o^2}{2m^*} \left[ 1/2 \left( \frac{k}{k_o} \right)^2 + r \left( \frac{k}{k_o} \right)^4 Y_4(\theta, \phi) + rt \left( \frac{k}{k_o} \right)^6 Y_6(\theta, \phi) \right] \quad (I-4)$$

as an expression for the constant energy surface;  $m^*$  is an effective mass,  $k_o$  is the radius of a sphere in  $k$  space which contains one electron per atom, and  $r$  and  $t$  are warping parameters. The values of  $Y_6$  in the three principal directions are:

$$Y_6(100) = 1, \quad Y_6(110) = -\frac{13}{8}, \quad Y_6(111) = \frac{16}{9}.$$

Although this approach is similar to that of García-Moliner, it has the advantage of eliminating parameters like  $A'$  from the final expression for the magneto-resistance coefficients. Furthermore, Olson and Rodriguez compute all three coefficients, allowing an expression for the transverse magneto-resistance of a polycrystal to be obtained directly, without any assumptions about the ratio of the longitudinal to transverse magneto-resistance. By using García-Moliner's expression for  $\bar{B}_t$ , the transverse magneto-resistance of a polycrystal, along with the results of Olson and Rodriguez we obtain

$$\frac{\Delta \rho}{\rho H^2} = \bar{B}_t = \left[ \frac{R}{\rho} \right]^2 [48.9 r^2 - 7.15 r^2 t + 750 (rt)^2] \quad (I-5)$$

where  $R$  is the calculated (free electron) value of the Hall constant and  $\rho$  is the resistivity at the temperature of the experiment.  $R$  is expressed in ohm-cm/gauss and  $\rho$  in ohm-cm. Since  $t$ , as obtained by fitting the expression (I-4) to Ham's  $E(k)$  curves, is of the order of unity, it is clear that the terms from  $Y_6$  contribute far more than those from  $Y_4$ . In Table I-1 we give the values of  $|r|$  obtained by fitting the expression (I-5), with the approximation that  $t$  may be set to 1, to Moliner's values of  $\bar{B}_t$ . The values of  $\rho$  are taken from Kittel [37]; the values of  $R$  from Mott and Jones [38]. The values of the parameter  $r$  that we obtain indicate considerably less warping than is obtained from the expansion (I-2), even though  $A$  and  $r$  are not directly comparable.

The behavior of the low temperature thermopower has been used by Ziman to make some estimate of the anisotropy of the Fermi surface in the alkalis [39]. The thermopower,  $Q$ , is defined by:

$$\vec{E} = Q \nabla T \quad (I-6)$$

where  $\vec{E}$  is the electric field in a metal and  $\nabla T$  is the temperature gradient. On a free electron picture  $Q$  should be negative, approximately proportional to  $T$ , and small, of the order of .1 microvolt/°C. at 10°K. Measurements on the alkalis show that at low temperatures  $Q$  can be either positive or negative or can even change sign with temperature, that it is not always linear in  $T$ , and that it may be of the order of several microvolts/°C. The large size of the effect at low temperature is due to the fact that the phonon distribution is not in equilibrium and contributes to the thermopower [40]. Bailyn pointed out that the sign of the lattice contribution to the thermopower can be either positive or negative [41]. This is because of the role played by umklapp processes in the lattice thermopower. The lattice power calculated by Ziman is proportional to  $-\langle \vec{s} \cdot \vec{q} \rangle$  where the  $\langle \rangle$  indicates an average over all electron-phonon interactions,  $\vec{q}$  is the phonon wave vector, and  $\vec{s}$  is given by:

$$\vec{s} = \vec{k} - \vec{k}' = \vec{K} + \vec{q} \quad (I-7)$$

$\vec{k}$  and  $\vec{k}'$  are the initial and final electron wave vectors and  $\vec{K}$  is a reciprocal lattice vector. If  $\vec{K} = 0$  we have a normal process,  $\vec{s}$  is parallel to  $\vec{q}$ .

the term in the  $\langle \quad \rangle$  is positive, and the contribution to the thermopower is negative. For an umklapp process, where  $\vec{K}$  is not 0,  $\vec{s}$  can be anti-parallel to  $\vec{q}$  and the contribution to the thermopower positive. In an extended zone scheme, the size of the smallest phonon wave vector with which an umklapp process may occur is determined by the shortest distance between adjacent Fermi surfaces and changes if the surfaces are warped. Ziman calculated the temperature dependence of the thermopower for various amounts of bulging of the Fermi surface and found he could fit the experimental data for sodium and potassium quite well. The rubidium and cesium data were not fitted in detail. For lithium, the thermopower is positive throughout the temperature range; this is taken to suggest that the Fermi surface actually touches the zone boundary. Ziman concludes that in sodium the surface is nearly spherical, and that the anisotropy increases as we go through the series potassium, rubidium, cesium and lithium.

Ziman's calculation is a rough one; he does not take the large anisotropy of the velocity of sound in alkalis into account and this could well change the size of the warping he obtains. However, we do expect that the differences between the various alkalis should show up in this calculation. In a more recent paper Bailyn suggests that differences in the anisotropy of the transverse phonon spectrum for the various alkalis may also be able to explain the observed thermopowers and that the relative importance of these two proposed causes is not at all clear [42].

We have seen that both the magneto-resistance data and the thermopower data have been used to infer that lithium is the alkali metal with the most anisotropic Fermi surface; the surface may even touch the zone face. Cohen and Heine [43] have inferred touching of the surface in lithium from the pressure dependence of the resistance. In all the alkali metals except lithium, the resistance initially decreases as pressure increases. The conductivity may be written as

$$\sigma = \frac{e^2}{4\pi^3 \hbar} \int v \tau(\vec{k}) dA \propto \overline{v\tau} A \quad (I-8)$$

where the integral is taken over the Fermi surface,  $v$  is the electron velocity,  $\tau(\vec{k})$  is the scattering time at point  $\vec{k}$ ,  $dA$  is an element of area on the Fermi

surface,  $\bar{v}$  and  $\bar{\tau}$  are average velocities and scattering times and  $A$  is the area of the Fermi surface. The usual explanation of the effect of pressure on the conductivity is that increasing pressure decreases the amplitude of the lattice vibrations, increasing  $\tau$  [44]. Cohen and Heine proposed that the effect in lithium is dominated by the increase of the area of contact with pressure; this can decrease the area of the Fermi surface and increase the resistivity. According to Bailyn [45] increased contact creates a narrower shape for the Fermi surface, with smaller cross sections; this decreases the velocities on the surface and increases the resistivity. Cohen and Heine also claim that the increased contact enhances scattering by umklapp processes and opposes the effect of the lattice vibrations on  $\tau$ . We have been able to draw Fermi surfaces in which increased contact increases the area of the Fermi surface. An example is the case where the unoccupied region of  $k$  space is spherical. Since the volume of this unoccupied region must stay constant and a sphere encloses this volume with the smallest possible surface area, any increased contact increases the area of the Fermi surface. This example points out that statements about the effect of touching should be accompanied by some picture of the original shape of the Fermi surface; without this, arguments on the effect of touching are not convincing.

Brooks [46] has pointed out that the decrease of the conductivity of lithium with pressure can be explained without invoking touching of the Fermi surface with the zone boundary. Calculations of the effective mass, such as those made by Brooks using the quantum defect method and summarized by Ham [47] show that  $m^*$  increases as the pressure increases. Since

$$v \propto dE/dk \propto 1/m^* \quad (I-9)$$

the average velocity  $\bar{v}$  will decrease with pressure. Likewise the decrease in the density of states factor  $|\nabla_{\mathbf{k}} E|$  in the expression for  $\tau$  (see Sec. IV, Eq. IV-37) lowers  $\tau$ .

The fact that the K X-ray emission for lithium does not drop sharply in intensity at the high energy end of the band has been used to infer strong deviations from free electron behavior [48]; this may indicate actual touching of Fermi surface with the zone boundary.

There is, then, no direct experimental information about the shape of the Fermi surface in the alkalis. What information we do have has been inferred from experiments on the transport properties. These transport properties depend on averages of scattering times and energy derivatives (electron velocities and effective masses) taken over the entire Fermi surface and yield useful information only if we have some model of the shape of the surface to start with. In the alkalis the expectation is that the Fermi surface is a warped sphere. The inferences that have been made agree that lithium shows severe warping and the Fermi surface may touch the zone boundary, that sodium has very little warping and that the warping probably increases as we go through the series potassium, rubidium and cesium.

#### D. The Fermi Surface as a Function of Pressure

With the availability of band calculations made at several values of lattice constant, theoretical predictions about the change in the shape of the Fermi surface with pressure can be made. The question arises as to possible experiments that will give information about the shape of the surface as a function of pressure. The high compressibilities of the alkali metals (Table I-1) make possible significant changes of lattice constant in the pressure range available in the laboratory. As we have seen, the direct techniques for studying the Fermi surface such as de Haas-van Alphen or acoustic attenuation measurements have not yet been applied to the alkalis, in large part because of the difficulty of growing single crystals and handling the metals. Even if these difficulties are overcome, helium temperature pressure measurements are possible only over a small pressure range, since the pressure transmitting fluid freezes with application of relatively low pressures. Even with the use of solid hydrogen as the pressure transmitting medium the pressure is still relatively low, of the order of 5000 atmospheres, and shear stresses are present which may introduce non-hydrostatic strain and produce additional defects due to plastic deformation [49]. In order to take advantage of the pressure range available in the laboratory, measurements at either room or nitrogen temperatures are needed.

Since no direct means of determining the Fermi surface are available, the next best possibility is to measure some transport properties under pressure and interpret the results in terms of changes of the Fermi surface and

of other parameters; preferably we would like to measure an effect that is sensitive to the shape of the Fermi surface alone.

The simplest transport property to measure is the conductivity. Unfortunately, this is quite insensitive to the shape of the Fermi surface and quite sensitive to the magnitude of the scattering time. This is best seen by noting the effect of warped surfaces of the form (I-4) on conductivity; Olson and Rodriguez give

$$\sigma = N e^2 \tau / m^* [ 1 - r^2 (0.190 + 1.85 t^2) ] \quad (I-10)$$

where  $N$  is the number of carriers/volume and  $\tau$  is the isotropic scattering time. If we remember that  $t$  is of the order of unity and that  $|r|$  is less than .1 (Table I-1) we now see that warping of a closed Fermi surface will change the conductivity by less than 2 percent from the value for a spherical surface. Since the observed effect of pressure on the conductivity of alkalis is to produce changes of the order of 50 percent in 15,000 atmospheres, we can see that changes in  $\tau$  and  $m^*$  far outweigh those in the shape of the surface.

On the other hand Eq. (I-5) for the magneto-resistance shows that this property is quite sensitive to the shape of the surface. Unfortunately, the magnitude of the magneto-resistance effect at room temperature is too small to be measured by ordinary techniques. Kapitza did manage to observe the magneto-resistance of sodium and lithium at room temperature by using pulsed fields of 300 kilogauss; he observed changes of resistance of less than 2 percent [50]. Since the effect goes as  $H^2$  ordinary dc magnetic fields of 10 to 30 kilogauss would produce resistance changes in the range from .002 percent to .02 percent. Reducing the temperature to the liquid nitrogen range would not produce a significant improvement. Kapitza found a 15 percent effect in lithium at this temperature; this would become a .15 percent effect with a 30 kilogauss dc field. It is only in the helium temperature range that the magneto-resistance becomes large enough, of the order of 10 percent, so that a pressure experiment might be feasible; however, in this range the available pressure is limited, as we have mentioned.

Another transport property of interest is the Hall effect. The Hall constant,  $R$ , is defined by

$$E_y = R J_x H_z \quad (I-11)$$

where  $E_y$  is the transverse electric field,  $J_x$  the current density, and  $H_z$  the magnetic field. Figure 1-1 shows the geometry involved;  $x, y, z$ , indicate direction. Derivations of the Hall constant based on a picture of free electrons give

$$R = 1/Nec \quad (I-12)$$

where  $e$  is the charge of the carriers and  $c$  the velocity of light. More accurate treatments of the Hall effect involve solving the Boltzmann transport equation and knowing  $E(\vec{k})$  and  $\tau(\vec{k})$ . The Hall constant is then given as the quotient of two integrals involving the scattering time and energy derivatives taken over the Fermi surface [51]. It can be shown that for  $\tau(\vec{k}) = \tau(E)$  and for spherical energy surfaces,  $E(\vec{k}) = E(|\vec{k}|)$ , the Hall constant is still given by Eq. (I-12). In general, anisotropy of the scattering time and of the energy surfaces will alter the expression for the Hall constant. We may then write

$$R = 1/Necn^* \quad (I-13)$$

where  $n^*$ , which we shall refer to as electrons/atom, is a factor which depends on the anisotropy of  $\tau(\vec{k})$  and  $E(\vec{k})$ , and is of the order of one. In Table 1-1 we have listed the values of  $n^*$  for the alkalis, computed from the values of the Hall constant given in the literature. From the computations of Olson and Rodriguez one can obtain the Hall constant for an energy surface of the form (I-4) and an isotropic scattering time. This gives

$$n^* = \frac{[1 - r^2 (.190 + 1.85 t^2)]^2}{1 - r^2 (5.14 + 81.2 t^2)} \quad (I-14)$$

We see that the change of  $n^*$  from its free electron value of unity depends only upon the warping of the surface. Expression (I-14) will always give  $n^*$  larger than unity. When we discuss our results in Sec. IV we shall give an expression for  $n^*$  which takes into account both warped energy surfaces and

anisotropic scattering times; in that case  $n^*$  may be either greater or less than one. We shall see there that the magnitude of the scattering time does not enter the expression for  $n^*$ ; only its anisotropy. Except for a direct volume dependence of  $N$ , we can attribute any changes in  $R$  with pressure to changes in  $n^*$ ; these changes are due to changes in the anisotropy of the Fermi surface and/or the anisotropy of the scattering time. If the measurement were performed in the impurity scattering range, where the scattering time is probably nearly isotropic, the results of a pressure measurement could be interpreted more directly in terms of changes of the anisotropy of the Fermi surface; in a room temperature measurement the scattering is by the lattice and we shall have to consider the effect of a possible anisotropy in the scattering time arising from the elastic anisotropy of the crystal. We shall see in Sec. IV that this can be quite important.

The expression (1-14) shows that the Hall effect is quite sensitive to anisotropy of the Fermi surface, considerably more so than the conductivity (1-8). It can be measured at room temperature, single crystal samples are not necessary, and since the scattering is dominated by the lattice, small amounts of impurities are not important. We decided to study the Hall effect in the alkali metals under pressure.

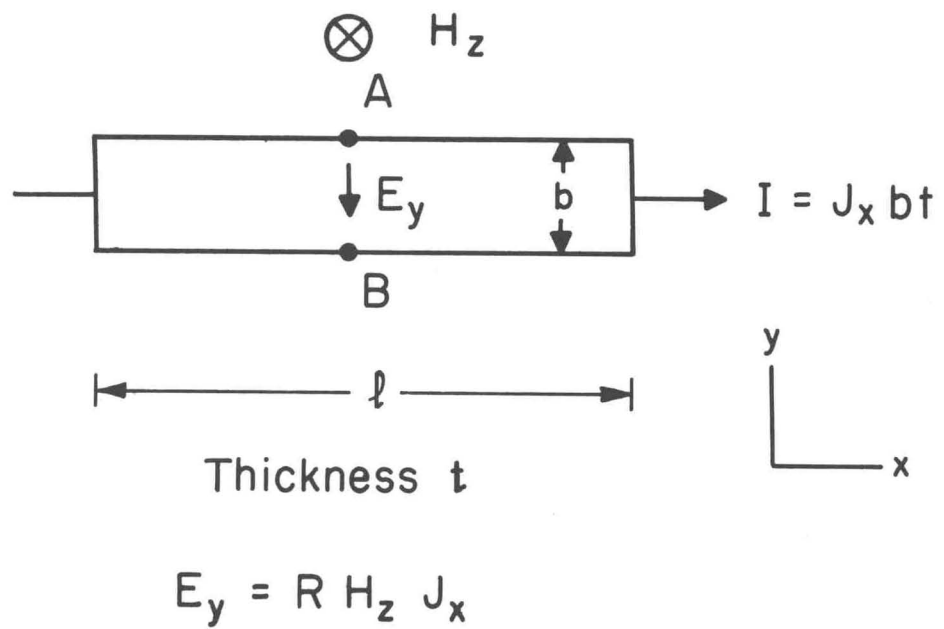


FIG. 1-1 THE HALL EFFECT

I. References

1. J. M. Luttinger, Proceedings of the Fermi Surface Conference, New York, p. 2 (1960).
2. J. M. Ziman, Electrons and Phonons, Oxford University Press, Oxford, England (1960) Chap. 2.
3. F. Ham, Proceedings of the Fermi Surface Conference, New York, p. 9 (1960).
4. W. Kohn and N. Rostoker, Phys. Rev. 94, 1111 (1954).
5. F. Ham, Solid State Physics, Academic Press, New York, 1, 127 (1955).
6. H. Brooks and F. Ham, Phys. Rev. 112, 344 (1958).
7. V. Heine, Proc. Roy. Soc. (London) A240, 361 (1957).
8. V. Heine, Proc. Roy. Soc. (London) A240, 340 (1957).
9. W. A. Harrison, Phys. Rev. 116, 555 (1954).
10. W. A. Harrison, General Electric Co. Memo Report MB-45 (1960).
11. W. A. Harrison, General Electric Co. Memo Report MB-43 (1959).
12. J. C. Phillips, Phys. Rev. 112, 685 (1958).
13. J. C. Phillips and L. Kleinman, Phys. Rev. 116, 287 (1959).
14. M. H. Cohen and V. Heine, Phil. Mag. Supp. 7, 395 (1958).
15. H. Brooks, N. 2 del Supplemento al Vol. 7, Series X, del Nuovo Cimento, 165 (1958).
16. R. G. Chambers, Can. J. Physics 34, 1395 (1956).
17. A. B. Pippard, 1954 Solvay Congress Report, Brussels, p. 123.
18. D. Shoenberg, Phil. Trans A245, 1 (1952).
19. B. Lax, Rev. of Mod. Physics 30, 122 (1958).
20. D. Shoenberg, Phil. Mag. 5, 105 (1960).
21. A. B. Pippard, Phil. Trans. A250, 325 (1957).
22. R. W. Morse, H. V. Bohm, J. D. Gavenda, Phys. Rev. 109, 1394 (1958).

23. M. H. Cohen, M. J. Harrison, and W. A. Harrison, *Phys. Rev.* 117, 937, (1960).
24. R. W. Morse, Proceedings of the Fermi Surface Conference, New York, p. 214 (1960).
25. M. Ya Azbel and E. A. Kaner, *J. Phys. Chem. Solids* 6, 113 (1958).
26. D. N. Langenberg and T. W. Moore, *Phys. Rev. Letters* 3, 328 (1959).
27. R. Olson and S. Rodriguez, *Phys. Rev.* 108, 1212 (1957).
28. N. E. Alekseevski and Yu. P. Gaidukov, *Soviet Physics JETP* 37, 481 (1960).
29. E. Justi and J. Kramer, *Physikalische Zeit.* 41, 105 (1940).
30. Reference 28.
31. F. García-Moliner, *Proc. Phys. Soc.* LXII, 996 (1958).
32. L. Davis, *Phys. Rev.* 56, 93 (1939).
33. H. Jones and C. Zener, *Proc. Roy. Soc.* A145, 268 (1934).
34. C. S. Barrett, *Phys. Rev.* 72, 245 (1948).
35. C. S. Barrett, *J. Inst. Metals* 84, 43 (1955).
36. Reference 27.
37. Charles Kittel, Introduction to Solid-State Physics, 1st ed., Wiley, New York, p. 240 (1953).
38. N. F. Mott and H. Jones, Theory of the Properties of Metals and Alloys, Dover, New York, p. 284 (1958).
39. J. M. Ziman, *Phil. Mag.* 4, 371 (1959).
40. Reference 2, p. 407.
41. M. Baily, *Phys. Rev.* 112, 1587 (1958).
42. M. Baily, Transport in Metals II, *Phys. Rev.* 120, 381 (1960).
43. Reference 14.
44. Reference 38, p. 271.

45. Reference 42.
46. H. Brooks, private communication.
47. Reference 5, p. 185.
48. D. H. Tombouliau, Handbuch der Physik, Springer Verlag, Berlin. 30, 272, (1957)
49. J. Hatton, Phys. Rev. 100, 681 (1955).
50. P. Kapitza, Proc. Roy. Soc. A123, 292 (1929).
51. A. H. Wilson, The Theory of Metals, Cambridge Univ. Press, p. 226, (1953).

## II. Experimental Techniques

### A. Electrical

#### 1. The measurement problem.

The voltage produced by a Hall effect sample is

$$V_H = RHI/t \quad (II-1)$$

where

- $V_H$  - Hall voltage
- H - magnetic field in gauss
- I - current in amps
- t - thickness in cm
- R - Hall constant in volt-cm/amp - gauss

We can estimate the Hall voltage produced by a typical alkali, sodium.

Using  $R = 21 \times 10^{-13}$  volt-cm/amp - gauss,  $H = 6000$  gauss,  $I = 3$  amps, and  $t = .05$  cm, we obtain  $V_H = .75$  microvolts. As we measure the voltage produced when the magnetic field is reversed we actually measure  $2V_H$  or 1.5 microvolts.

If we estimate a change of about 10 percent in the Hall voltage in  $15,000 \text{ kg/cm}^2$  and wish to measure this change to at least 10 percent, we must resolve changes of 1 percent in  $V_H$ . This means we need a measuring system that can resolve  $10^{-8}$  volts.

#### 2. The choice of an ac or dc method.

Hall voltage measurements may be performed using either an ac or dc system. In an ac system a dc magnetic field and an ac sample current can be used. The Hall voltage is then an ac voltage having the same frequency as the sample current. Such a system is described in detail by Lavine [1, 2]. Its advantages include the elimination of contact, thermoelectric, and thermomagnetic potentials. Furthermore, ac amplifiers provide sensitive detectors. Lavine also pointed out a serious defect of the ac method. The high currents, of the order of an ampere, flowing through the sample cause it to vibrate in the

magnetic field. This induces spurious voltages in the system, since the sample with its associated Hall leads forms a closed loop vibrating in a magnetic field. These vibrations may be eliminated by clamping the sample rigidly. In our work we used originally a modification of Lavine's equipment. Considerable effort was spent in developing ways of mounting the sample that would eliminate vibrations. Unfortunately, clamping the sample to prevent vibrations conflicts with the requirement that a pressure sample be mounted in such a way as to leave it free to expand and contract. We were finally able to mount our specimens so as to prevent audible sample vibrations. When we encountered the problem of irreproducibility on samples of rubidium we decided to look for spurious ac voltages by doing a dc check measurement. The dc measurement on rubidium still gave results that varied from sample to sample. This difficulty was overcome when we prepared the sample so as to avoid oxidation, in the manner described below. The dc measurements generally gave less scatter on Hall voltage vs. pressure curves than the ac ones, although at least part of the difference may be due to the better sample preparation techniques used later in the experiment. However, the dc measurement also gave resistance as a function of pressure, while the ac one did not; in addition it was faster and more convenient to use and eliminated the possibility of spurious voltages due to vibrations. We finally adopted the dc measuring system to be described. The agreement between the ac and dc results will be discussed in Sec. III, but was fairly good.

### 3. Description of the dc measuring system.

Figure 2-1 shows a block diagram of the entire electrical system. The sample current of 3 amperes is provided by two six volt storage cells in parallel. Sample current was measured by a Weston model 931 ammeter. This meter could easily be read to 1/3 percent at full scale. The voltage produced at the Hall probes was measured by the Rubicon potentiometer and galvanometer amplifier described below.

The Rubicon No. 2767 microvolt potentiometer [3] is an instrument in which the spurious thermal electromotive forces originating within the instrument have been reduced to less than .01 microvolt. It incorporates a reversing key which instantaneously changes the polarity of the galvanometer

connections. The potentiometer is adjusted until reversing the galvanometer connections produces no deflection at the detector. In this way the presence of constant thermal voltages in the detector circuit does not affect the potentiometer balance. Furthermore, the detector will see twice the out-of-balance voltage while the potentiometer is being balanced and the detector sensitivity is effectively doubled.

Use of the Rubicon potentiometer required that we have a detector which would resolve a voltage of .01 microvolt. To achieve this sensitivity we constructed the galvanometer amplifier pictured in Fig. 2-2. Light from the source, S, passes through the aperture, A, in the partition separating the light source from the rest of the galvanometer. It is focused onto the mirror of the primary galvanometer, G, by a double convex lens, L, reflected onto the plane mirror M, and forms a circular spot on the two matched "EEL" selenium photocells<sup>†</sup>, P<sub>1</sub> and P<sub>2</sub>. The photocells are mounted on a modified microscope stage<sup>††</sup>, T, and can be moved in the direction of the arrows by turning the shaft R. The photocells are connected so that their voltages oppose and the output of the pair is fed to the secondary galvanometer. The shaft R is used to move the photocells until there is no deflection on the secondary galvanometer when there is no input to the system. A signal at the primary galvanometer G changes the light balance on the photocells and produces a deflection of the secondary galvanometer.

The galvanometer amplifier was built on a piece of 2 inch steel channel 24 inches long and was enclosed in aluminum. The light source, S, and its associated transformer, X, were separated from the rest of the system by an aluminum partition which prevented light from the source from reaching the photocells and also prevented convection currents from the light bulb from moving the galvanometer mirror. The primary galvanometer was supported

-----  
<sup>†</sup> Electronic Equipment Limited, 101 Leadenhall St., London E.C. 3, England.

<sup>††</sup> Micronta mechanical stage, available from Radio Shack, Inc. Boston, Mass.

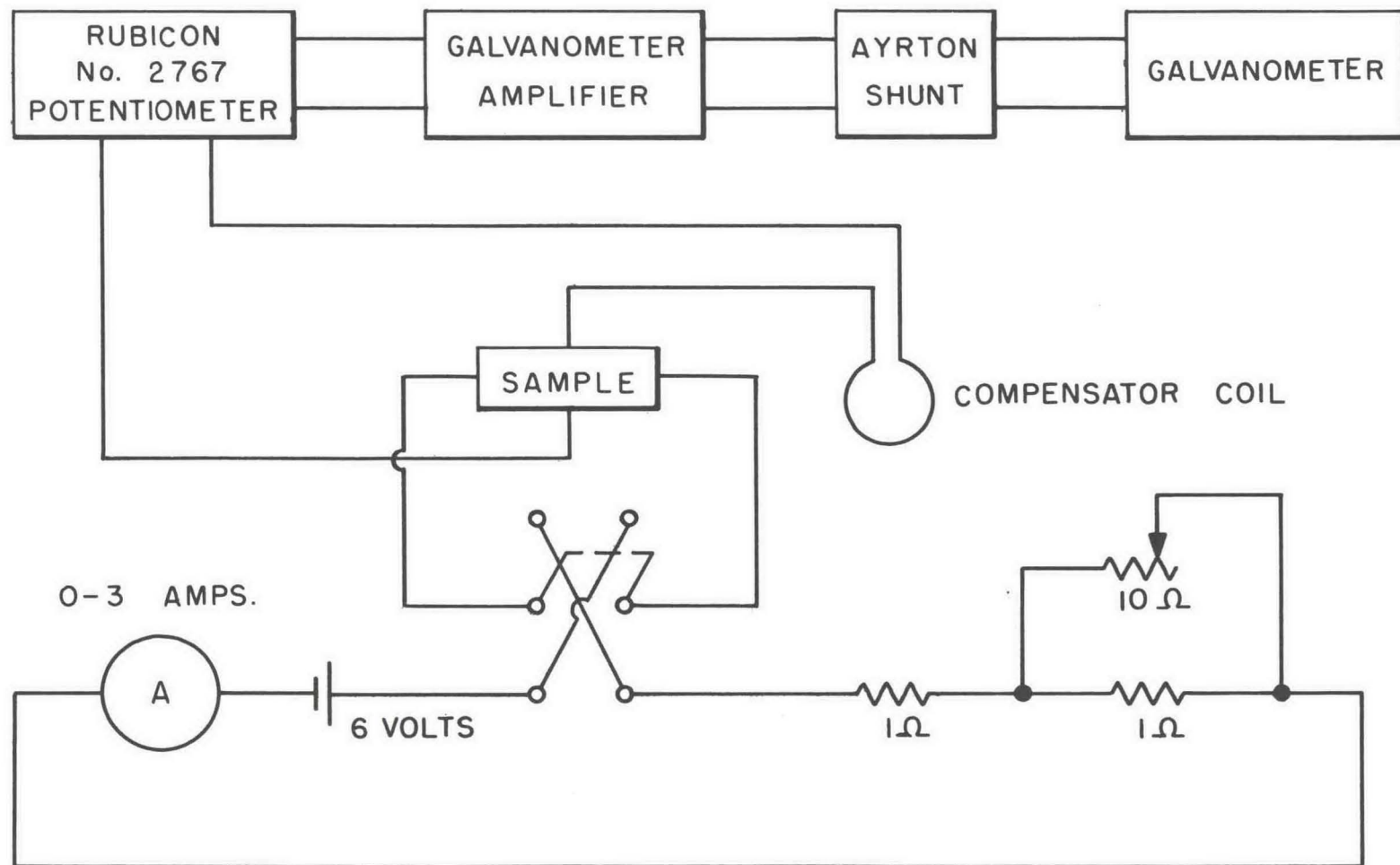


FIG. 2-1 HALL VOLTAGE MEASURING CIRCUIT.

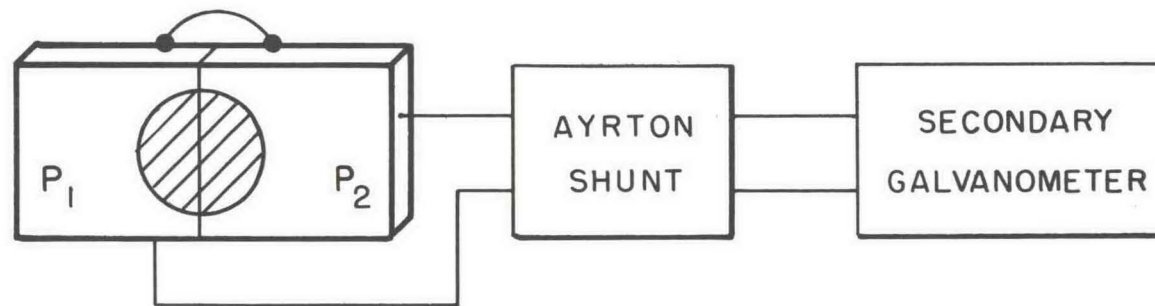
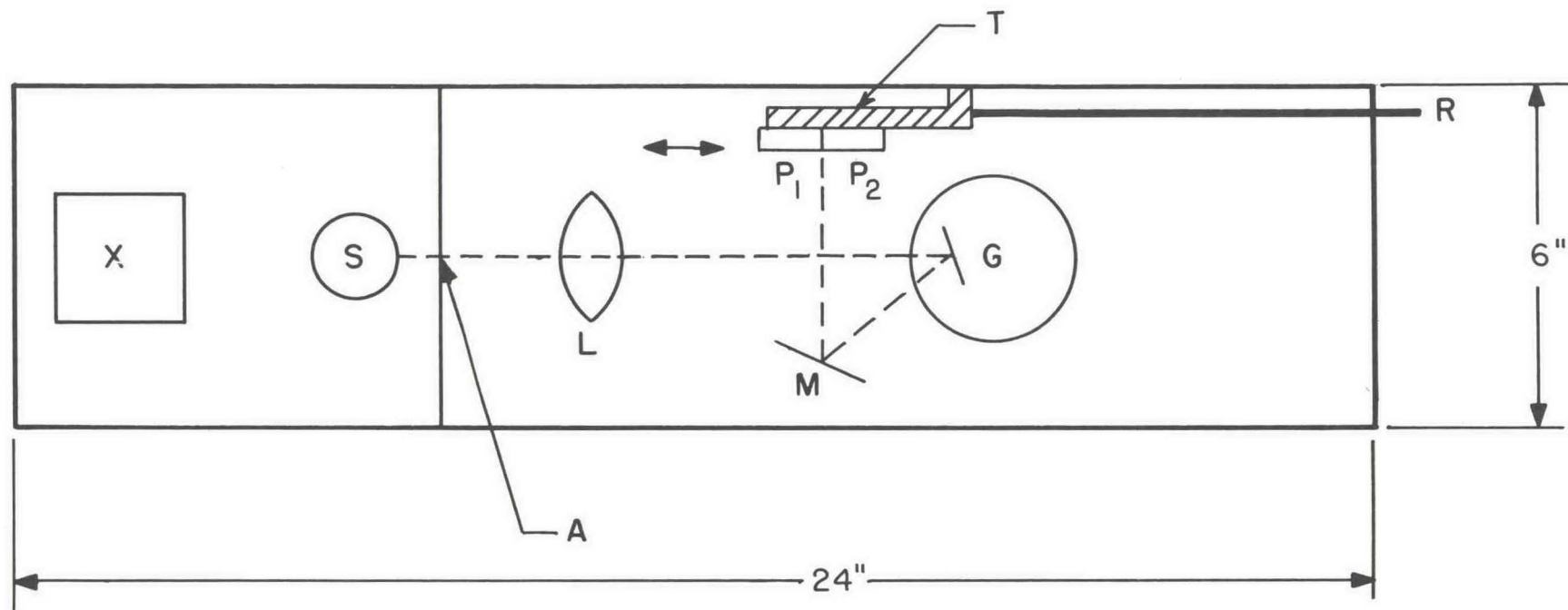


FIG. 2-2 GALVANOMETER AMPLIFIER.

by three pads of 1/4 inch thick rubber under the leveling screws. The entire unit rested on a piece of 3/4 inch thick steel plate supported by a heavy 2' x 2' table. The latter was insulated from the floor by a piece of sponge rubber 1 inch thick and one yard square. These precautions were necessary to eliminate the sensitivity of the system to vibrations in the floor caused by normal building activity.

The primary galvanometer, G, was a Leeds and Northrup type HS unit with a voltage sensitivity of  $1.8 \times 10^{-7}$  volts/mm for 1 meter path length. The optical path length in the galvanometer amplifier was about .3 meter so the sensitivity of the primary system is approximately  $60 \times 10^{-8}$  volts input/mm deflection at the photocells. The sensitivity of the entire system, as measured by using a voltage divider to give an input of  $10^{-7}$  volts and noting the secondary galvanometer deflection, is approximately  $10^{-8}$  volts/mm. The gain of the system is approximately 60. The secondary galvanometer was a Leeds and Northrup 2430G.

The detection system could have been made more sensitive by improving the optical system. Galvanometer amplifiers have been made with gains of 2000-3000 [4]. Such gain is difficult to use, because of attendant drift, and negative feedback is often used to reduce the gain and increase the stability. The sensitivity we achieved using a simple optical system without negative feedback was adequate and no improvements were made. We considered the galvanometer amplifier preferable to commercially available chopper amplifiers, which had a noise level of .03 microvolt and were moderately expensive.

The magnet was of laboratory design, with 7 inch pole pieces and a 2 inch gap. The power supply was unregulated, using selenium rectifiers in a bridge circuit. The maximum field available was 8750 gauss. The magnet was calibrated by proton resonance, but the field was set by adjusting the current measured by a Weston Model 430 1/4 percent accuracy ammeter.

The compensator is a loop of wire with an enclosed area of about one square inch mounted on a formica rod and placed in the magnetic field. The coil can be rotated so that the enclosed flux varies. Small variations in

magnetic field, caused by current fluctuations, induce varying voltages in the loop formed by the Hall leads and the sample. The compensator coil, connected in series with the Hall leads, is rotated until the voltage induced in it exactly cancels that induced in the sample loop and the drift disappears. The magnitude of the field fluctuations, as measured using a search coil and the galvanometer amplifier, was about 4 gauss at a field of 3700 gauss.

These field variations of approximately .1 percent would not cause measurable variations in the Hall voltage. On the other hand, the voltages induced in the Hall loop are quite measurable; they are of the order of .1 microvolt. The compensator eliminated the effect of the field fluctuations without actually regulating the power supply. Slow, steady drifts of magnetic field can change the Hall voltage but can be detected by monitoring the magnet current.

#### 4. Spurious voltages.

Low level Hall voltage measurements are made difficult by thermoelectric and thermomagnetic effects which can produce spurious voltages. Fortunately, most of these effects were not of concern to us, as long as they did not change in the time required to take a reading. The voltage measured by the potentiometer is

$$V = V_R + V_H + V(H) + V(H^2) + V_S, \quad (\text{II-2})$$

where

$V_R$  - voltage due to the IR drop between Hall probes

$V_H$  - Hall voltage

$V(H)$  - all other voltages linear in H

$V(H^2)$  - all voltages quadratic in H

$V_S$  - spurious voltages which are independent of H

Calling the voltage produced with the field in one direction  $V_1$  and that with the field reversed  $V_2$  we have

$$|V_1 - V_2| = |2V_H + 2V(H)| \quad (\text{II-3})$$

provided we have made the measurements so quickly that  $V_R$  and  $V_S$  have not changed.

Table 2-1 defines three thermomagnetic effects;  $\Delta T$  and  $V$  refer to the amount that the temperature of the potential at point A in Fig. 1-1 is greater than that at point B. The Ettingshausen effect is the transverse temperature gradient which occurs when we have a longitudinal current and a transverse magnetic field; it is the thermal analogy of the Hall effect. The Nernst effect is the transverse voltage produced when there is a temperature gradient along the sample and a magnetic field perpendicular to it. The Righi-Leduc effect is the transverse thermal gradient caused by the same conditions. The effects are evaluated for the values of field, current, and dimensions corresponding to our experiment. The value of  $dT/dx$  used,  $1^\circ \text{C/cm}$ , is almost certainly too high, as the mass of the bomb surrounding the sample acts as a constant temperature bath. As the Ettingshausen and Righi-Leduc coefficients are not known for the alkalis, we estimate the effect by using the value for copper [5]. These coefficients are probably smaller in the alkalis, where the Fermi surface is more nearly spherical than in copper. The thermoelectric power of a potassium-steel thermocouple is 22 microvolts/ $^\circ \text{C}$ . [6]; hence the voltage due to a Righi-Leduc temperature of  $1.4 \times 10^{-3} \text{ }^\circ \text{C}$  is .03 microvolt. For a more reasonable value of  $dT/dx$  we can ignore the thermomagnetic effects.

The Nernst and Righi-Leduc effects are usually eliminated by reversing the sample current and making a measurement before the temperature gradient can reverse sign. This requires a reversing switch in the input to the potentiometer as  $V_R$ , the dominant term in  $V$ , changes sign. Since such a reversing switch could introduce thermoelectric voltages, we decided to do the measurement without current reversal.

Throughout the measurements we tried to maintain a precision of 1 percent on an individual voltage measurement. This figure was dictated to a large degree by the potentiometer, which was specified free of thermal voltages greater than .01 microvolt. Since two readings were needed for each value of  $2 V_H$  obtained, this voltage was obtained within .02 microvolt, or to a precision of about 1 percent for typical values of  $2 V_H$ .

We can estimate the effect of the various parts of the system on the precision of the measurement. The potentiometer, as mentioned above, may contribute thermal voltages of .01 microvolt. Most of these probably stay constant over short periods of time, with the exception of the emf. . . due to the reversing switch, which may change each time the key is pressed.

The magnet current can be set to 1/3 percent. A regulated power supply was not used, as frequent checking of the magnet current minimized the effect of current drifts and allowed us to achieve the desired precision.

Successive readings of  $V_H + IR$  at constant pressure varied by amounts ranging from 1 part in 500 to 1 part in 5000. Since the IR drop is of the order of 50 microvolts, this corresponds to changes of several hundredths of a microvolt. This change is too large to be due to magnetic field variations and is due either to sample current fluctuations or to thermal voltages caused by variations of sample temperature. We did not isolate the cause of these changes but minimized their effect by taking pairs of voltage readings rapidly. These drifts were the most important limitation on the precision of the individual Hall voltage measurements.

Slow, visible, oxidation of the sample sometimes occurred. Such oxidation would decrease the thickness of the sample and cause the atmospheric pressure Hall voltage to increase with time, as was observed. Such oxidation during a run can cause hysteresis in the  $V_H$  vs. pressure curves, reducing their precision. We found we could obtain some runs with a hysteresis of less than 1 percent.

On successive runs of the same sample the normalized Hall voltages at fixed pressure generally differed by less than 2 percent. In most cases, with the exception of potassium, the reproducibility from sample to sample was about the same as from run to run; specific comments on each metal are included in Sec. III. Since a good run with 1 percent precision on individual values of  $V_H$  defined a curve to better than 1 percent, the ultimate limit on the precision of the measurements came from the presence of some hysteresis in most runs and from the variation between samples mentioned above.

HP6

Ettingshausen Effect

$$\Delta T = \frac{\text{PHI}}{t}$$

$$\text{Cu; } P = -1.6 \times 10^{-10} \frac{\text{°C-cm}}{\text{amp-gauss}}$$

Nernst Effect

$$V = QHb \frac{dT}{dx}$$

$$\text{Li; } Q = 1.6 \times 10^{-2} \frac{\text{volts}}{\text{gauss} \cdot \text{°C}}$$

Righi-Leduc Effect

$$\Delta T = SHb \frac{dT}{dx}$$

$$\text{Cu; } S = -2.3 \times 10^{-7} (\text{gauss})^{-1}$$

---

For  $I = 3$  amperes,  $B = 6000$  gauss,  $t = .05$  cm,  $b = 1$  cm,  $d = 4$  cm,  $\frac{dT}{dx} = \frac{1\text{°C}}{\text{cm}}$

---

$$\Delta T = -5 \times 10^{-5} \text{°C}$$

$$V = 10^{-9} \text{ volts}$$

$$\Delta T = -1.4 \times 10^{-3} \text{°C}$$

Table 2-1

The Ettingshausen, Nernst and Righi-Leduc Effects

### B. High Pressure Apparatus

The high pressure system is shown schematically in Fig. 2-3. The hydraulic ram and the intensifier were obtained from Professor Bridgman. A hand pump is used to force oil into the intensifier cylinder. The intensifier compresses the pressure transmitting fluid, pentane, in the low pressure, high compressibility region. After a pressure of about  $1500 \text{ kg/cm}^2$  is attained, the large hydraulic press is used to move the piston and piston head down the upper cylinder, compressing the pentane further. After the piston head has moved about  $1/2$  inch it is below the intensifier connection and the latter is no longer subject to high pressure.

The upper cylinder is connected to the beryllium copper bomb, suspended between the magnet pole pieces, by  $1/8$ " O.D.  $\times$   $.020$ " I.D., stainless steel tubing. The bomb, Fig. 2-4, was used at pressures up to  $15,000 \text{ kg/cm}^2$ . It was eventually destroyed in an explosion and replaced by one of identical design. We believe pentane under high pressure leaked past the terminal plug and remained temporarily sealed in by the drive plug. Pressure was transmitted to the thin walled ( $3/8$ ") portion of the bomb and ruptured it.

The sealing arrangement at both ends of the bomb is shown in Fig. 2-5. Initially we were able to seal both ends of the bomb using only lead and aluminum washers; eventually the packing hole belled out and we needed to add a cold rolled steel washer to seal reliably.

The terminal plug used was a modification of the design normally used in this laboratory. Because of the high sample currents we needed, larger cones and wires were used. The Bridgman tubing seal at the other end of the bomb needed to be almost completely within the  $.625$  inch packing hole to prevent it from mushrooming or shattering under pressure. Detailed descriptions of the high pressure techniques used may be found in the literature [7,8].

The pressure was determined by measuring the change of resistance of a manganin coil on a bridge [9]. The gauge coil was calibrated against another manganin coil which served as a laboratory standard. At the conclusion of the measurements we checked our gauge against the mercury transition

at  $7640 \text{ kg/cm}^2$  (at  $0^\circ\text{C}$ ) and found a difference of  $90 \text{ kg/cm}^2$ . This error may be due to the fact that the manganin gauge was in the apparatus when the beryllium-copper bomb exploded and the resulting rapid pressure change may have altered the properties of the manganin slightly. The pressure measurements are therefore accurate to better than 1.5 percent. The techniques involved in the mercury calibration have been described by Bridgman [ 10].

### C. Sample Preparation

The alkali metals are highly reactive and very compressible; these characteristics made it difficult to prepare suitable samples of the alkalis. Since the alkalis react rapidly with oxygen, whenever possible, electrical measurements on them have been performed by enclosing them in glass. Hall effect samples have been made by forming thin molds of glass or quartz containing platinum electrodes and distilling the alkali metal into them [ 11, 12]. This procedure protects the surface of the sample and allows the metal to be purified by distillation. It is not, however, useful for pressure work. The glass constrains the alkali and prevents it from contracting freely under pressure. The pressure in the sample is not necessarily hydrostatic. Finally, pressure can break the contacts to the thin platinum electrodes.

Bridgman, in his work on the pressure dependence of the resistance of the alkali metals was able to make wires of alkalis and connections to them by means of spring clips [ 13]. This leaves the sample free to contract under pressure. The contacts obtained are not always reliable and may open under pressure. This technique is not useful for Hall measurements where the mounting must be such as to maintain the sample's shape and orientation under pressure. Furthermore, some attempts to make samples of this kind show it is extremely difficult to attach four spring clip contacts to a sample without tearing it.

The sample preparation method finally adopted represented several compromises. In order to expose the metal to the pressure fluid we had to accept some surface oxidation. In order to make reliable contacts and to keep the sample orientation fixed it was necessary to constrain the sample somewhat.

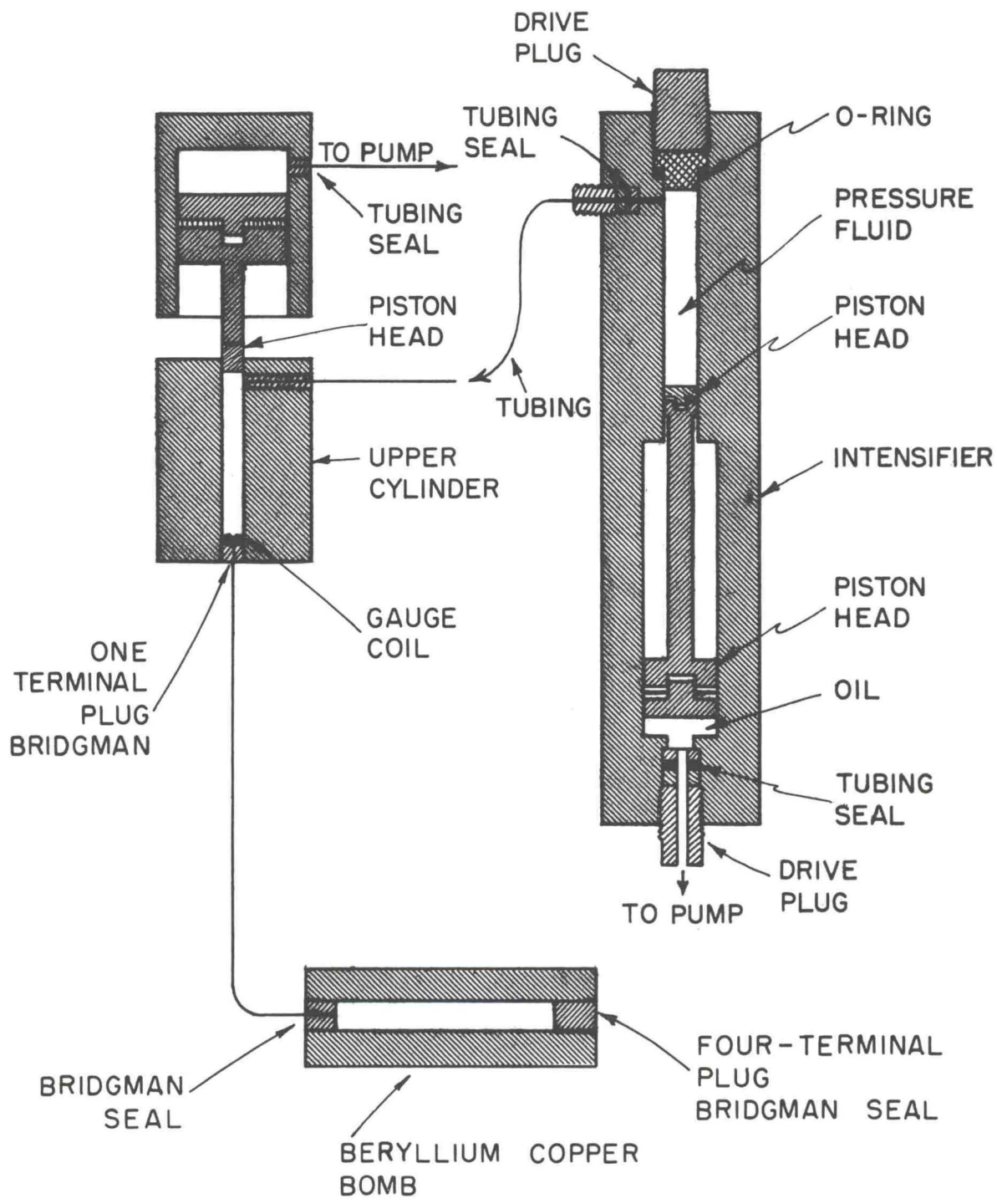
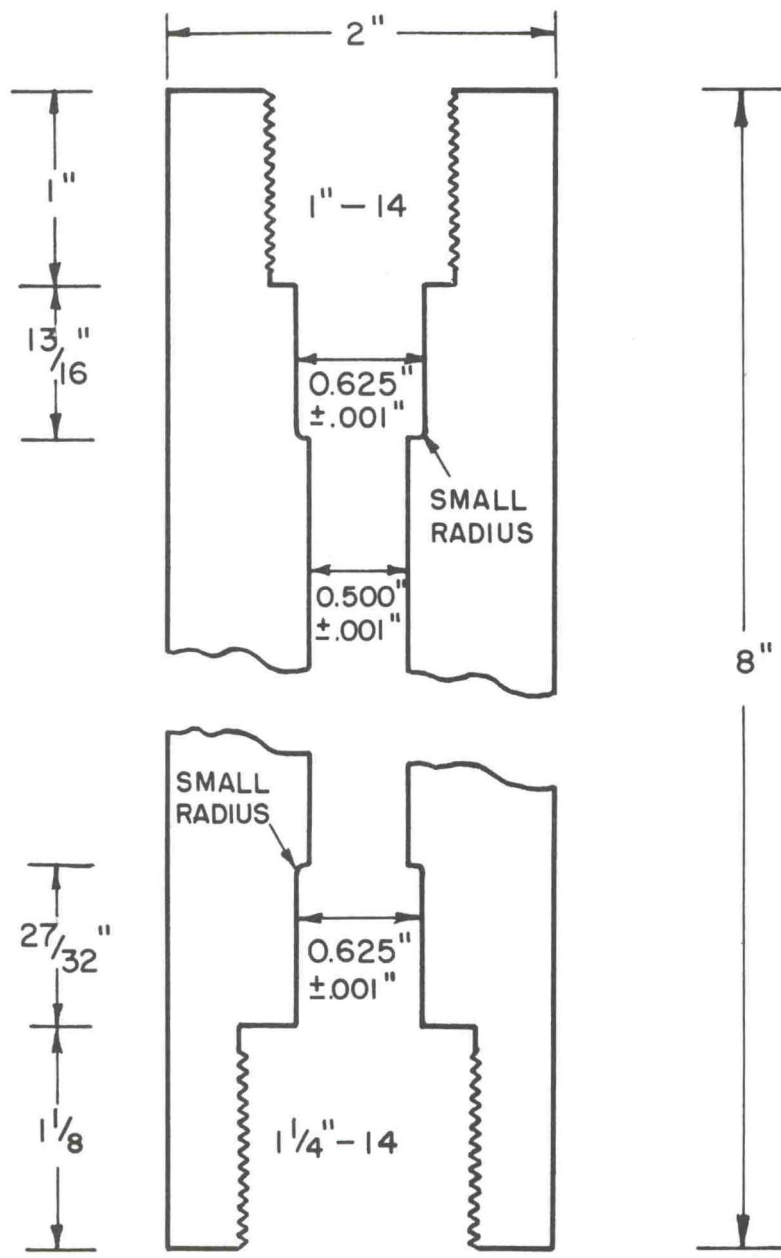


FIG. 2-3 SCHEMATIC DIAGRAM OF 15,000 kg/cm<sup>2</sup> HIGH PRESSURE APPARATUS



Be Cu ROCKWELL C 39

FIG. 2-4 BERYLLIUM COPPER BOMB

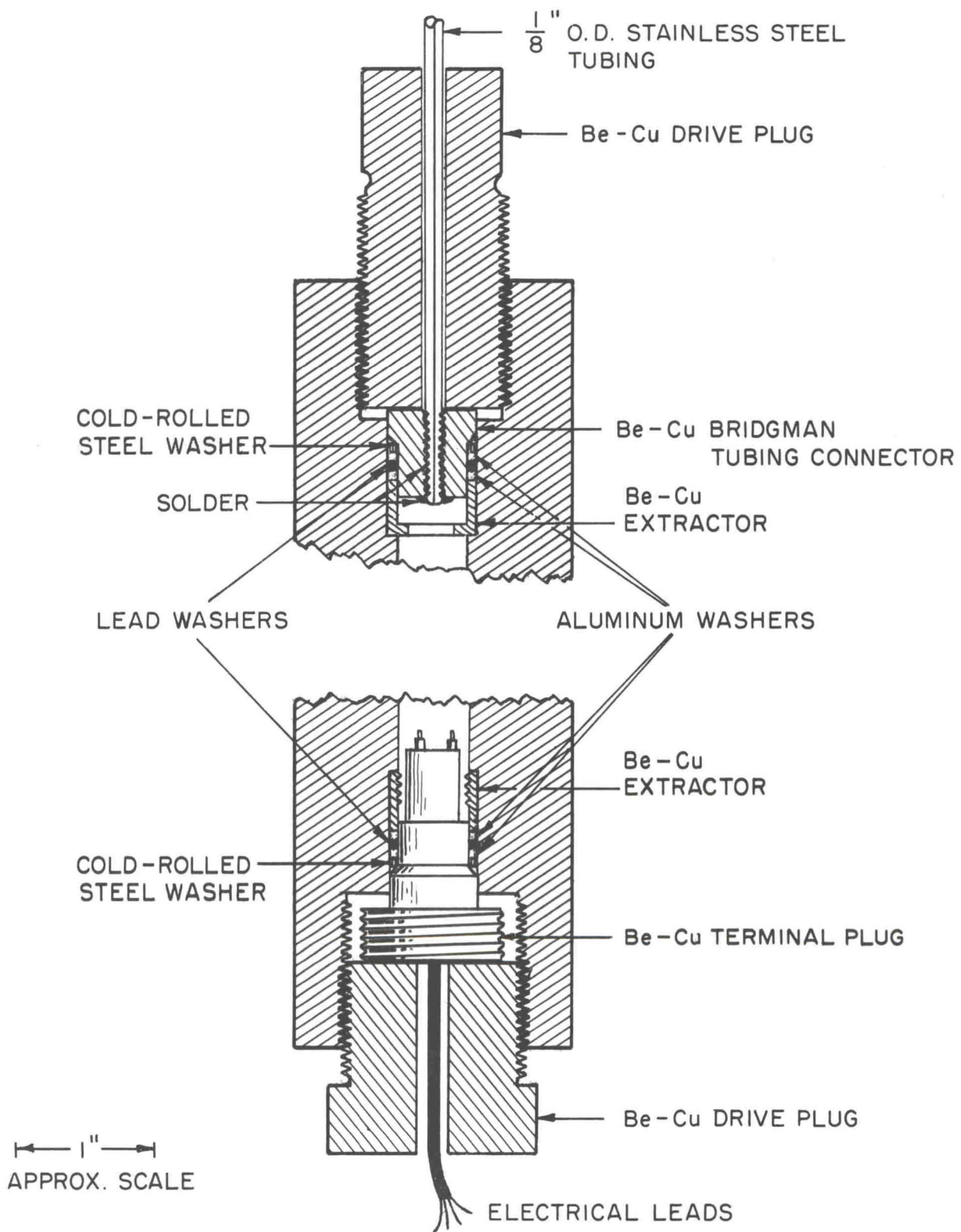


FIG. 2-5 BERYLLIUM-COPPER BOMB-SEALING DETAIL

The sample holder that was finally used is shown in Fig. 2-6. The holder is designed to push onto a four-terminal plug. The current contacts are pieces of stainless steel which fit over either end of the alkali sample and are tightened down with screws. This construction assures a large area, low resistance contact and reduces the possibility of heating at the contacts. The Hall probes are an integral part of the sample and have a width of about  $1/16$  inch. They are about  $1/8$  inch long and terminate in "ears" about  $1/8$  inch wide and  $3/4$  inch long. There are two  $3/32$  inch diameter stainless steel pins imbedded in the formica body of the sample holder; part of the formica and of the stainless steel pins has been cut away to provide a flat metal contact on either side of the holder. The "ears" of the sample are bent over the holder and clamped to these contacts by the two stainless steel plates. Thus a large area contact is achieved for the Hall leads even though the actual probes remain thin. The groove milled in the formica holder was used for forming samples of rubidium and cesium. These metals were molded till they filled the groove and then scraped until the surface was flush with the sample holder. This gave a reasonably uniform sample thickness.

In the case of lithium, sodium, and potassium, the thickness of the sheets of alkali was measured by a  $.001$  inch dial comparator gauge. Samples varied in thickness by about  $\pm .001$  inch over their length. Since most samples were over  $.010$  inch thick, the samples were thus uniform to  $\pm 10$  percent. In the case of rubidium and cesium, which were formed directly on the sample holder, the thickness was not measured.

We were primarily interested in the relative changes of the Hall voltage under pressure, rather than its absolute value. However, the length to width ratio in our case, approximately 3, is such that the difference between our measured voltage and the true Hall voltage is less than 1 percent. This one percent correction is computed for a geometry applicable to a semiconductor; namely, the ends of the samples are equipotentials and the Hall voltage electrodes are point probes [14]. Neither of these conditions are exactly fulfilled in our case; in particular, the finite size of the Hall probes can distort the current flow lines so that they are no longer parallel to the long side of the sample.

Non-uniformity in the thickness of the sample introduces uncertainty in the absolute value of the Hall constant, but as long as the sample geometry is unchanged under hydrostatic pressure the relative change in the Hall constant is unaffected. The sample should be flat and without "wrinkles"; for the latter can give a magnetic field normal to wrinkled portions of the surface that is less than the applied field. If such wrinkled portions straighten out under pressure, the orientation of portions of the sample is effectively changed and a spurious pressure dependence would result. Such behavior would probably make itself evident through hysteresis in the Hall voltage vs. pressure curves.

The samples were formed and mounted in a bath of Deo Base<sup>†</sup>, a light mineral oil. Rubber gloves were used in order to avoid contaminating the Deo Base with moisture. This technique was adopted after some attempts to make samples in a dry box filled with nitrogen gas. The metal surfaces remained cleaner and assembling the sample holder was easier in the Deo Base bath. In the case of lithium, sodium, and potassium a slice of metal was cut from a chunk of alkali. It was rolled into a sheet about .020 inch thick, bent over the sample holder and contacts attached. The sample was then trimmed to form the Hall contacts and the "ears" shown in Fig. II-6. The sample holder was next pushed onto the four-terminal plug and the entire unit was quickly transferred to the bomb where the pentane prevented oxidation. The film of mineral oil remaining on the sample protected it from oxidation during the transfer.

Each of the alkali metals presented some special problems of handling. Lithium was the hardest metal and was difficult to cut and roll. Furthermore, since lithium did not deform readily, it was hard to get the stainless steel current contacts to dig into the metal and form large area, low resistance contacts. This was remedied by placing a piece of sodium between the lithium and the stainless steel contact; the soft sodium made good contact to both the lithium and the stainless steel.

-----  
<sup>†</sup> Available from Howe and French, Boston, Mass.

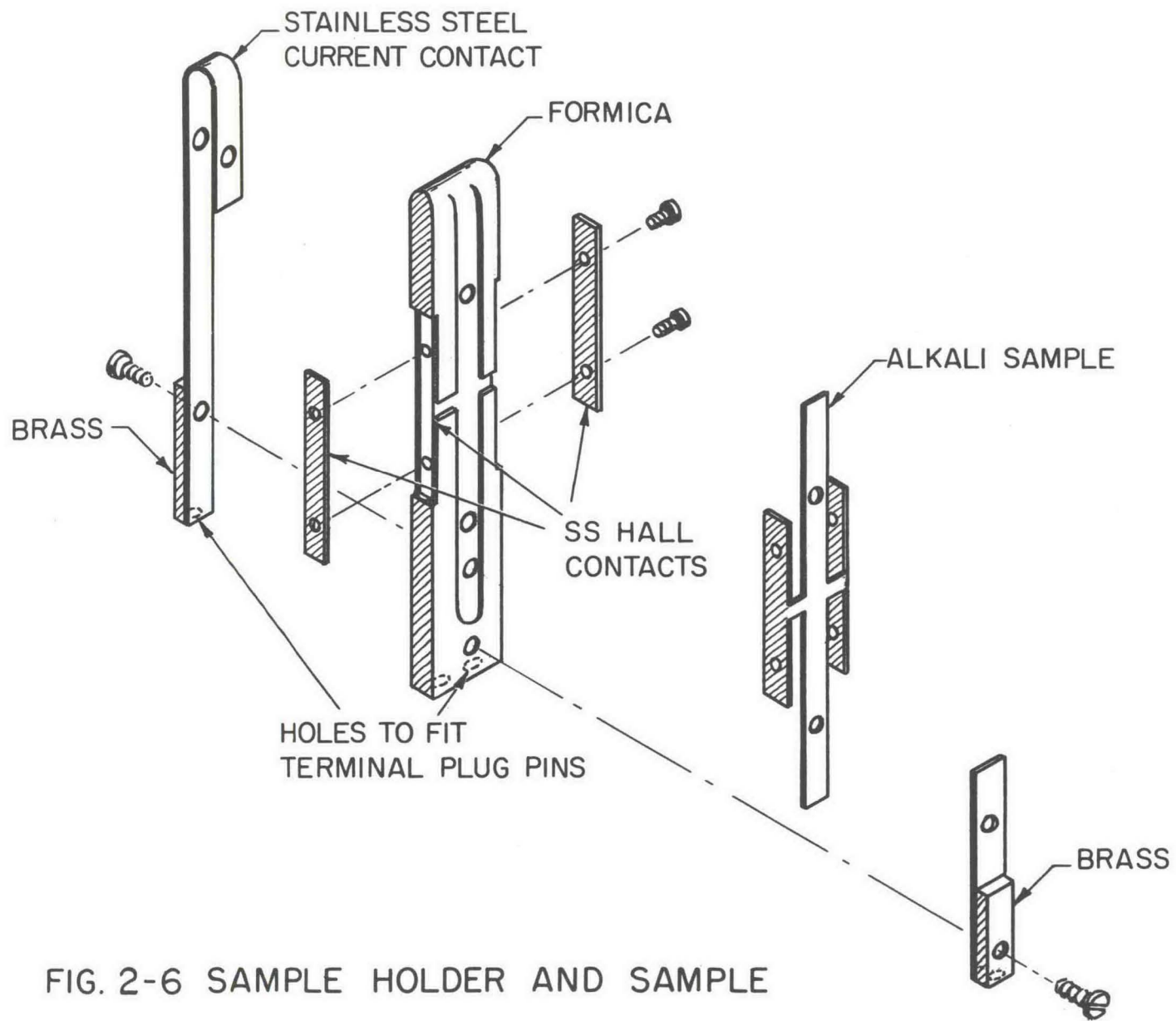


FIG. 2-6 SAMPLE HOLDER AND SAMPLE

Sodium and potassium were not difficult to handle under oil. After the Deo Base had been purified by reacting alkali chips with it, reasonably clean surfaces could be maintained. These metals, as well as lithium, were soft enough to allow sheets of thickness from .007 inch to .035 inch to be made using a small adjustable set of rollers.

The lithium and potassium were cleaned by heating to above the melting point under forepump vacuum. The sodium was cleaned by melting it under oil. Chunks of the metal were placed in a small stainless steel boat about 1/2" by 1/2" by 3" long. Inclusions of oxide or dirt rose to the top of the ingot and could be removed. Better purification using distillation was not considered necessary since the metal surface would suffer some oxidation as soon as it was placed in oil. We were concerned with producing samples that were macroscopically homogeneous, but not necessarily pure in the sense of having low residual resistance. As long as the impurity scattering was small compared with the lattice scattering at room temperature, the sample was "pure" as far as we were concerned. The lithium was obtained from Fairmount Chemical Co., the sodium from Merck and Co., and the potassium from Mallinckrodt Chemical Co.

Rubidium and cesium were considerably more difficult to handle than the other alkalis. These metals, sealed in one gram glass vials, were obtained from A. D. MacKay Co. and Fairmount Chemical Co. We initially tried to remove the metal from the vials by placing them in a heater and letting the molten liquid flow out under oil. This was not satisfactory as we obtained several small globules of metal, each of which was too small to make a sample. If we pressed several globules together the resulting sample would have an oxide film inside it.

These metals oxidized rapidly even when kept under oil at room temperature. Furthermore, the oxide was soluble in the metal [15]. As oxide formed, it dissolved in the pure metal forming an alloy which was liquid at room temperature.

The final solution was to make the rubidium and cesium samples in chilled oil. The tray containing the Deo Base was placed on a block of polyfoam which had been hollowed out and filled with dry ice. The oil in the

tray was maintained at a temperature of  $0^{\circ}\text{C} - 5^{\circ}\text{C}$ . Both the Deo Base and the pressure transmitting fluid, pentane, were purified by reacting them with globules of sodium-potassium alloy, a liquid. The metal was removed from the glass vial by pushing it out with a small formica rod. The slugs of metal obtained were molded by hand, using gloves, to approximately the shape and size needed, placed on the sample holder and contacts made while the metal surface was still clean. The surface generally had a dull silver-gray color, indicating some oxidation. Unoxidized rubidium and cesium have a bright silver color, while metal immersed in uncleaned oil would become black. The sample surface was further protected by placing some silicone stopcock grease on it and then covering it with a sheet of .003 inch Mylar plastic, the latter held down by the screws which tightened the current contacts. The sample was transferred to the bomb in the same way as the other alkalis.

#### D. Measurements as a Function of Temperature

The temperature measurements on lithium were made using a glass dewar with 2 inch O.D. and 1-1/2 inch I.D. and the unit shown in Fig. 2-7. The unit fitted inside the dewar and a seal was made at the top using a rubber gasket made from a plurostopper<sup>†</sup>. The region above the liquid nitrogen and around the glass tube formed a closed chamber which could be connected to a mechanical pump. By pumping on the liquid nitrogen it could be cooled below its freezing temperature, to about  $-216^{\circ}\text{C}$ . The region above the glass tube was sealed using the brass plate and an "O" ring. It was pumped out and filled with helium exchange gas. A formica rod, one end of which was made into a sample holder similar to the pressure one, screwed onto the top brass plate. A heater, consisting of a piece of copper tubing wound with resistance wire, fitted around the sample holder. The temperature was measured using a copper-constantan thermocouple located at the sample. Temperatures below  $-196^{\circ}\text{C}$  were measured by calibrating our thermocouple at the nitrogen point and using the value  $dE/dT = 16$  microvolts/ $^{\circ}\text{C}$  given by Scott [16] for the thermoelectric power at  $-196^{\circ}\text{C}$ . The electrical connections were

-----  
<sup>†</sup> Available from Bethlehem Apparatus Co., Hellertown, Penn.

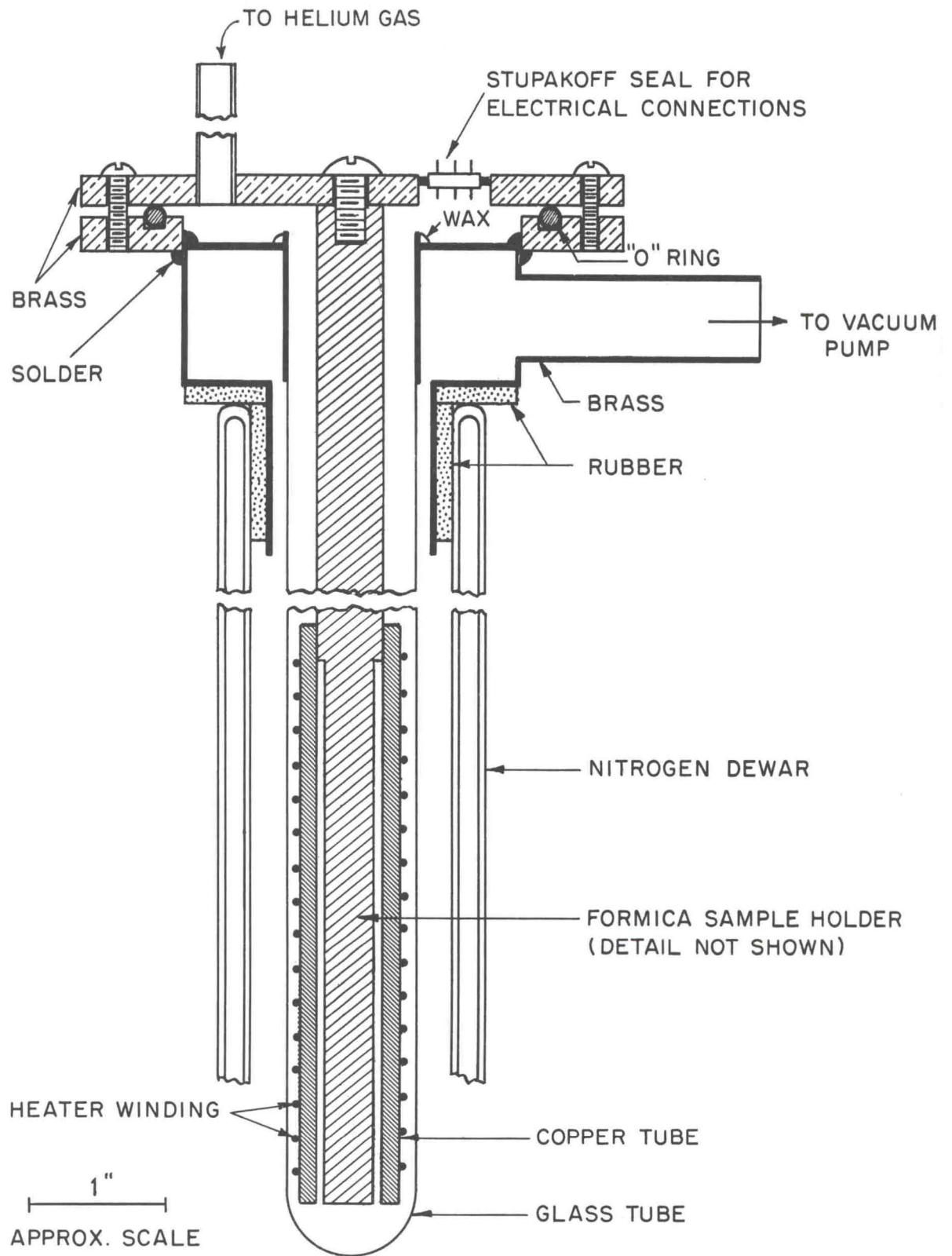


FIG. 2-7 LOW TEMPERATURE MEASUREMENT APPARATUS

brought out through a Stupakoff<sup>†</sup> seal; the thermocouple and Hall voltage leads were brought right through the pins and sealed in with wax, avoiding extra junctions.

Below liquid nitrogen temperature, an equilibrium temperature was obtained by allowing the mechanical pump to pump continuously on solid nitrogen. No attempt was made to maintain a vapor pressure higher than that obtained by continuous pumping, i. e., to obtain intermediate temperatures. Temperatures above liquid nitrogen temperature were obtained by setting the current through the heater to a fixed value and waiting for thermal equilibrium.

Because the Hall constant of sodium, potassium, rubidium, and cesium did not vary significantly between room and nitrogen temperatures, no attempt was made to measure it at intermediate temperatures. Sodium and potassium were measured by immersing the formica sample holder rod directly into the dewar filled with liquid nitrogen. Cesium and rubidium were measured using the same sample holder and terminal plug as in the pressure experiments. A piece of formica tube, closed at one end, was filled with mineral oil and the sample holder enclosed in it. This served to protect these highly reactive metals from accidental exposure to air.

-----

<sup>†</sup> Available from Stupakoff Ceramic and Mfg. Co., Latmore, Penn.

II. References

1. J. M. Lavine, Phys. Rev. 114, 482 (1959).
2. J. M. Lavine, Technical Report No. 225, Cruft Laboratory, Harvard University (1956).
3. Bulletin 270, p. 4, Rubicon Co., Philadelphia, Pa.
4. J. S. Preston, J. Sci. Instr. 23, 173 (1946).
5. International Critical Tables VI, McGraw-Hill Co., New York, p. 420, (1929).
6. Handbook of Chemistry and Physics, 35th Edition, Chemical Rubber Publishing Co., Cleveland, p. 2380 (1953).
7. P. W. Bridgman, The Physics of High Pressures, G. Bell and Sons, Ltd., London (1949).
8. W. Paul, G. B. Benedek, and D. M. Warschauer, Rev. Sci. Instr. 30, 874 (1959).
9. D. M. Warschauer and William Paul, Rev. Sci. Instr. 29, 675 (1958).
10. P. W. Bridgman, Rev. Sci. Instr. 24, 400 (1953).
11. F. J. Studer and W. D. Williams, Phys. Rev. 47, 291 (1935).
12. E. Krautz, Z. Naturf. 5a, 13 (1950).
13. P. W. Bridgman, Proc. Amer. Acad. 72, 157 (1938).
14. Hans Lippman and Friedrich Kuhrt, Z. Naturf. 13a, 474 (1958).
15. P. W. Bridgman, Phys. Rev. 27, 68-86 (1926).
16. R. B. Scott, Temperature, Its Measurement and Control in Science and Industry, Reinhold Publishing Co., p. 210 (1941).

### III. Experimental Results

#### A. The Hall Voltage and $n^*$ vs. Pressure

The Hall effect data were taken by measuring the Hall voltage at fixed magnetic field (6310 gauss) and sample current (3 amperes) at approximately twelve points in the pressure range from 1 to 15,000 kg/cm<sup>2</sup>. Only one value of the magnetic field was used since our earlier ac measurements had verified the anticipated linear relation between  $V_H$  and field. Figure 3-1 shows a typical voltage vs. field curve, obtained on sodium by the ac method. The thickness of the samples ranged from .007 inch to .050 inch. No absolute values of the Hall constants will be plotted on the pressure curves because they would depend on a relatively inaccurate thickness measurement and because our prime interest was in relative changes of the Hall constant. The temperature was slightly below room temperature, because the bomb was in contact with the cooled magnet yoke.

Although the curves we present are for dc measurements, in some cases there are also data available from the earlier ac measurements. The ac data were obtained by measuring  $V_H$  vs. field at a fixed pressure and plotting the slope of this curve vs. pressure. These data are discussed where applicable. The scatter on the ac data is generally greater than in the dc case. Furthermore, there is always a question as to whether the ac data is affected by spurious voltages induced by sample vibrations; such vibrations would be damped by the increased viscosity of pentane under pressure and could give a pressure dependent voltage. Much of the ac data were obtained on samples that had not been cleaned by melting and outgassing under vacuum and contained inclusions of oxide or gas. The dc data are based on cleaned samples, as free of oxide and large inhomogeneities as we could produce.

The lithium data are from the two best runs (those with the least scatter) out of four. The curve for one of these runs is shown in Fig. 3-2. The two runs were on different samples and gave Hall voltage decreases of 1.4 percent and 1.5 percent in 10,000 kg/cm<sup>2</sup>. The slopes were obtained using a least squares fit.

If all four dc runs are considered, the average of the least square slopes gives a decrease of 1.9 percent in 10,000 kg/cm<sup>2</sup> with a root mean square deviation of .4 percent. The only ac data are based on measure-

ments on unclean material and on curves with more scatter. Seven runs on five different samples give an average decrease of 3.5 percent in  $10,000 \text{ kg/cm}^2$  with a root mean square deviation of .8 percent. The slopes of the individual curves were obtained from a straight line fitted by eye, rather than by least squares as in the case of the final dc data.

The sodium data are based on four runs on three different samples ranging in thickness from .007 inch to .026 inch. The average of the least square slopes is a decrease of 3.4 percent in  $10,000 \text{ kg/cm}^2$ . The root mean square of the deviations is .4 percent. A typical curve is shown in Fig. 3-3.

The ac data for cleaned sodium, based on three runs on two different samples, gives an average decrease of 3.3 percent in  $10,000 \text{ kg/cm}^2$  with an rms deviation of .5 percent. The data on uncleaned sodium, based on three runs, gives a 4.7 percent decrease with an rms deviation of .6 percent. The slopes in the ac case again come from visual fits.

The data for two potassium samples are shown in Fig. 3-4. Despite many runs the curves for different samples did not agree. The curves are chosen to indicate the difference between data obtained from different samples and the approximate range of the value of  $V_H$  at  $15,000 \text{ kg/cm}^2$ . A total of twelve runs on seven samples was performed. Since some of the curves were not linear, the percentage decrease in  $V_H$  at  $10,000 \text{ kg/cm}^2$  was used as a rather arbitrary way of characterizing them. The average decrease is 6.2 percent, with an rms deviation of 1.6 percent.

Twelve ac runs on seven samples of cleaned potassium yielded a decrease of 7.9 percent in  $10,000 \text{ kg/cm}^2$  with an rms deviation of 2.9 percent. The lack of reproducibility between different samples makes it impossible to compare meaningfully the ac and dc data, other than to say they are not in gross disagreement.

The ac measurements at one point seemed to indicate a correlation between the size of the pressure effect and sample thickness. Accumulation of more data did not support this correlation. In Fig. 3-5 we show the percentage decrease in  $V_H$  in  $10,000 \text{ kg/cm}^2$  vs. sample thickness for the twelve dc runs on potassium and for the four dc runs on sodium.

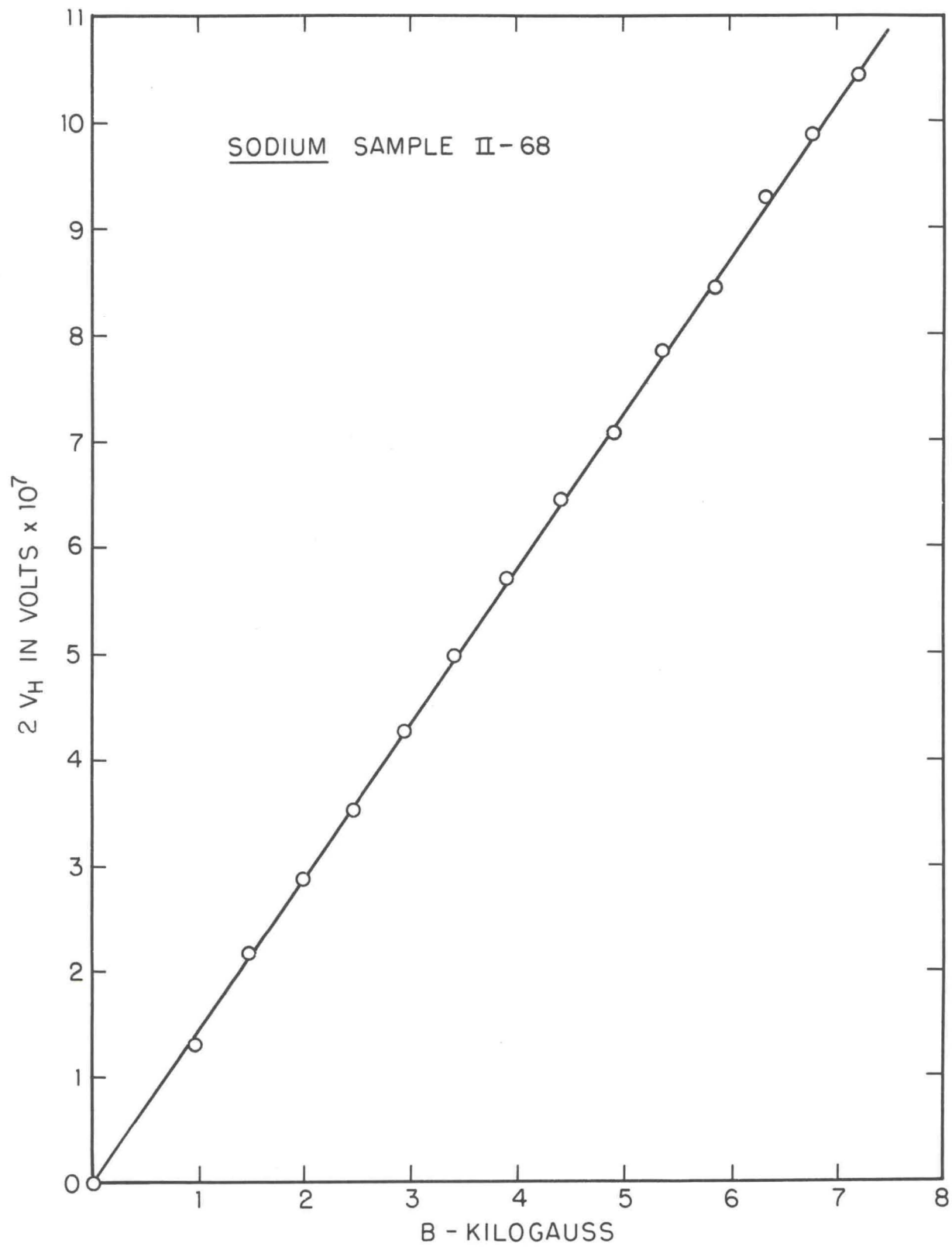


FIG. 3-1 HALL VOLTAGE x 2,  $2V_H$ , VS. MAGNETIC FIELD.  
A.C. MEASUREMENTS

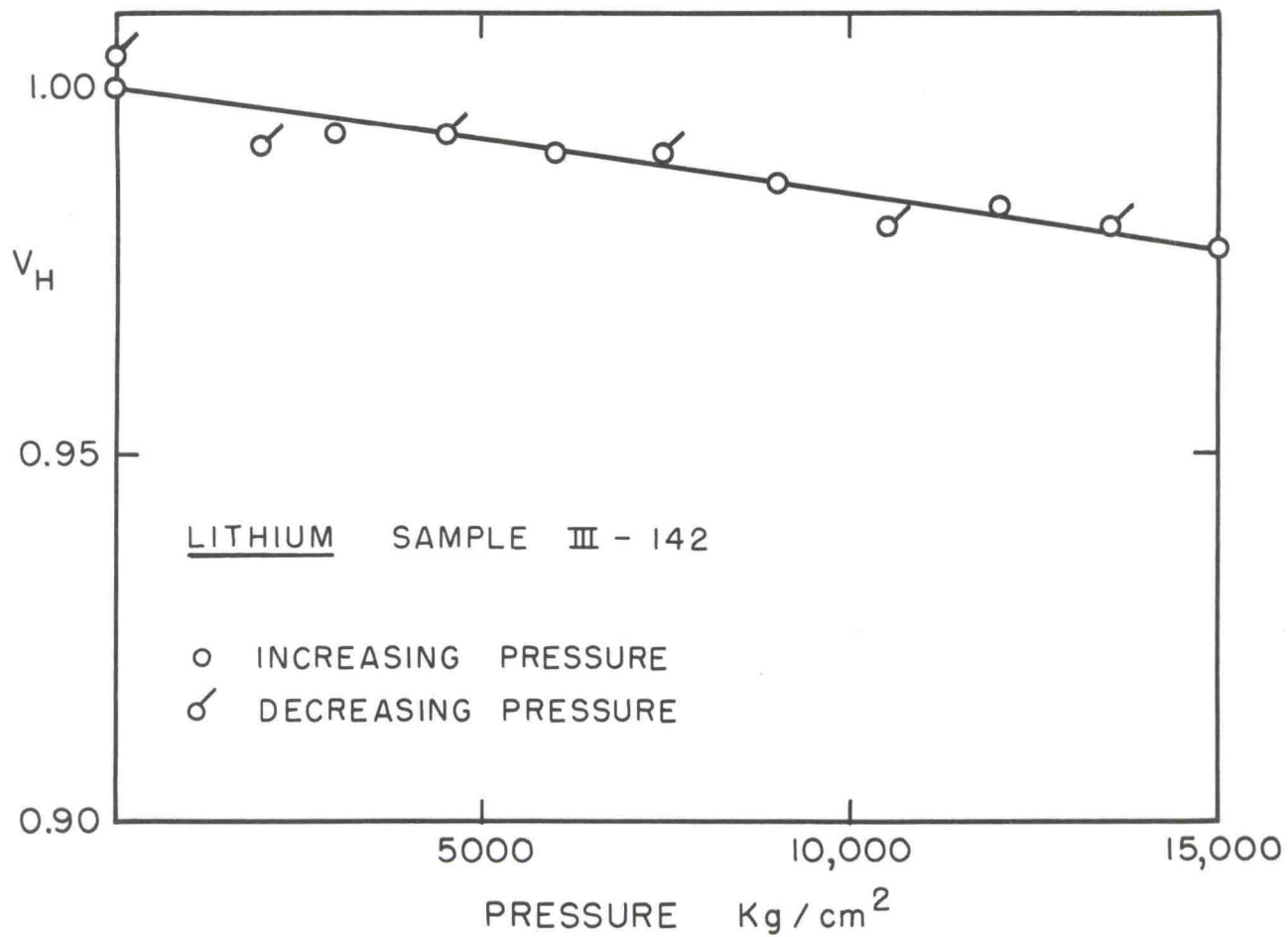


FIG. 3-2  $V_H$ , NORMALIZED HALL VOLTAGE VS. PRESSURE

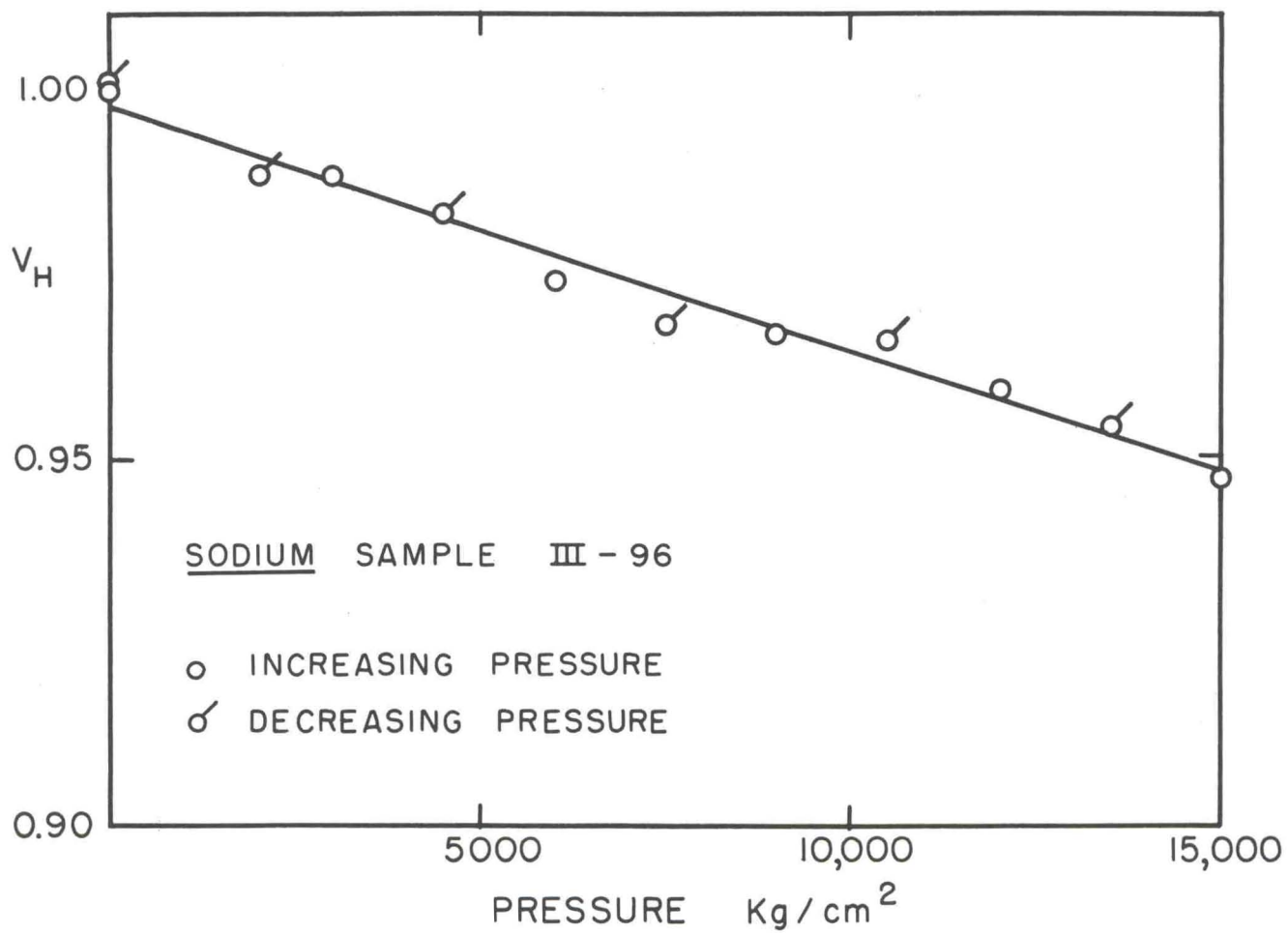


FIG. 3-3  $V_H$ , NORMALIZED HALL VOLTAGE VS. PRESSURE

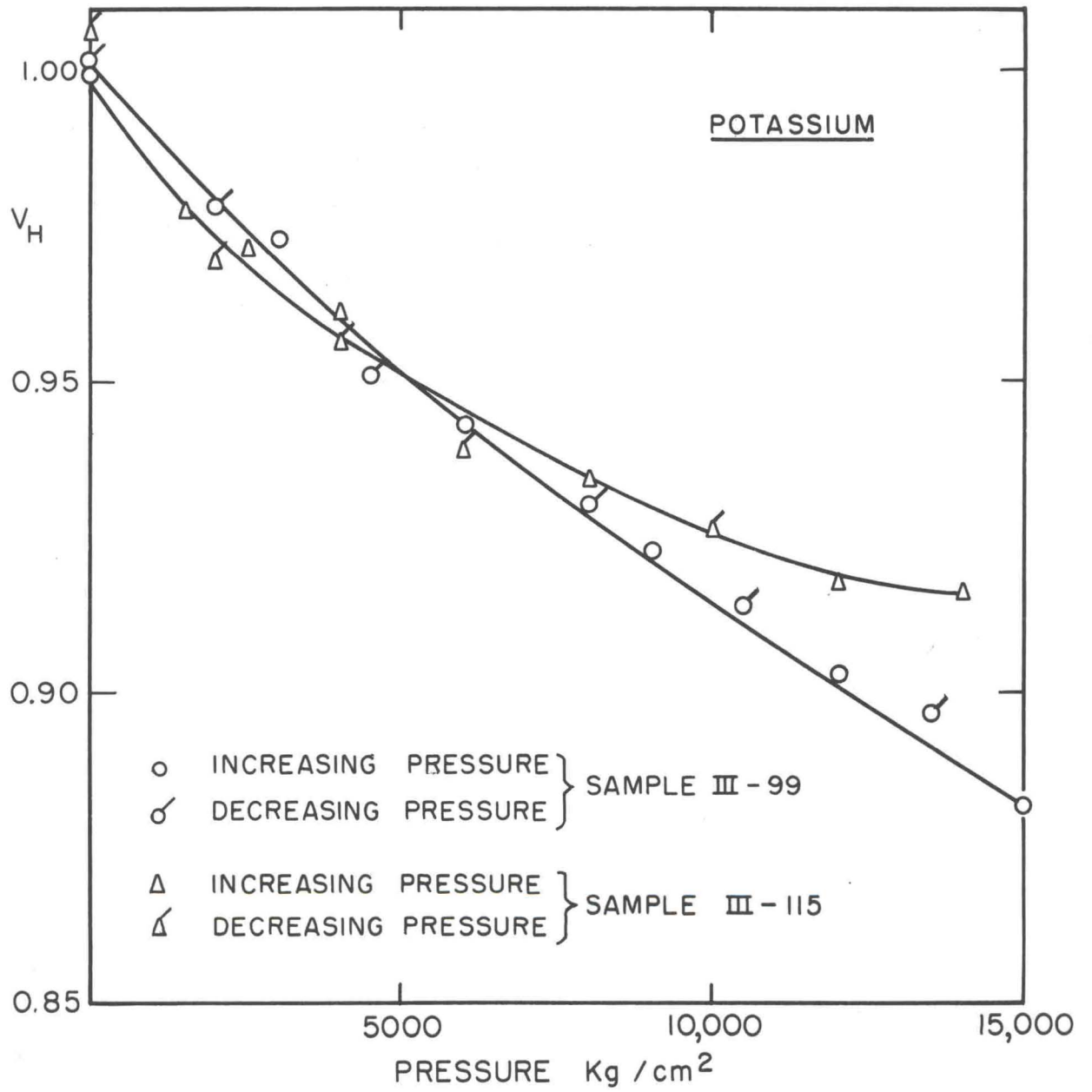


FIG. 3-4  $V_H$ , NORMALIZED HALL VOLTAGE VS. PRESSURE

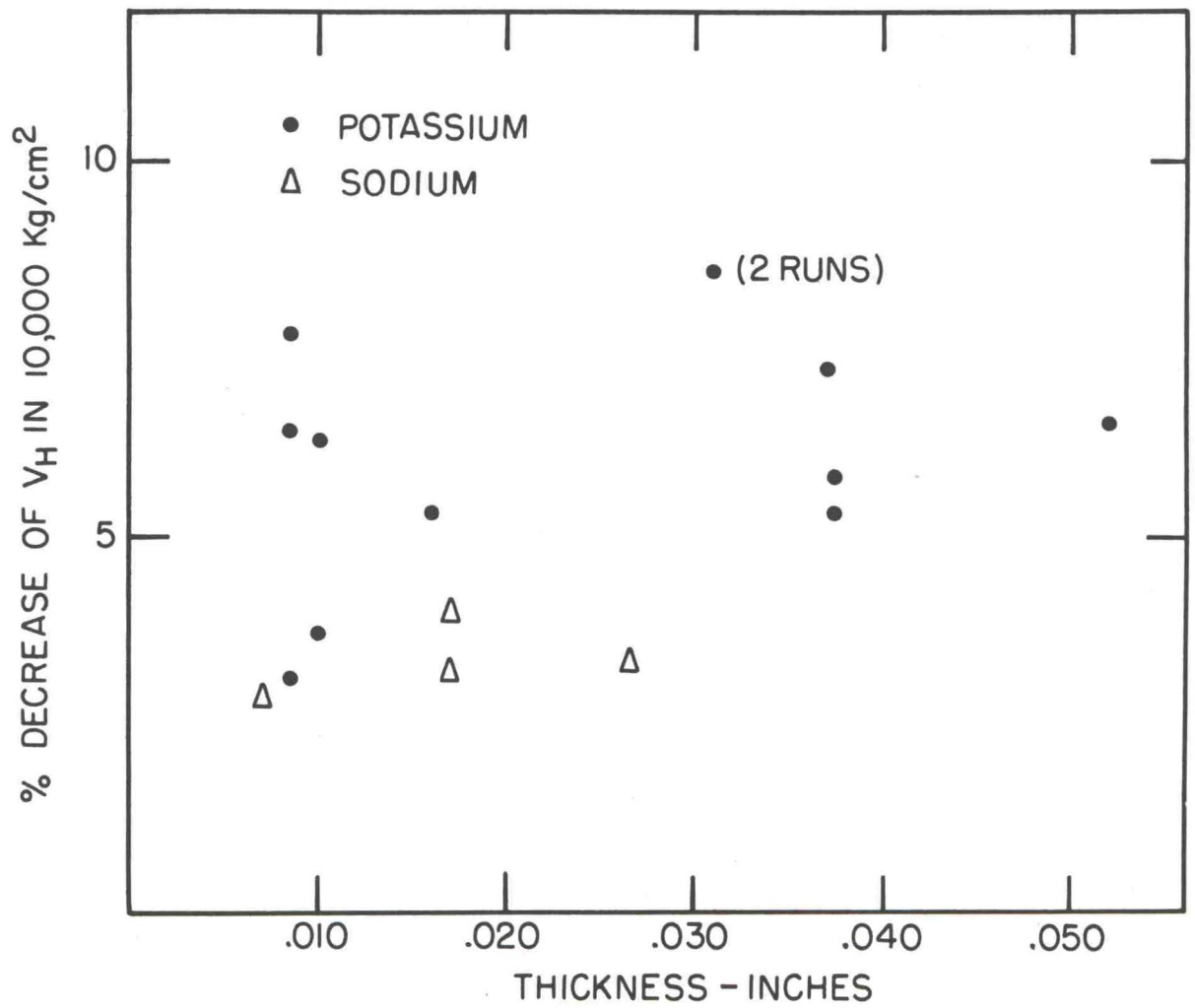


FIG. 3-5 DECREASE OF  $V_H$  IN 10,000 Kg/cm<sup>2</sup> VS. SAMPLE THICKNESS. D.C. MEASUREMENTS

Although the data on potassium were not as reproducible from sample to sample as the sodium data, and the decrease in  $V_H$  at a fixed pressure is not an entirely satisfactory way of describing the curve, we include these data because of the large number of runs and the wide range of thicknesses covered.

The resistance versus pressure curve for potassium was anomalous insofar as it consistently differed from the data of Bridgman [1]. Our value of .4 for the normalized resistance at  $15,000 \text{ kg/cm}^2$  is in sharp disagreement with Bridgman's value of .22. Figure 3-6 shows a typical curve of normalized resistance vs. pressure for potassium, as well as the data of Bridgman.

We suspected that our sample holder might be acting as a constraint on the compressible potassium and decided to repeat Bridgman's experiment, which used a free wire of potassium. We made a potassium wire by extruding the metal through a brass die and attached four Be-Cu contacts. Although difficulty with the contacts caused sample current fluctuations and made it impossible to get accurate curves, the value of the normalized resistance at  $15,000 \text{ kg/cm}^2$ , .4, was confirmed.

As the behavior of resistance versus pressure was the same for a free wire and for a sample mounted on our holder, we concluded that our sample holder was not constraining the specimens and that the Hall voltage data obtained with it were representative of free samples of alkalis. The fact that the rubidium resistance data, discussed below, are in substantial agreement with Bridgman's results even though rubidium is more compressible than potassium also indicates that the sample holder is not acting as a constraint.

Figure 3-7 shows a typical Hall voltage curve for rubidium. After sample preparation techniques had been revised so as to avoid working oxide into the metal, reproducibility was good. The final data are based on two samples used in a total of five runs; in four of these runs the decrease of  $V_H$  in  $15,000 \text{ kg/cm}^2$  was between 12 percent and 13 percent while in the fifth it was 9 percent. All the ac data on rubidium were taken before the sample preparation techniques had been improved and show the same lack of reproducibility as the early dc data.

Figure 3-8 shows a curve of normalized resistance vs. pressure for rubidium as well as the data of Bridgman for bare wires of this metal. The resistance data sometimes showed hysteresis, but the shape of the curve agrees with Bridgman's work. Many runs were made before we learned to make clean, one-piece, samples which gave reproducible Hall voltage data; the resistance data, on the other hand, were much less sensitive to the method of making the sample. Thirteen runs on various rubidium samples gave an average normalized resistance at  $15,000 \text{ kg/cm}^2$  of .35 with an rms deviation of .036. It should be pointed out that one can have hysteresis in the resistance curves without having it in the Hall voltage curves, since any slight tearing at the Hall leads changes the effective spacing between the voltage probes and thus the measured IR drop. The Hall voltage depends only on the thickness of the sample and will not show hysteresis because of tearing. The location of the voltage probes, appropriate for a Hall measurement, gives probe spacing comparable to the probe size and is not a good geometry for resistance measurements. In view of this, the agreement with Bridgman's data is satisfactory.

A typical Hall voltage curve for cesium is shown in Fig. 3-9. Two samples were used and a total of six runs performed. The measurements were at approximately  $14^\circ\text{C}$ . The normalized Hall voltage at  $15,000 \text{ kg/cm}^2$  was between .61 and .64 for all six runs and a well defined curve was obtained. The rms deviation on intermediate points is about 1.5 percent.

The resistance of cesium under pressure exhibited considerable hysteresis and it was only after several runs on the same sample that the resistance minimum found by Bridgman became apparent. Because of the hysteresis the data could not be checked quantitatively against Bridgman's data; the shape of the curve was in agreement with his work. The possibility of tearing the sample Hall leads is even greater here than in rubidium, since the compressibility is greater.

The curves of  $n^*$  vs. pressure were obtained from the experimental curves using the relation

$$n^* = \frac{V(P)}{V_H(P) t(P)} \quad (\text{III-1})$$

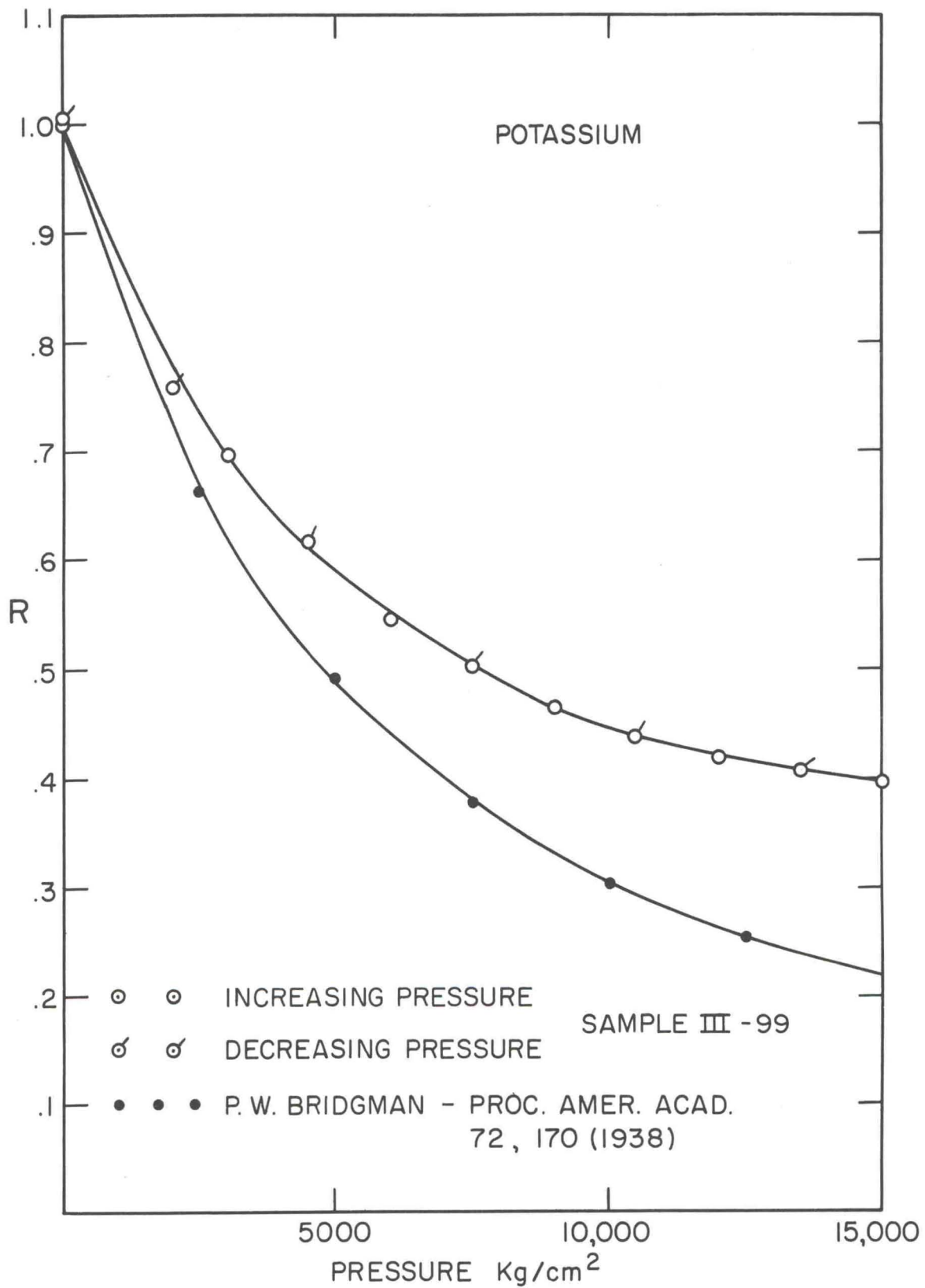


FIG. 3-6 NORMALIZED RESISTANCE R, vs. PRESSURE

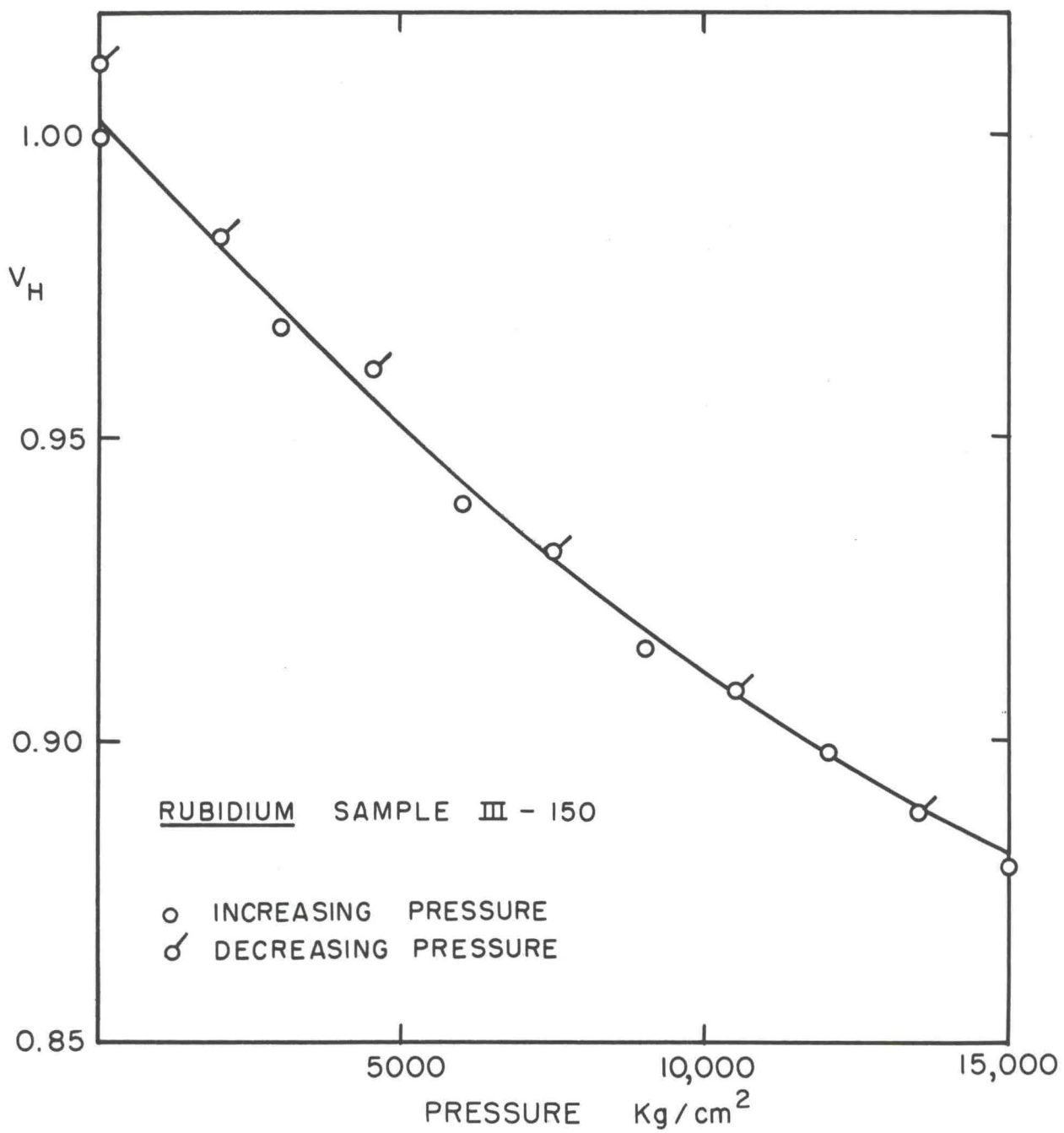


FIG. 3-7  $V_H$ , NORMALIZED HALL VOLTAGE VS. PRESSURE

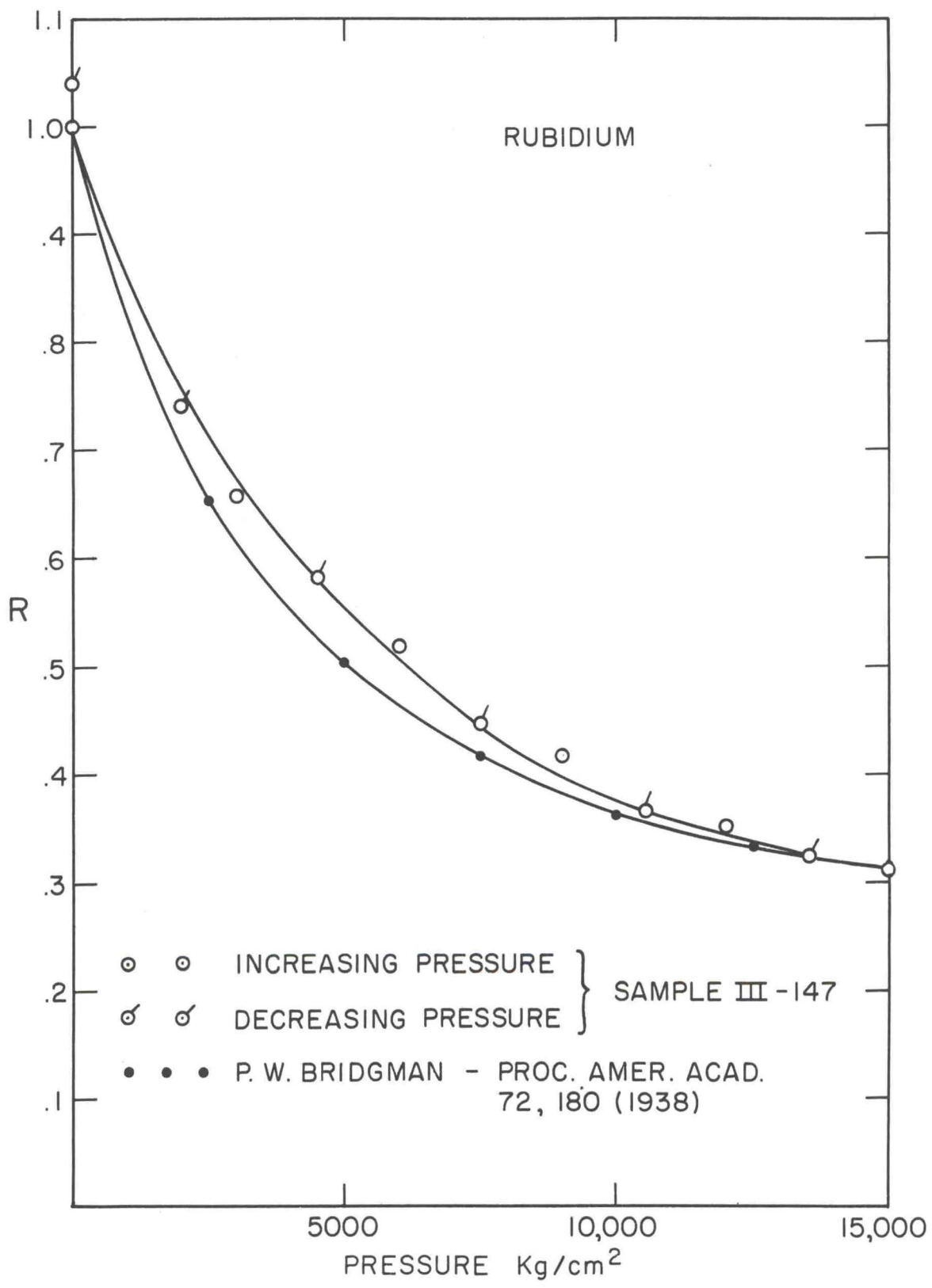


FIG. 3-8 NORMALIZED RESISTANCE R, vs. PRESSURE

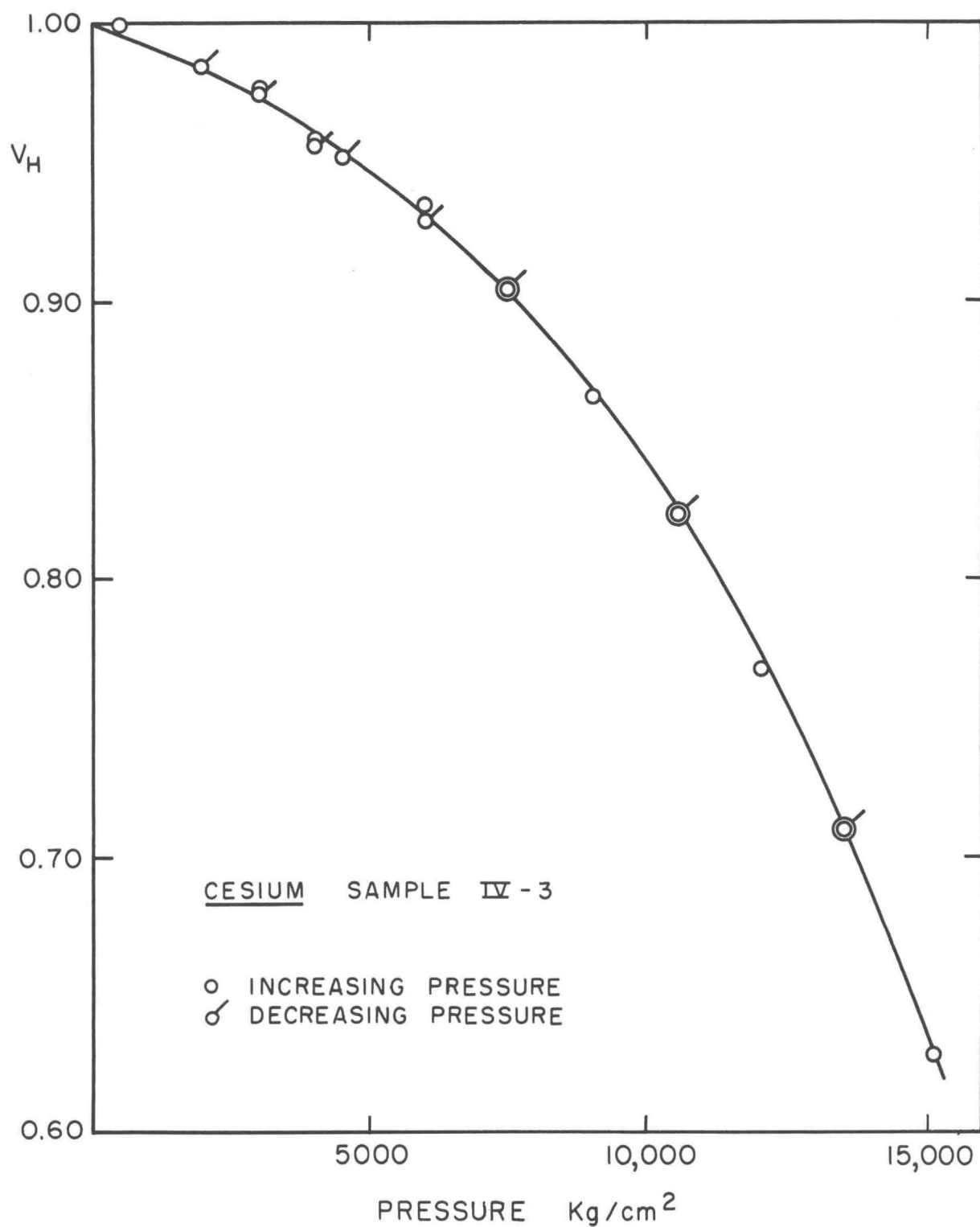


FIG. 3-9  $V_H$ , NORMALIZED HALL VOLTAGE VS. PRESSURE

where  $t(P)$  is the linear dimension of the alkali metal as a function of pressure,  $V(P)$  is its volume, and  $V_H(P)$  is the normalized Hall voltage.  $V(0) = t(0) = 1$ .  $t(P)$  corrects for the change of Hall voltage due to the change of thickness of the sample under pressure and  $V(P)$  corrects for the change of electron density under pressure. The values of  $V(P)$  are taken from Bridgman's compressibility data [2,3]; the values of  $t(P)$  are computed from  $V(P)$ .  $n^*$  is normalized to unity at atmospheric pressure.

The curves of  $n^*$  for lithium and sodium shown in Figs. 3-10 and 11 were computed from the average of the least square slopes of  $V_H$  vs. pressure for the four sodium samples and two lithium samples. The curves of  $n^*$  for potassium, rubidium, and cesium, shown in Figs. 3-12, 13 and 14, were obtained from values of  $V_H$  read from the curves for specific samples. This was done as a matter of convenience, as we were interested in fitting the general shape of the  $n^*$  vs. pressure curve and for this purpose the curve for a typical sample was sufficiently accurate. In the case of potassium, where the Hall voltage curves differed between samples, we give  $n^*$  for the same two samples III-99 and III-115 whose curves of  $V_H$  vs. pressure appear in Fig. 3-4. These curves indicate the direction, size, and range of the effect in potassium, but because of the limited reproducibility their details cannot be considered meaningful.

#### B. Hall Voltage and $n^*$ vs. Temperature

Figure 3-15 shows  $n^*$  vs. temperature for lithium. The values of  $n^*$  are computed directly from the measured values of  $V_H$  by using the value of the thermal expansion coefficient given by Bridgman [2]. All the points were taken as temperature increased, since when the heater was on, the nitrogen boiled away too rapidly to permit a series of points at decreasing temperatures to be measured.

Table 3-1 shows the values of normalized Hall voltage at room and nitrogen temperatures for sodium, potassium, rubidium, and cesium. Values of  $n^*$  are also given except for the case of cesium, where no value of the thermal expansion coefficient is available [4].

C. Absolute Values of  $n^*$ 

In the course of interpreting the results we became concerned with the absolute value of  $n^*$ ; in particular we noticed that the literature values of the Hall constant for sodium and potassium gave  $n^*$  greater than unity (Table 1-1). We expected, for reasons that will be given in Sec. IV, that  $n^*$  should be less than one and decided to compute the absolute value of the Hall constant from our data where possible. In Fig. 3-16, 17, and 18 we plot  $2V_H$  vs. the reciprocal sample thickness for lithium, sodium and potassium. In fitting a straight line to the points we gave more weight to those points corresponding to thick samples, since the relative error in the thickness of these samples is less.

Table 3-2 lists the free electron calculated values of the Hall constant, the values of Hall constant obtained from the slopes of the lines in Figs. 3-16 to 3-18, and the values of  $n^*$ . For convenience we also include the values of  $n^*$  corresponding to the literature values of Hall constant, which have already been tabulated in Table 1-1.

We believe the electrical portion of our measurement is accurate to better than 2 percent; the accuracy of the voltage measurement is about 1 percent and the current and magnetic field measurements are each accurate to better than 1/2 percent. The thickness measurement, accurate to .001", gives a 10 percent error on the thin (.010") samples and an error of less than 5 percent on the thicker (.020" to .050") samples. Since the latter were favored in fitting the data, we estimate the error due to the thickness measurement as 5 percent. The overall accuracy of the measurement is 7 percent. The literature values of  $n^*$  from the work of Studer and Williams [5], who quote an accuracy of 6 percent for sodium and 5 percent for potassium, disagree with ours. We shall discuss the reasons for expecting  $n^*$  to be less than unity in Sec. IV.

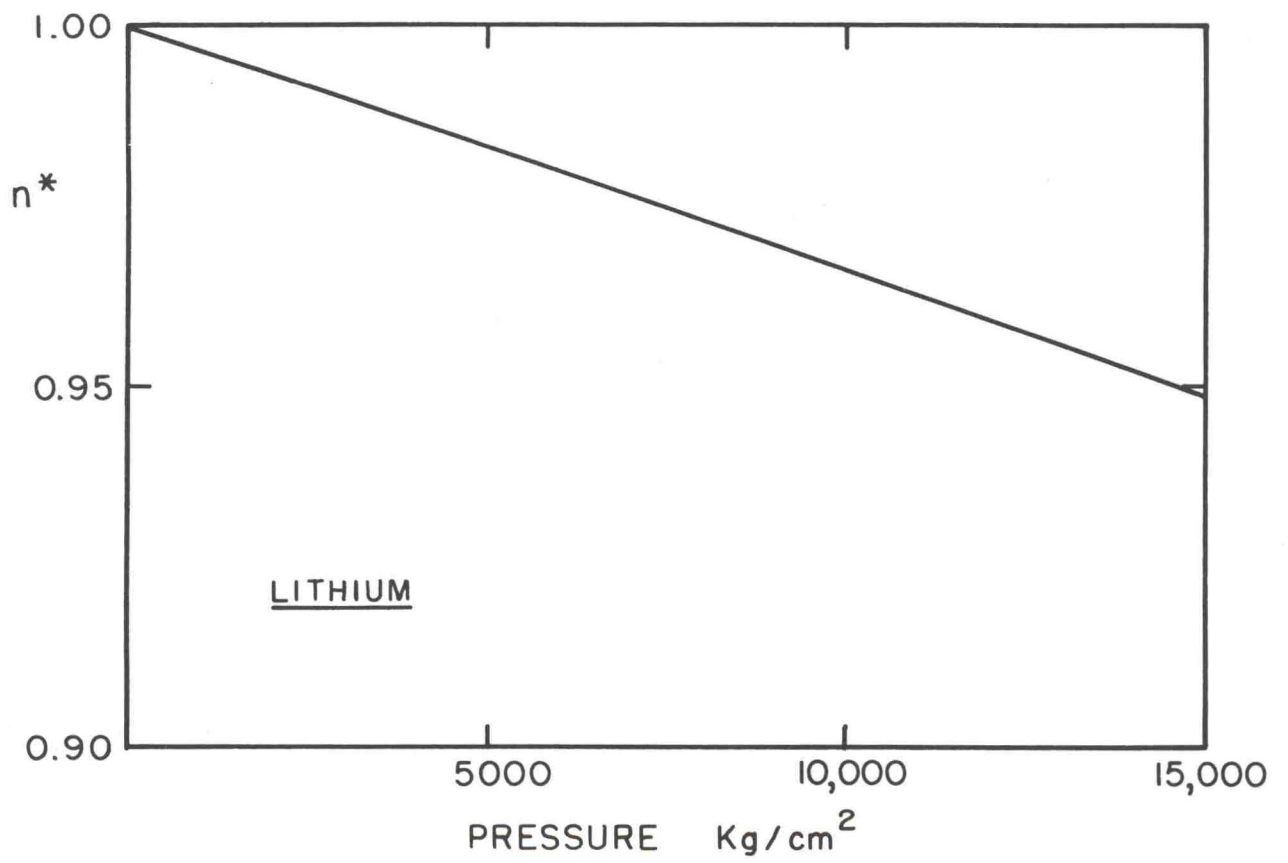


FIG. 3-10  $n^*$ , NORMALIZED ELECTRONS/ATOM VS. PRESSURE

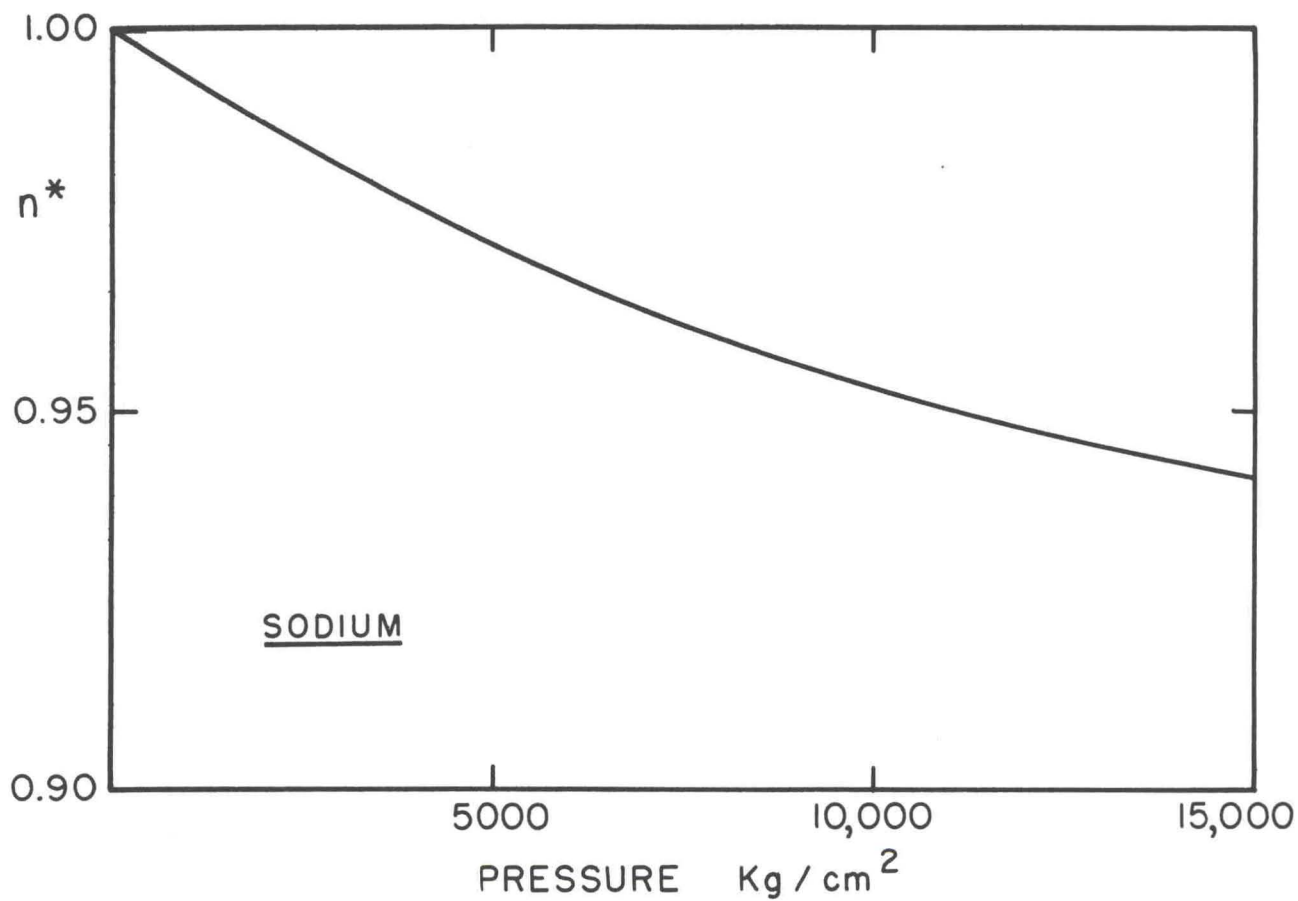


FIG. 3-11  $n^*$ , NORMALIZED ELECTRONS/ATOM VS. PRESSURE

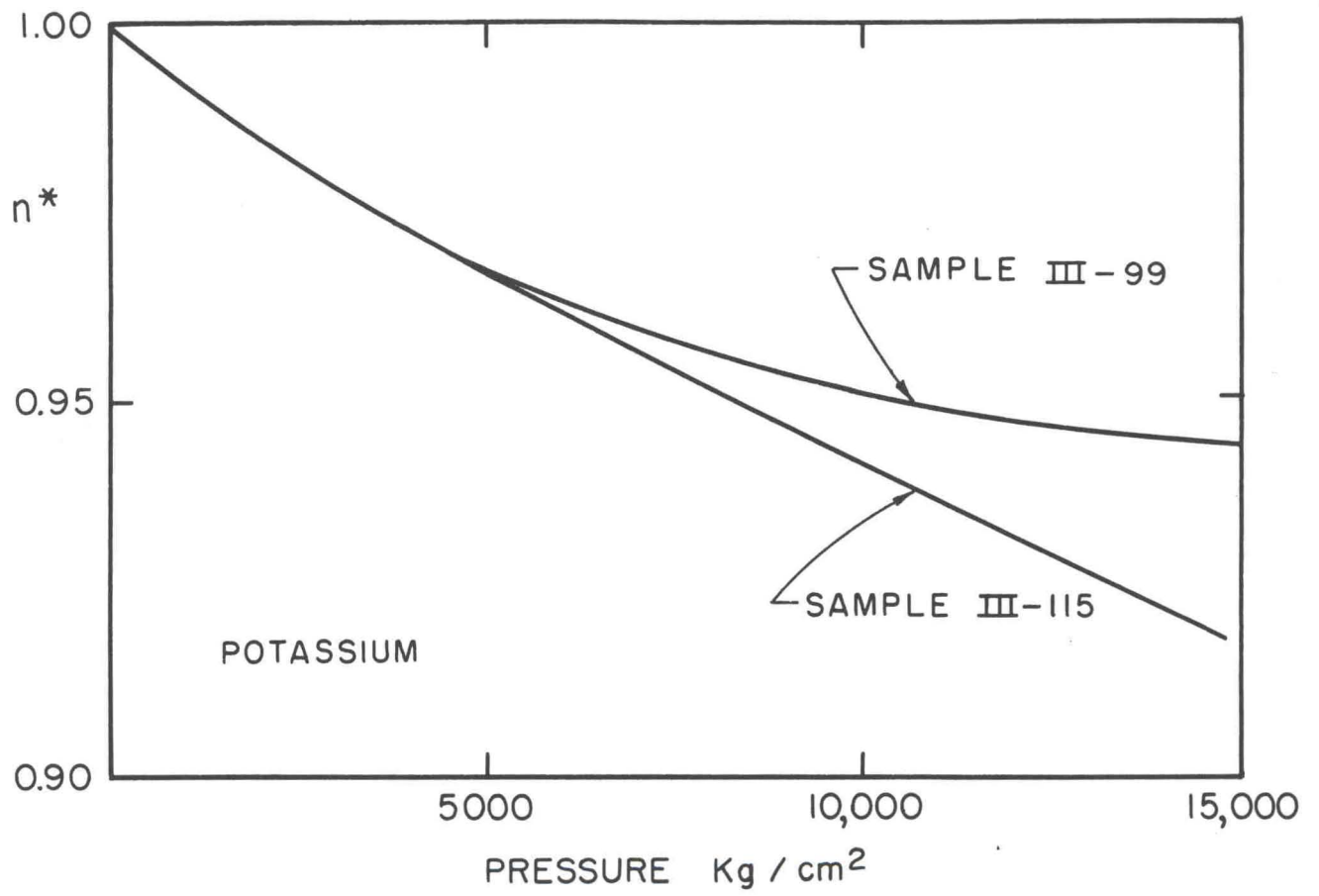


FIG. 3-12  $n^*$ , NORMALIZED. ELECTRONS/ATOM VS. PRESSURE.

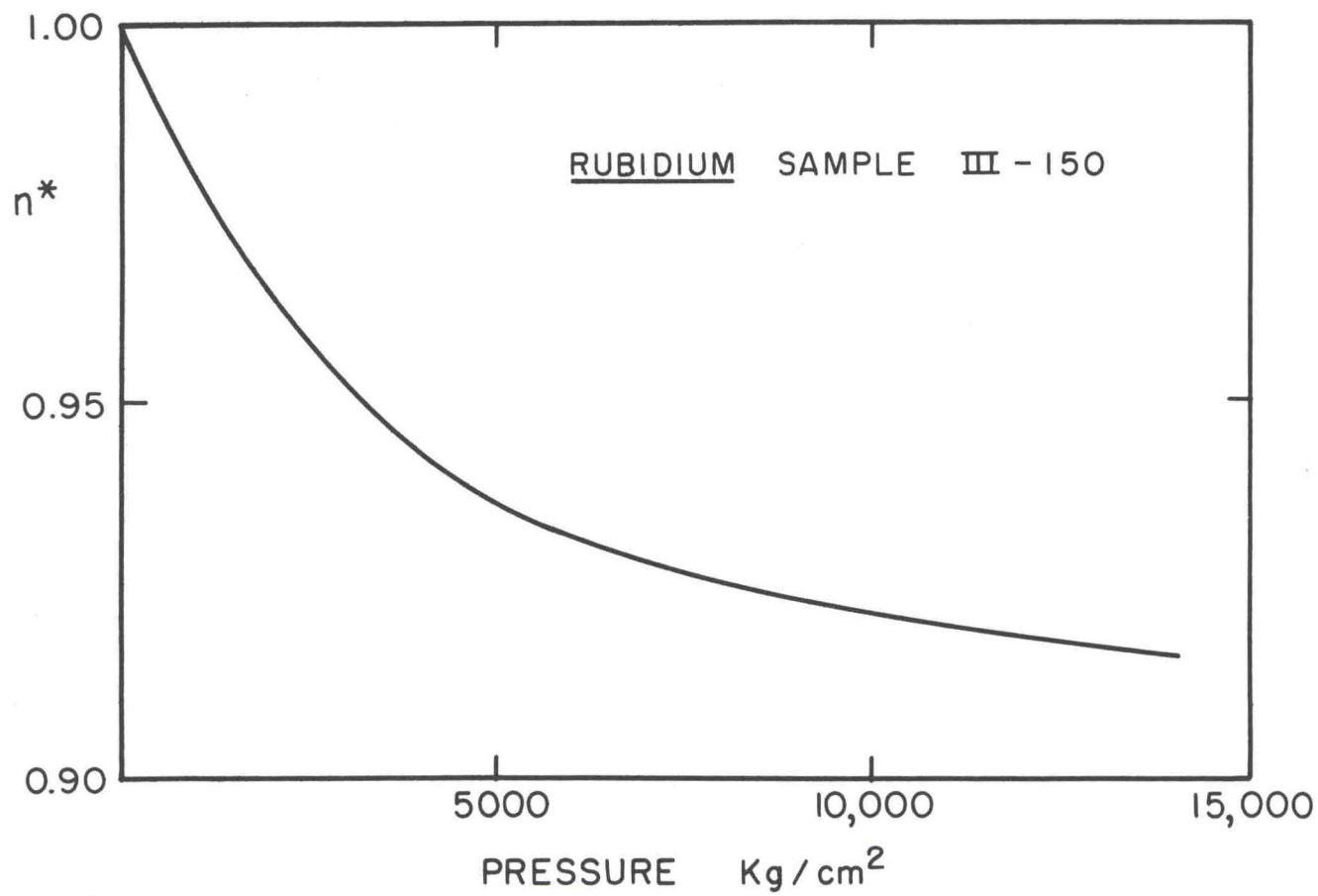


FIG. 3-13  $n^*$ , NORMALIZED ELECTRONS/ATOM VS. PRESSURE

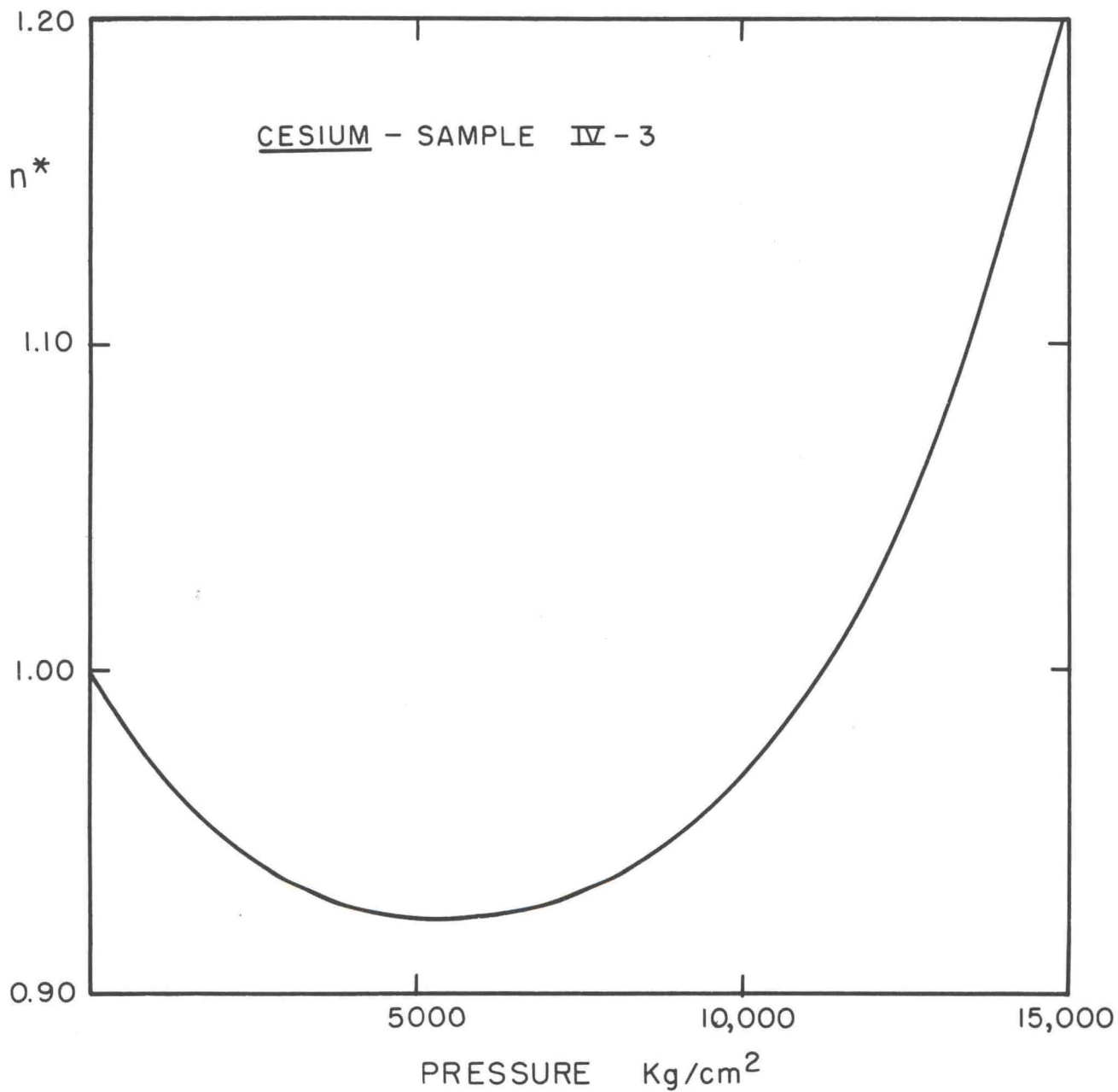


FIG. 3-14  $n^*$ , NORMALIZED ELECTRONS/ATOM VS. PRESSURE

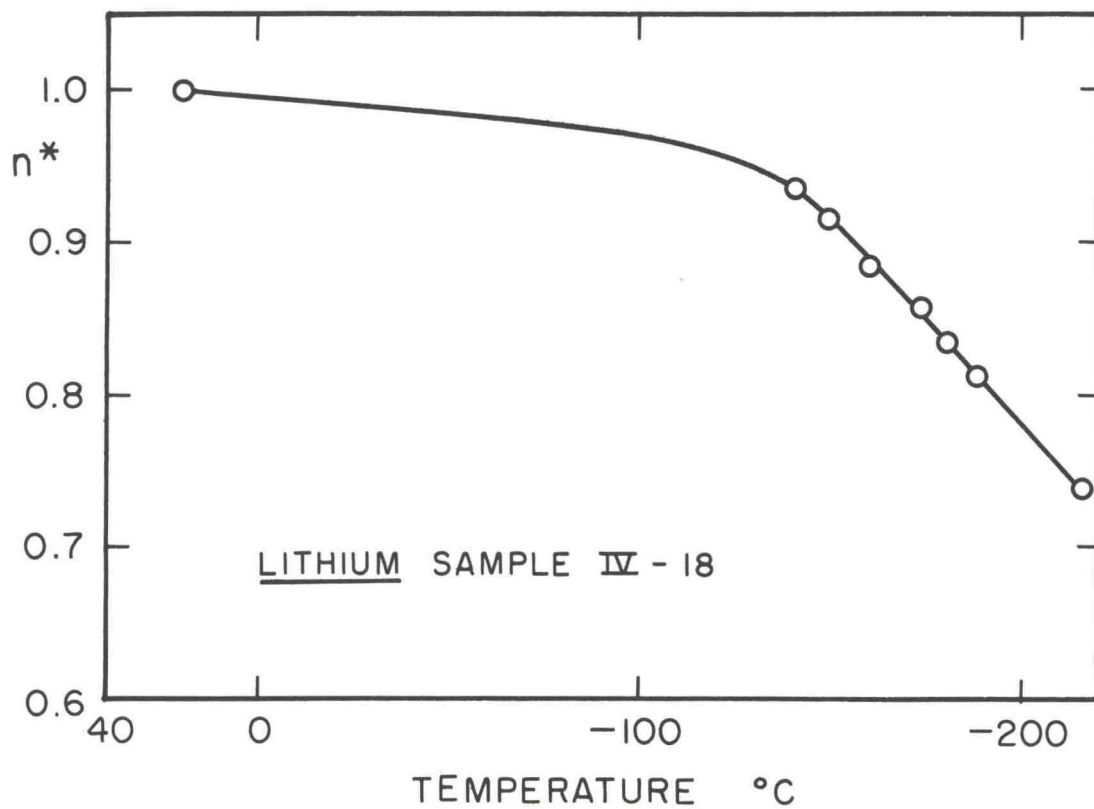


FIG. 3-15  $n^*$ , NORMALIZED ELECTRONS/ATOM VS. TEMP.

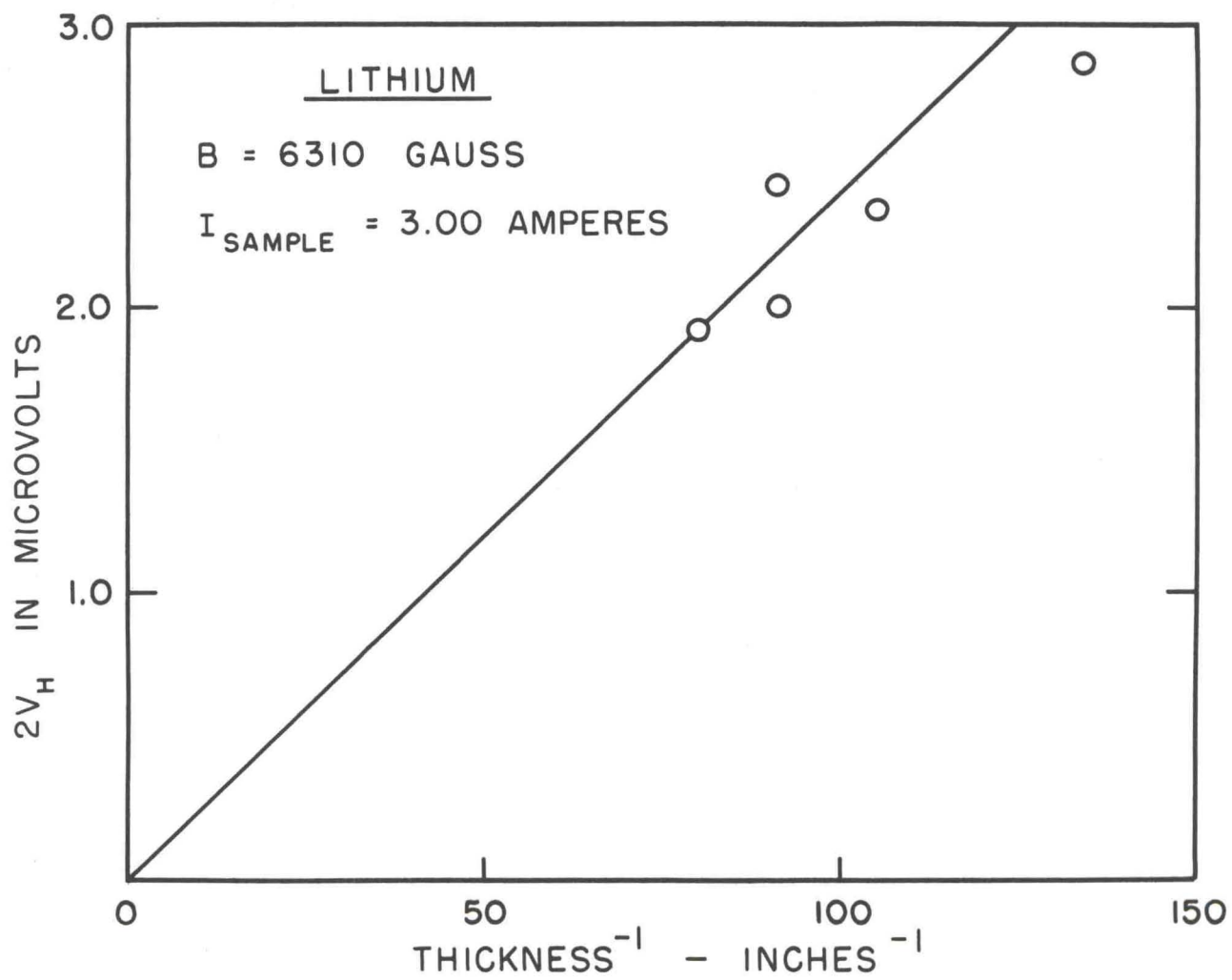


FIG.3-16 HALL VOLTAGE x 2, 2V<sub>H</sub>, VS. SAMPLE THICKNESS<sup>-1</sup>

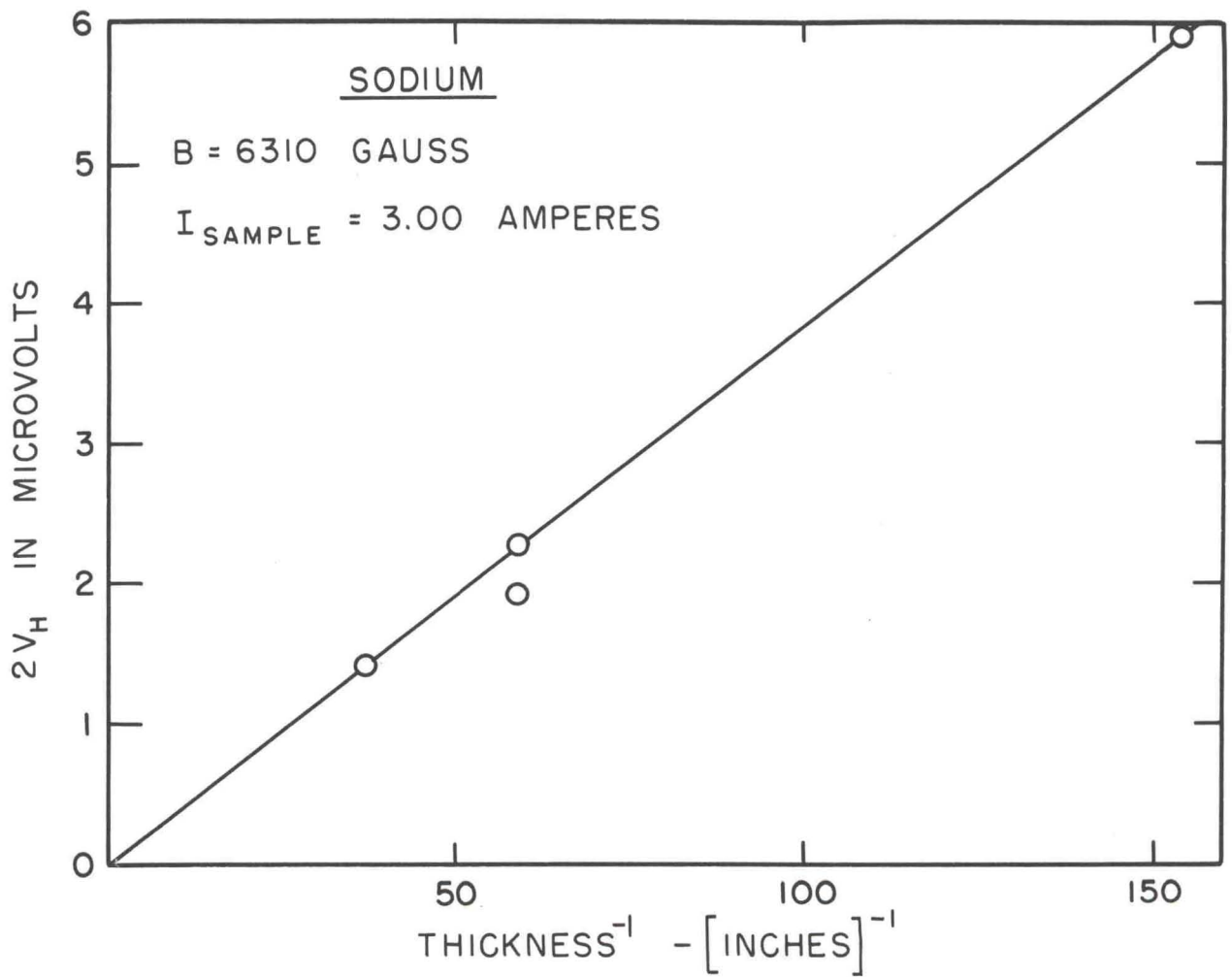


FIG. 3-17 HALL VOLTAGE x 2, 2V<sub>H</sub>, VS. SAMPLE THICKNESS<sup>-1</sup>

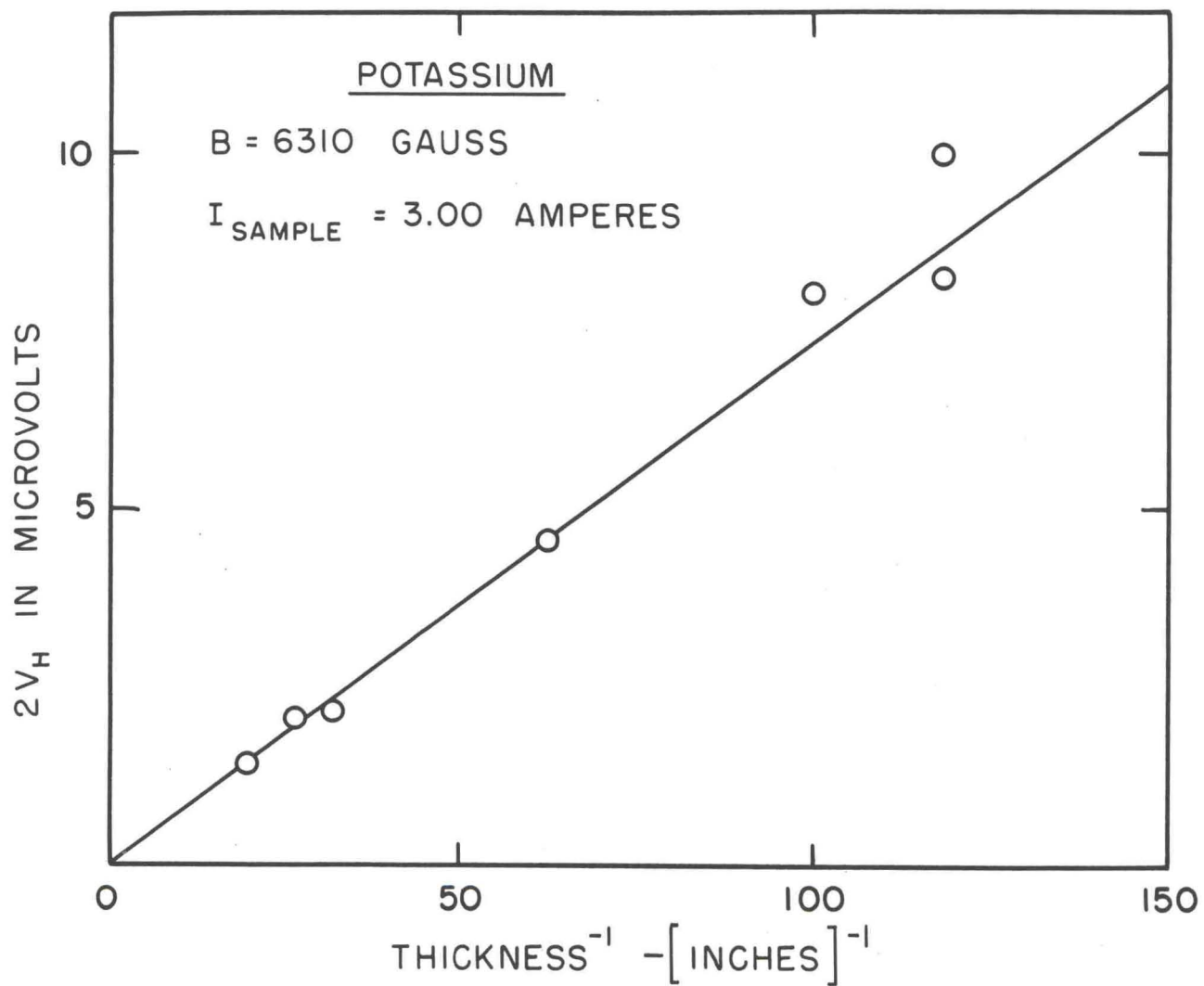


FIG. 3-18 HALL VOLTAGE  $\times 2$ ,  $2V_H$ , VS. SAMPLE THICKNESS<sup>-1</sup>

Metal	Temp.	$V_H$ Normalized	$n^*$ Normalized
<u>Cesium</u>	R. T.	1.000	
	77°K	.973	
	R. T.	1.000	
<u>Rubidium</u>	R. T.	1.000	1.00
	77°K	.971	1.00
	R. T.	1.003	
<u>Potassium</u>	R. T.	1.000	1.00
	77°K	.981	.98
	R. T.	1.007	
<u>Sodium</u>	R. T.	1.000	1.00
	77°K	1.000	.97
	R. T.	1.003	

Table 3 - 1

Hall Voltages of Four Alkali Metals at Room and Liquid  
Nitrogen Temperatures

	Li	Na	K
$R_{\text{calc.}} \times 10^{13}$			
$\frac{\text{volt-cm}}{\text{amp-gauss}}$	13.5	24.5	46.5
$R_{\text{exp}} \times 10^{13}$	15.5	25.8	49.0
$\frac{\text{volt-cm}}{\text{amp-gauss}}$			
$n^*$	.87	.95	.95
$n^*$ from literature values of R- (see Table I-1)	.79	1.17	1.11

Table 3-2

Hall Constants for Lithium, Sodium and Potassium

III. References

1. P. W. Bridgman, Proc. Am. Acad. Arts Sci. 72, 178 (1938).
2. P. W. Bridgman, Proc. Am. Acad. Arts Sci. 70, 93-94 (1935).
3. P. W. Bridgman, Phys. Rev. 27, 68 (1926).
4. The thermal expansion for sodium, potassium, and rubidium is taken from American Instit. of Physics Handbook, McGraw-Hill Co., New York, 4-52 (1952).
5. F. J. Studer and W. D. Williams, Phys. Rev. 47, 291 (1935).

IV. DiscussionA. Expressions for  $n^*$ 

The results of the pressure measurements show two important features. First, for the elements lithium, sodium, potassium, and rubidium the value of  $n^*$  decreases as the pressure increases. Second, in cesium  $n^*$  goes through a minimum as the pressure increases.

In Sec. I, Eq. (I-13), we saw that for a warped, nearly spherical, Fermi surface of the type described by Eq. (I-4) and for an isotropic scattering time  $\tau(\vec{k}) = \tau(E)$ ,  $n^*$  is always greater than unity. Increases in the absolute values of the warping parameters,  $r$  and  $t$ , cause  $n^*$  to increase. If we consider the Fermi surface to be nearly spherical at atmospheric pressure and to distort under pressure, as is suggested by Ham's calculations, then  $n^*$  is initially unity and increases with increasing pressure. As our data cannot be fitted on this model we may consider the possibility that the surface is already warped at atmospheric pressure and that one of the warping parameters increases in absolute magnitude with increasing pressure while the other decreases in such a manner as to decrease  $n^*$ . The energy vs.  $k$  curves obtained by Ham are in most cases identical for the 100 and 111 directions for all lattice constants; this condition fixes the ratio of the warping parameters and eliminates the possibility that they change in opposite directions. The magnitude of the warping parameters obtained from Ham's work increases as the lattice constant is decreased from the atmospheric pressure value. This is shown later for an expansion of the wave vector, rather than energy, in fourth- and sixth-order Kubic harmonics; as far as the change in the magnitude of the warping coefficients is concerned the two expansions are similar. We are thus unable to fit the experimental data with a theory that considers only warping of the Fermi surface in the sense of Eq. (I-4).

We now consider the effect on the value of  $n^*$  of anisotropic scattering times,  $\tau(\vec{k})$  and warped Fermi surfaces. This involves the evaluation of integrals of energy derivatives and scattering times over the Fermi surface; explicit expressions for these integrals are given by Wilson [1]. The work involved in evaluating them is considerable; fortunately, Cooper and Raimis have evaluated them for the case of anisotropic scattering times and warped Fermi surfaces that are described by Kubic harmonics [2,3]. These

authors express the length of the wave vector to the Fermi surface by:

$$k = k_0 [1 + AY_4(\theta, \phi) + A_1 Y_6(\theta, \phi)] \quad (IV-1)$$

The Kubic harmonics  $Y_4(\theta, \phi)$  and  $Y_6(\theta, \phi)$  are combinations of spherical harmonics having cubic symmetry; they are given by [4]

$$Y_4(\theta, \phi) = 5/2 [x^4 + y^4 + z^4 - 3/5] \quad (IV-2)$$

and

$$Y_6(\theta, \phi) = 231/2 [x^2 y^2 z^2 - Y_4(\theta, \phi)/55 - 1/105] \quad (IV-3)$$

where  $x = \sin \theta \cos \phi$ ,  $y = \sin \theta \sin \phi$  and  $z = \cos \theta$ . In the principal directions the values of the Kubic harmonics are:

$$\begin{array}{lll} Y_4(100) = 1 & Y_4(110) = -1/4 & Y_4(111) = -2/3 \\ Y_6(100) = 1 & Y_6(110) = -13/8 & Y_6(111) = 16/9 \end{array}$$

Similarly they write

$$\left( \frac{\partial k}{\partial E} \right)_{E_F} = k_0' [1 + BY_4(\theta, \phi) + B_1 Y_6(\theta, \phi)]; \quad (IV-4)$$

the derivative is taken at the Fermi energy  $E_F$ . The scattering time is also expanded in Kubic harmonics;

$$\tau = \tau_0 [1 + CY_4(\theta, \phi) + C_1 Y_6(\theta, \phi)] \quad (IV-5)$$

The expression for  $n^*$  may be obtained from Eq. (8) of Ref. [3]:

$$\begin{aligned} n^* = 1 + 4/21 [9A^2 - 18A(C - B) - (C - B)^2] \\ + 8/13 [20A_1^2 - 40A_1(C_1 - B_1) - (C_1 - B_1)^2] \end{aligned} \quad (IV-6)$$

The expression is correct to second-order in the coefficients of  $Y_4$  and  $Y_6$ . We note that the value of  $n^*$  depends on the anisotropy of the scattering time, but not on its magnitude. As we expect,  $n^* = 1$  for spherical surfaces

and isotropic scattering times. Furthermore, we see that the terms in  $AC$  and  $A_1 C_1$  can give a decrease of  $n^*$  as the warping, ( $|A|$  and  $|A_1|$ ), increases, provided  $A$ ,  $A_1$ ,  $C$ , and  $C_1$  have the proper sign. Once an anisotropic scattering time is introduced, increased warping of the Fermi surface does not necessarily increase  $n^*$ .

The expression of the warping in this manner has introduced two more coefficients,  $B$  and  $B_1$ , which did not appear when the energy was expanded in Kubic harmonics as in Eq. (I-4). However,  $B$  and  $B_1$  are not independent of  $A$  and  $A_1$ . In Appendix 1 we derive the relations between  $B$ ,  $B_1$  and  $A$ ,  $A_1$  on the assumption that the warping is small.

### B. Calculation of the Warping Parameters

We obtained the warping parameters  $A$  and  $A_1$  from the computations of Ham [5] for the alkali metals. Ham's data give electron energy vs.  $ka/2\pi$ , where  $a$  is the lattice constant, for the 100, 110 and 111 directions. If the Fermi energy is known, we can use these curves to obtain the length of the  $k$  vector at the Fermi surface for the three principal directions. Equation (IV-1) can then be used to obtain three equations, from which  $k_0$ ,  $A$  and  $A_1$  can be computed.

The Fermi level can be obtained by a simple procedure. The Fermi surface must enclose a volume in  $k$  space which contains all the electronic states of the valence electrons. The density of states in  $k$  space per unit volume of crystal is  $1/4\pi^3$  and a b.c.c. crystal with lattice constant  $a$  and one valence electron/atom has  $2/a^3$  valence electrons/unit volume. For a spherical Fermi surface the radius,  $k_s$ , is given by

$$\frac{1}{4\pi^3} k_s^3 4\pi/3 = 2/a^3 \quad (\text{IV-7})$$

or

$$ak_s/2\pi = .62 \quad (\text{IV-8})$$

When the Fermi surface is distorted by warping, the enclosed volume must remain unchanged from the spherical case. For warping of the form (IV-1) Cooper and Raimes [6] give the enclosed volume as

$$V = 4\pi/3 k_0^3 [1 + .57 A^2 + 1.85 A_1^2] \quad (IV-9)$$

We shall see later that  $|A| < .04$  and  $|A_1| < .09$  for all the alkali metals; in addition  $A$  and  $A_1$  are always negative. Under these conditions the contribution of the terms in  $A^2$  and  $A_1^2$  to the expression in the bracket is less than 2 percent. To a good approximation the volume enclosed by the warped Fermi surface is just that of a sphere with radius  $k_0$ , and since the enclosed volume must equal that of the Fermi sphere,  $k_0$  equals  $k_s$  and

$$k_0 a/2\pi = .62 \quad (IV-9a)$$

The data of Ham were fitted by choosing a level of energy such that the maximum and minimum values of  $ka/2\pi$  for this energy averaged to .62. The values of  $A$ ,  $A_1$ , and  $k_0$  for this energy were computed using Eq. (IV-1) and values  $ka/2\pi$  given by Ham's  $E$  vs.  $k$  curves. If the value of  $k_0 a/2\pi$  obtained differed by more than 1 percent from .62 we repeated the procedure for a different value of energy.

In Table 4-1 we tabulate the results of this procedure. Since the actual curves of  $E$  vs.  $k$  are not shown we give the value of  $ak/2\pi$  at the Fermi energy for the principal directions. The last figure on the values for  $A$  and  $A_1$  is given even though the precision of the fit and of the  $E$  vs.  $k$  curves used does not justify it; rounding off would obscure some of the changes of warping parameter with lattice constant. In addition, the values of  $A$  and  $A_1$  for cesium are sensitive to the choice of Fermi energy since  $k$  changes very rapidly with energy in this particular case. In Table 4-2 we give values of the warping parameters for lattice constants corresponding to atmospheric pressure and to  $15,000 \text{ kg/cm}^2$ ; these values are obtained from a linear interpolation between the values of lattice constant shown in Table IV-1.

Examination of Table 4-1 shows that the  $k$  vectors in the 100 and 111 directions are usually equal; for this case (IV-1) leads to the condition  $A = .47 A_1$ . We have used this relation in computing  $B$  and  $B_1$  for values of

$A_1$  between .00 and -.08, using the expressions given in Appendix 1. The result can be expressed as

$$B/A = B_1/A_1 = 3.3 - 60 A_1, \text{ for } A_1 < 0. \quad (\text{IV-10})$$

### C. Dependence of $n^*$ on Pressure

We have obtained a range of values for  $A$  and  $A_1$  from Ham's work and we can express  $B$  and  $B_1$  in terms of  $A$  and  $A_1$ . We now notice that the terms arising from the sixth-order Kubic harmonics dominate the expression for  $n^*$  Eq. (IV-6). Using the relation (IV-10) for  $B$  and setting  $C = 0$  we find that the terms in  $A$  and  $B$  contribute only about 1 percent to  $n^*$  for  $|A| \leq .03$ . We can simplify the fitting of the data with no significant error by considering only the contribution of terms in  $A_1$ ,  $B_1$ , and  $C_1$  to  $n^*$ . The expression for  $n^*$  then becomes:

$$n^* = 1 + 12.3 A_1^2 - 24.6 A_1 (C_1 - B_1) - .615 (C_1 - B_1)^2 \quad (\text{IV-11})$$

A non-zero value of  $C_1$  can cause  $n^*$  to decrease as  $|A_1|$  increases. Investigation of the behavior of  $n^*$  vs.  $A_1$  for different forms of  $C_1$  is straightforward but tedious. In Fig. 4-1 we give some curves of  $n^*$  vs.  $A_1$  obtained using Eq. (IV-11) with the supplementary condition (IV-10) and various forms of  $C_1$ . The values  $C_1 = -.3$  and  $C_1 = -.4$  were chosen because they represent the simplest non-zero  $C_1$ 's and because their magnitude gives values of  $n^*$  for  $A_1 = 0$  that are in the same range as the observed values in the alkalis. The values  $C_1 = -.3 + 4.5 A_1$  and  $C_1 = -.4 + 5 A_1$  are chosen because the terms in  $A_1$  approximately cancel the terms in  $A_1^2$  occurring in the expression for  $n^*$  and give a steeper initial slope of the  $n^*$  vs.  $A_1$  curve. Certain features of these curves should be noted.

They show that  $n^*$  can decrease as the warping,  $|A_1|$ , increases; the experimental data and Ham's calculations do not conflict.

The size of the changes in  $n^*$  produced by changes in  $A_1$  of the magnitude indicated by Table 4-2 is consistent with the size of the observed changes. Looking at the part of the curve before the minimum we see that changes in  $A_1$  of .02 produce changes of the order of 10 percent in  $n^*$ .

HP6

Metal	a atomic units	$\frac{ak_{100}}{2\pi}$	$\frac{ak_{110}}{2\pi}$	$\frac{ak_{111}}{2\pi}$	A	A <sub>1</sub>
Li	8.11	.613	.623	.613	-.002	-.005
	6.65	.607	.634	.613	-.011	-.011
	5.34	.575	.665	.590	-.031	-.037
Na	10.04)	No anisotropy				
	8.11)					
	6.65)					
K	11.46	.625	.640	.625	-.003	-.007
	10.05	.620	.620	.620	0	0
	8.11	.585	.675	.575	-.013	-.049
Rb	12.57	.611	.629	.611	-.004	-.009
	10.74	.605	.627	.605	-.005	-.011
	9.05	.560	.680	.560	-.028	-.061
Cs	13.35	.600	.655	.600	-.013	-.027
	11.46	.580	.670	.580	-.021	-.045
	10.04	.495	.655	.495	-.041	-.088

Table 4-1

Warping Parameters for Alkali Metals Computed

from Data of F. Ham

HP6

Metal	Pressure kg/cm <sup>2</sup>	a atomic units	A	A <sub>1</sub>
Li	1	6.64	-.011	-.011
	15,000	6.42	-.015	-.015
K	1	9.85	-.001	-.003
	15,000	9.00	-.007	-.026
Rb	1	10.64	-.006	-.015
	15,000	9.55	-.021	-.047
Cs	1	11.44	-.021	-.045
	15,000	10.01	-.041	-.088

Table 4-2

Warping Parameters of Alkali Metals  
at Two Pressures, Computed  
from Data of F. Ham

The value of  $n^*$  passes through a minimum and then rises rapidly; no additional assumptions need be introduced to account for the observed minimum of  $n^*$  for cesium.

The experimental data are semi-quantitatively fitted using non-zero  $C_1$ 's of the form shown in Fig. 4 -1. A quantitative fit does not seem feasible at this stage; some theoretical guidance as to the form of  $C_1$  is needed. It is a striking feature of the semi-quantitative fit that the magnitude of  $C_1$  is much greater than that of  $A_1$ . It is also worth noting that while the consideration of non-zero  $C_1$ 's was forced upon us by the direction of the change in  $n^*$ , a non-zero value of  $C_1$  is also needed in order to account for the magnitude of the change in  $n^*$  in sodium and lithium, where the change in  $A_1$  is very small. However, several difficulties should be considered.

Ham's data give the warping for sodium as zero both at atmospheric pressure and at  $15,000 \text{ kg/cm}^2$  and make it impossible to attribute the change in  $n^*$  to the pressure dependence of  $A_1$ . On the other hand, the existence of the low temperature magneto-resistance implies, subject to the reservations mentioned in Section I, that there is a small anisotropy of the Fermi surface. If this is so, we expect the anisotropy to change with pressure; if  $C_1$  is large enough the small change in  $A_1$  might account for the observed effect.

The change in  $A_1$  for lithium is small, (.004); to account for the observed change in  $n^*$ , about 5 percent, we choose a value for  $C_1$  of  $-.4 + 5A_1$  to obtain a sufficiently steep initial slope on the  $n^*$  vs.  $A_1$  curves. The value of  $n^*$  for lithium at atmospheric pressure obtained from the curve for  $C_1 = -.4 + 5A_1$  is .78; this is in agreement with the fact that the absolute value of  $n^*$  for lithium is substantially less than one (Table III-2). The absolute values of  $n^*$  for the other alkali metals are larger and much closer to unity; this suggests that the value of  $C_1$  for lithium should be different from that for the other alkalis.

Most of the curves of  $n^*$  vs.  $A_1$  have minima for values of  $|A_1|$  less than the atmospheric pressure  $|A_1|$  computed for cesium; this is not true for the curve with  $C_1 = -.4 + 5A_1$ , but the values of  $n^*$  at  $A_1 = -.045$  are much too low. To fit the cesium data we must postulate that the atmospheric

pressure warping for cesium is considerably less than that given by Ham's data; a value for  $A_1$  of  $-.01$  or  $-.02$  is probably needed. Since the work of Ham indicates that in cesium the Fermi surface nearly touches the zone boundary, it is possible that the drastic change in the behavior of  $n^*$  vs. pressure at the minimum is due to the beginning of contact with the zone face. In this case the discussion of the data in terms of the Cooper and Raimes description of the Fermi surface is unreliable. Since the only case in which a minimum in  $n^*$  vs. pressure has been observed may be explained in terms of the Fermi surface touching the zone face, it may be worth repeating that  $C_1$  was introduced primarily to yield a decrease in  $n^*$  with increasing  $|A_1|$  rather than a dependence showing a minimum.

From Fig. 4 - 1 we see that another result of anisotropic scattering times is that the values of  $n^*$  for  $A_1 = 0$  are always less than one. Since the literature values of  $n^*$  for sodium and potassium were greater than unity we used our Hall effect data where thickness measurements were available to obtain the absolute value of the Hall constant and  $n^*$ . The results were presented in Table 3 - 2. Although the measurements of Studer and Williams [7] were made on double distilled material in glass and should be reliable, the large  $n^*$  for sodium, 1.17, is unacceptable. Ham's data indicate that the Fermi surface in sodium is spherical; the magneto-resistance and thermo-power experiments discussed in Sec. I also suggest that the surface is nearly spherical. If  $A$  and  $A_1$  are zero and  $C_1 \neq 0$ ,  $n^*$  is less than one. Small  $A_1$ , of the order of  $-.01$ , and fairly large  $C_1$ , of the order of  $+.3$ , can make  $n^*$  greater than one, but only by about 2 percent. In view of this we suspect the value of  $n^*$  obtained from the data of Studer and Williams and prefer our own. The same objection applies to their potassium data, which give  $n^* = 1.11$ . The only other Hall data on sodium are the 1886 measurements of Ettingshausen and Nernst [8], which give  $n^* = .98$ . If we accept our values of  $n^*$  for sodium and potassium, the atmospheric pressure value of  $n^*$  is less than one for all the alkalis; the proposed explanation for this is the existence of a non-zero  $C_1$ .

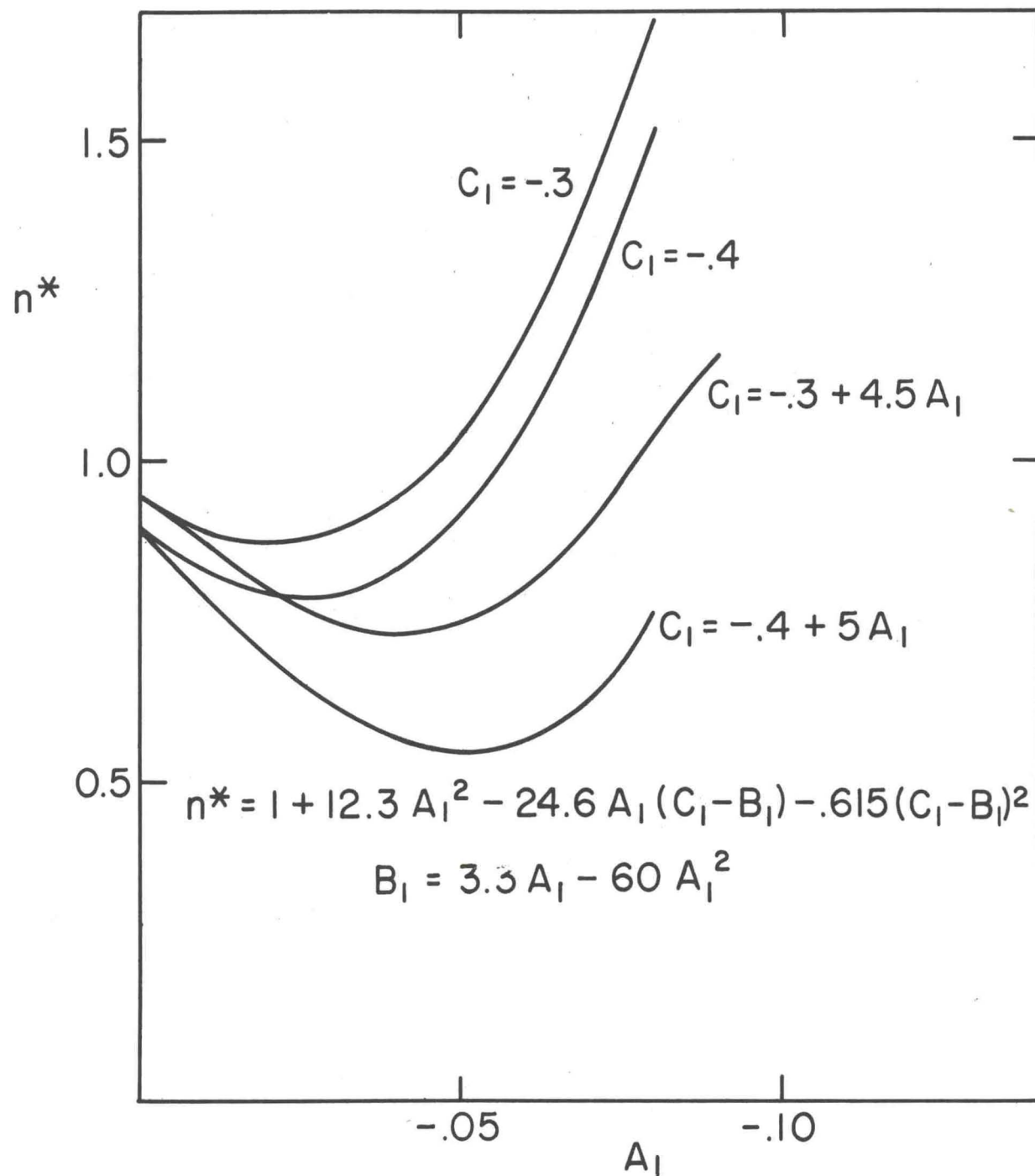


FIG. 4-1  $n^*$ , electrons/atom, vs.  $A_1$

The slight decrease in the size of the pressure effect that occurred when we cleaned our samples and made them more homogeneous, discussed in Sec. III, might be due to a decrease in  $|C_1|$ . There is no reason for expecting our cleaning process to decrease  $|C_1|$  rather than increase it; however, changes in  $|C_1|$  can provide a reason for the dependence of the size of the pressure effect on sample homogeneity. Furthermore, the large differences in the size of the rubidium pressure effect with different samples, observed before we made clean, one-piece rubidium samples, can be understood on the same basis.

The initial dependence of the pressure data on sample preparation raises the question of whether the pressure results would be altered by further cleaning of the sample. Since the inhomogeneities removed were relatively large and should vary from sample to sample, we take the reproducibility finally achieved to indicate that the cleaning process has eliminated most of the effect of inhomogeneities. If the cleaning process could be carried further, as by the growth of single crystals and the consequent elimination of grain boundaries, we expect that at worst the size of the pressure effect would decrease. We do not expect the direction of the pressure effect to change. It was the direction of the pressure effect that forced us to consider anisotropic scattering times; this anisotropy is the dominant feature of the interpretation. The proposal that the scattering time is anisotropic is unaltered by the presence of some scattering due to inhomogeneities, although the exact size of the anisotropy might be altered. This is not crucial for us since we cannot fit the data in detail and are concerned only with the order of magnitude of the anisotropy,  $|C_1|$ . The assumption is made here that the scattering is dominated by the lattice vibrations and the effect of inhomogeneities is relatively small, so that most of the anisotropy must be attributed to lattice scattering.

The pressure data and the changes in the warping parameter  $A_1$  obtained from Ham's calculations agree semi-quantitatively if we consider anisotropic scattering times with values of  $C_1$  of about  $-.3$ . We must now examine possible sources of the proposed anisotropy in  $C_1$ .

### D. The Scattering Time

In the last section we found that in order to fit the experimental data we needed to introduce an anisotropic scattering time  $\tau(\vec{k})$ . In this section we shall indicate possible sources of this anisotropy and make some estimate of its order of magnitude.

It is tacitly assumed that the scattering time for the case of applied electric and magnetic fields is the same as that for an applied electric field only. We follow the derivation of the expression for  $\tau(\vec{k})$  given by Mott and Jones [9], modifying it only at those places where assumptions that lead to an isotropic  $\tau$  are introduced.

If the distribution function is given by  $f(\vec{k})$ , the probability that a state at  $\vec{k}$  is occupied, then in the steady state

$$\left(\frac{\partial f(\vec{k})}{\partial t}\right)_{\text{fields}} + \left(\frac{\partial f(\vec{k})}{\partial t}\right)_{\text{collisions}} = 0. \quad (\text{IV-12})$$

We write the distribution function as

$$f(\vec{k}) = f_0 + \left(\frac{\partial f(\vec{k})}{\partial t}\right)_{\text{fields}} \tau(\vec{k}) \quad (\text{IV-13})$$

where  $f_0$  is the Fermi-Dirac distribution function. We take the  $z$  axis along that particular direction in  $k$  space for which we wish to compute  $\tau(\vec{k})$  and apply the electric field  $F$  along this direction. Since

$$dk_z/dt = eF/\hbar \quad (\text{IV-14})$$

the equilibrium Fermi-Dirac distribution is shifted in  $k$  space and becomes

$$f(\vec{k}, t) = f_0(k_z - eFt/\hbar, k_y, k_x) \quad (\text{IV-15})$$

We now assume spherical constant energy surfaces so that  $E(\vec{k}) = E(|\vec{k}|)$ ; thus

$$\frac{f(\vec{k}) - f_0}{\tau(\vec{k})} = \left(\frac{\partial f(\vec{k})}{\partial t}\right)_{\text{fields}} = -\frac{\partial f_0}{\partial k_z} \frac{eF}{\hbar} = -\frac{\partial f_0}{\partial E} \frac{\partial E}{\partial k} \frac{k_z}{k} \frac{eF}{\hbar} = -\left(\frac{\partial f(\vec{k})}{\partial t}\right)_{\text{collisions}} \quad (\text{IV-16})$$

Then  $\left(\frac{\partial f(\vec{k})}{\partial t}\right)_{\text{collisions}}$  is evaluated by taking the difference between the number of collisions into a volume element at  $\vec{k}$  and the number out of it; by considering only transitions between states of equal energy, we obtain

$$\left(\frac{\partial f(\vec{k})}{\partial t}\right)_{\text{coll.}} = [1 - f(\vec{k})] \int f(\vec{k}') P_{\vec{k}'\vec{k}} dS' - f(\vec{k}) \int [1 - f(\vec{k}')] P_{\vec{k}\vec{k}'} dS' \quad (\text{IV-17})$$

Here  $P_{\vec{k}\vec{k}'} dS'$  is the probability per unit time of an electron making a transition from a state  $\vec{k}$  to a state  $\vec{k}'$ , both of which lie on the same spherical surface of constant energy;  $dS'$  is an element of area about the state  $\vec{k}'$ . The form of  $P_{\vec{k}\vec{k}'}$  is given in Eq. (IV-23);  $U_{\vec{k}\vec{k}'}$  and  $U_{\vec{k}'\vec{k}}$ , the transition probabilities between volume elements in  $k$  space, are equal by detailed balancing. Since we have assumed spherical energy surfaces,  $|\nabla_{\vec{k}} E|$  in Eq. (IV-23) is constant on a surface of constant energy and

$$P_{\vec{k}\vec{k}'} = P_{\vec{k}'\vec{k}} \quad (\text{IV-18})$$

Then

$$\left(\frac{\partial f(\vec{k})}{\partial t}\right)_{\text{coll.}} = \int_{\text{Fermi sphere}} [f(\vec{k}') - f(\vec{k})] P_{\vec{k}\vec{k}'} dS' \quad (\text{IV-19})$$

Substituting for  $f(\vec{k}')$ ,  $f(\vec{k})$  from Eq. (IV-13) and dividing through by

$\tau(\vec{k}) \left(\frac{\partial f(\vec{k})}{\partial t}\right)_{\text{fields}}$ , and using the expression for  $\left(\frac{\partial f(\vec{k})}{\partial t}\right)_{\text{fields}}$  from Eq. (IV-16) we obtain

$$\frac{1}{\tau(\vec{k})} = \int_{\text{Fermi sphere}} \left[ 1 - \frac{\tau(\vec{k}') k'_z}{\tau(\vec{k}) k_z} \right] P_{\vec{k}\vec{k}'} dS' \quad (\text{IV-20})$$

Equation (IV-20) for  $\tau(\vec{k})$  is an integral equation. In order to estimate the anisotropy of  $\tau(\vec{k})$  we shall set  $\tau(\vec{k}')/\tau(\vec{k}) = 1$  inside the integral. This may be regarded as the first step of an iteration procedure for finding  $\tau$ . Since we chose our electric field ( $z$  axis) along the direction  $\vec{K}$  for which we are computing  $\tau(\vec{k})$  we have

$$k_z = k_s \quad \text{and} \quad k'_z = k_s \cos \theta \quad (\text{IV-21})$$

where  $\theta$  is the angle between  $k$  and  $k'$ . Let  $\phi$  be the angle between the plane of  $k$  and  $k'$  and the  $z$ - $x$  plane. Then

$$\frac{1}{\tau(\vec{k})} = k_s^2 \int_0^\pi d\phi \int_0^{2\pi} [1 - \cos \theta] |\sin \theta| P_{\vec{k}, \phi}(\theta) d\theta. \quad (\text{IV-22})$$

We have chosen these limits on  $\theta$  and  $\phi$  because of the possibility that  $P_{\vec{k}, \phi}(\theta) \neq P_{\vec{k}, \phi}(-\theta)$ ; this possibility arises because for an arbitrary direction of  $\vec{k}$  the section of the Brillouin zone for phonons centered on the tip of the  $k$  vector is not symmetrical about the line  $\theta = 0$ . A phonon may be available for a normal process with angle  $\theta$  but not for one with the angle  $-\theta$ . We would like to evaluate the inner integral numerically and prefer to include the effect of asymmetries in it.

We now consider the form of  $P_{\vec{k}, \phi}(\theta)$ . Perturbation theory gives

$$P_{\vec{k}, \phi}(\theta) = \frac{1}{4\pi^2 \hbar} \frac{|U_{kk'}|^2}{|\nabla_k E| |k'|} \quad (\text{IV-23})$$

where  $U_{kk'}$  is the matrix element of the perturbing potential  $U$  taken between the initial electron state  $\psi_k$  and the final state  $\psi_{k'}$  [10]; unit crystal volume is assumed. We shall be interested only in the perturbation due to lattice vibrations, since at room temperature these dominate the scattering of electrons. We then write

$$\begin{aligned} U(\vec{r}) &= \sum_{\vec{l}} V[\vec{r} - \vec{l} - \vec{R}(\vec{l})] - V(\vec{r} - \vec{l}) \\ &= - \sum_{\vec{l}} \vec{R}(\vec{l}) \cdot \nabla V(\vec{r} - \vec{l}); \end{aligned} \quad (\text{IV-24})$$

where  $V(\vec{r} - \vec{l})$  is the potential at  $\vec{r}$  associated with the ion at lattice point  $\vec{l}$  and  $\vec{R}(\vec{l})$  is the displacement at  $\vec{l}$ .  $V(\vec{r} - \vec{l})$  includes both the potential due to the ion core and to the electrons that shield the core. The wave functions are

written in the Bloch form

$$\psi_{\vec{k}}(\vec{r}) = e^{i\vec{k} \cdot \vec{r}} u_{\vec{k}}(\vec{r}) \quad (\text{IV-25})$$

We write the matrix elements as

$$U_{\vec{k}\vec{k}'} = - \sum_{\vec{l}} \vec{R}(\vec{l}) \cdot \int_{\text{crystal}} \psi_{\vec{k}'}^*(\vec{r}) \nabla V \psi_{\vec{k}}(\vec{r}) d\vec{r} \quad (\text{IV-26})$$

and by changing the origin to the lattice point at  $\vec{l}$  so that  $\vec{r}' = \vec{r} - \vec{l}$

$$U_{\vec{k}\vec{k}'} = - \sum_{\vec{l}} \vec{R}(\vec{l}) e^{-i(\vec{k} - \vec{k}') \cdot \vec{l}} \int \psi_{\vec{k}'}^*(\vec{r}') \nabla V \psi_{\vec{k}}(\vec{r}') d\vec{r}' \quad (\text{IV-26a})$$

Bailyn [11] has computed the integral in Eq. (IV-26a) in a calculation that uses the Hartree-Fock equation for the electrons. We follow his notation and express the integral as

$$\int_{\text{crystal}} \psi_{\vec{k}'}^*(\vec{r}) \nabla V(\vec{r}) \psi_{\vec{k}}(\vec{r}) d\vec{r} = \hat{s} [JS] \quad (\text{IV-27})$$

$$\text{where } \hat{s} = \frac{\vec{k} - \vec{k}'}{|\vec{k} - \vec{k}'|}.$$

We are ignoring normalization factors. J denotes the contribution to the matrix element of the ion core alone and S denotes a shielding factor which includes the effect of the electron cloud about the core and the exchange hole.

If we now express the displacement  $\vec{R}(\vec{l})$  in terms of lattice waves, we have

$$\vec{R}(\vec{l}) = \sum_p \sum_{\vec{q}} \hat{e}_{\vec{q},p} a_{\vec{q},p} e^{-i\vec{q} \cdot \vec{l}} \quad (\text{IV-28})$$

where  $\hat{e}_{\vec{q},p}$  is a unit vector which depends on  $\vec{q}$ , the lattice vibration or phonon wave number and the polarization p.  $a_{\vec{q},p}$  is the amplitude of the vibration.

Then

$$U_{kk'} = - \sum_{\vec{q}} \sum_{\vec{l}} e^{-i(\vec{k} - \vec{k}' + \vec{q}) \cdot \vec{l}} a_{\vec{q},p} \sum_p \hat{e}_{\vec{q},p} \cdot \hat{s} [JS(\theta)] \quad (IV-29)$$

the sum over  $\vec{l}$  yields the condition

$$\vec{k} - \vec{k}' + \vec{q} = \begin{cases} \vec{K}, \text{ a reciprocal lattice vector} \\ 0 \end{cases} \quad (IV-30)$$

and a value N, the number of ions.

Since  $\vec{k}$  and  $\vec{k}'$  are specified and we have restricted  $\vec{q}$  to lie in the 1st Brillouin zone,  $\vec{q}$  is specified and the sum over  $\vec{q}$  reduces to a single term.

The value of  $a_{\vec{q}}$  comes from the matrix element for a phonon annihilation (creation) operator and is given by [12]

$$a_{\vec{q},p} = \left[ \frac{\hbar}{2NM\nu_{\vec{q},p}} \right]^{1/2} \times \begin{cases} (\bar{n}_{\vec{q},p})^{1/2} & \text{annihilation of phonon} \\ \text{or} \\ (\bar{n}_{\vec{q},p} + 1)^{1/2} & \text{creation of phonon} \end{cases} \quad (IV-31)$$

where M is the mass of the ion and  $\nu_{\vec{q},p}$  the frequency of the phonon  $\vec{q}$ .

$\bar{n}_{\vec{q}}$  the equilibrium occupation number is given by the Bose-Einstein factor;

$$\bar{n}_{\vec{q}} = \frac{1}{e^{h\nu_{\vec{q}}/kT} - 1} \quad (IV-32)$$

For the high temperature limit  $h\nu/kT \ll 1$  and  $a_{\vec{q}}$  becomes

$$a_{\vec{q}} = \left[ \frac{\hbar}{2NM\nu_{\vec{q}}} \frac{kT}{h\nu_{\vec{q}}} \right]^{1/2} \quad \text{High Temperature Limit} \quad (IV-33)$$

We write this as

$$a_{\vec{q},p} = \frac{B^{1/2}}{N\omega_{\vec{q},p}} \quad (IV-34)$$

where  $\omega_{\vec{q},p}$  is now the angular frequency of the phonon with wave vector  $\vec{q}$  and polarization  $p$ . We introduce the  $1/N$  to cancel the  $N$  from the sum Eq. (IV-30).

Then

$$U_{\vec{k},\vec{k}'} = \sum_{p=1,2,3} \frac{B^{1/2}}{\omega_{\vec{q},p}} JS(\theta) \hat{e}_{\vec{q},p} \cdot \hat{s} \quad (\text{IV-35})$$

and dropping the sum over  $p$  with the understanding that we will consider the polarization that gives the largest contribution to  $U_{\vec{k}\vec{k}'}$ , we obtain

$$P_{\vec{k},\phi}^{\vec{q}}(\theta) = \frac{B}{4\pi^2 \hbar |\nabla_{\vec{k}} E|_{\vec{k}'}} \frac{[JS(\theta)]^2 (\hat{e}_{\vec{q},p} \cdot \hat{s})^2}{\omega_{\vec{q},p}^2} \quad (\text{IV-36})$$

Lumping all the uninteresting constants together into  $D$ , we have

$$\frac{1}{\tau(\vec{k})} = D \int_0^\pi d\phi \int_0^{2\pi} d\theta \frac{(1 - \cos \theta) |\sin \theta| [JS(\theta)]^2 (\hat{e}_{\vec{q},p} \cdot \hat{s})^2}{\omega_{\vec{q},p}^2 |\nabla_{\vec{k}} E|_{\vec{k}'}} \quad (\text{IV-37})$$

We now consider the sources of anisotropy in  $\tau(\vec{k})$ . The density of states factor  $\frac{1}{|\nabla_{\vec{k}} E|_{\vec{k}'}}$  is, strictly speaking, isotropic since we assumed spherical constant energy surfaces to derive Eq. (IV-20). For a warped surface, one could assume Eq. (IV-20) was still valid and compute  $\tau(\vec{k})$  using the density of states factor. An anisotropic state density will act as a weighting factor in the integral; for the case of an alkali we can estimate its magnitude using Eq. (IV-4).

$$|\nabla_{\vec{k}} E| = 1 / \left( \frac{\partial k}{\partial E} \right)_{E_F} = \frac{1}{k'_0 [1 + B Y_4 + B_1 Y_6]} \quad (\text{IV-38})$$

Equation (IV-10) gives  $B_1$  in terms of  $A_1$ . For a typical value of  $A_1$ ,  $-.02$ ,  $B_1 = -.09$  and noting the values of  $Y_6$  in the principal directions we see that the density of states factor varies by about  $\pm 10$  percent from its average value. This is a relatively weak weighting factor, compared with the effect of  $\omega_{\vec{q},p}^2$ .

We now write

$$\omega_{\vec{q},p} = c_{\vec{q},p} q \quad (\text{IV-39})$$

and choose for  $c_{\vec{q},p}$  the velocity of sound in the elastic limit (small  $q$ ). While this is incorrect for large  $q$ , the differences in the elastic limit velocities for different polarizations and for different directions of propagation are quite large and this approximation indicates the relative importance of different branches of the phonon spectrum and of different directions of the same branch, even though the individual  $q$ 's within a branch are not correctly weighted. We indicate the choice of the elastic limit sound velocity by writing  $c_{\hat{q},p}$ , where  $\hat{q}$  is a unit vector in the direction of  $\vec{q}$ . In Table 4-3 we list expressions for the velocity of sound squared times the density for the three principal directions and evaluate the expressions using the elastic constants for potassium, as given in Table 4-1 [13]. The point is that  $c_{\hat{q},p}^2$  varies by about a factor of six between the various transverse modes and is substantially larger for the longitudinal modes than for the transverse ones. This weights the contribution of the transverse phonons to the integral more strongly than that of the longitudinal ones. Furthermore, it means that transitions using certain phonons, namely 110 phonons polarized 110 will be weighted very much more strongly than others. Transitions from a given initial state  $\vec{k}$  on the Fermi surface to those final states for which the transition probability is large, involve many different phonon directions and so average the different sound velocities to some extent. Since the angular terms in the integral weight certain values of the scattering angle,  $\theta$ , heavily and since the phonon direction for a fixed scattering angle depends on the initial state  $\vec{k}$  we do not expect the variations in sound velocity to average out completely, although we do expect that the averaging will make the anisotropy of  $\tau(\vec{k})$  considerably less than that of  $c_{\hat{q},p}^2$ . The numerical values in Table 4-3 indicate how bad the assumption of an elastically isotropic solid, usually made in computing  $\tau$ , is for the alkali metals.

The term  $1/q^2$  in the integral for  $1/\tau(\vec{k})$  depends on the initial state  $\vec{k}$  for those processes in which  $K \neq 0$  in Eq. (IV-30). For a normal process, in which  $K = 0$ ,  $\vec{q}$  depends only on the angle  $\theta$  between  $k$  and  $k'$ . In an umklapp (U.K.) process, in which  $K \neq 0$ ,  $\vec{q}$  depends not only on  $\theta$ , but also on

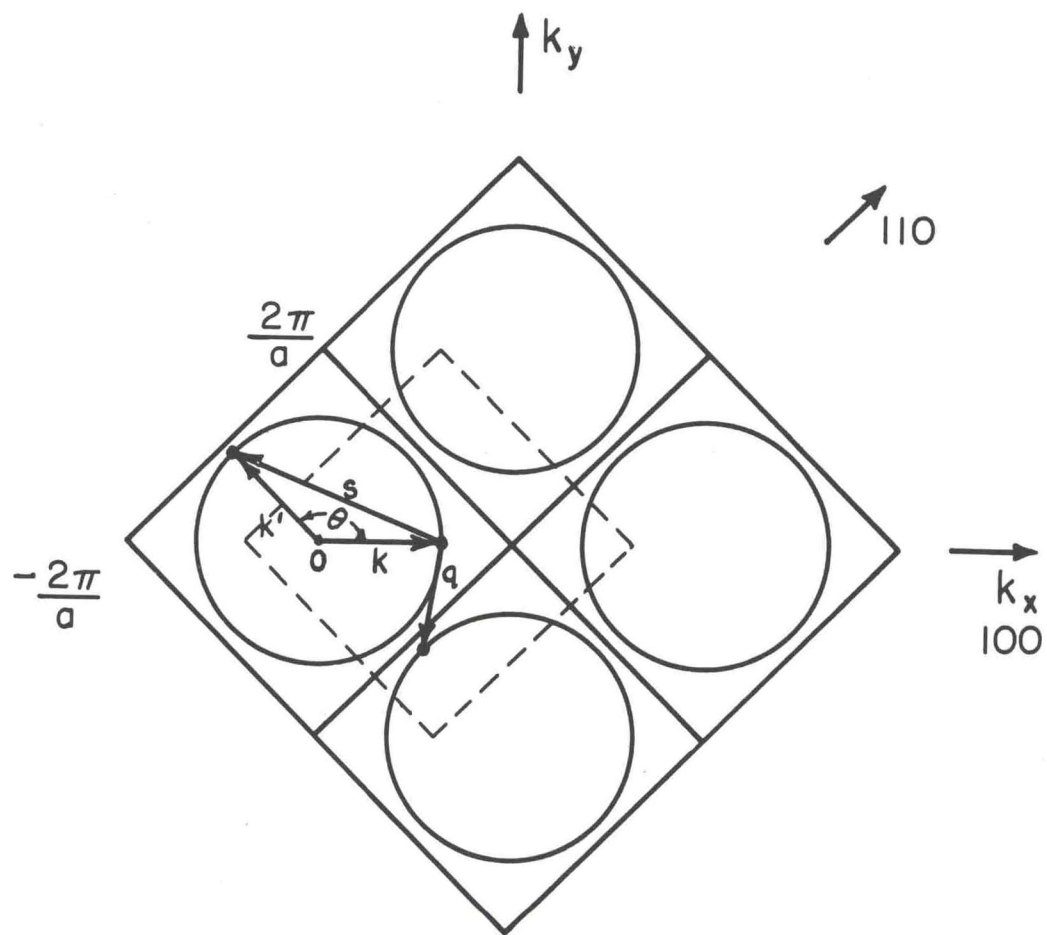


FIG. 4-2 CROSS SECTION, IN 001 PLANE, OF BRILLOUIN ZONES FOR B.C.C. METAL.

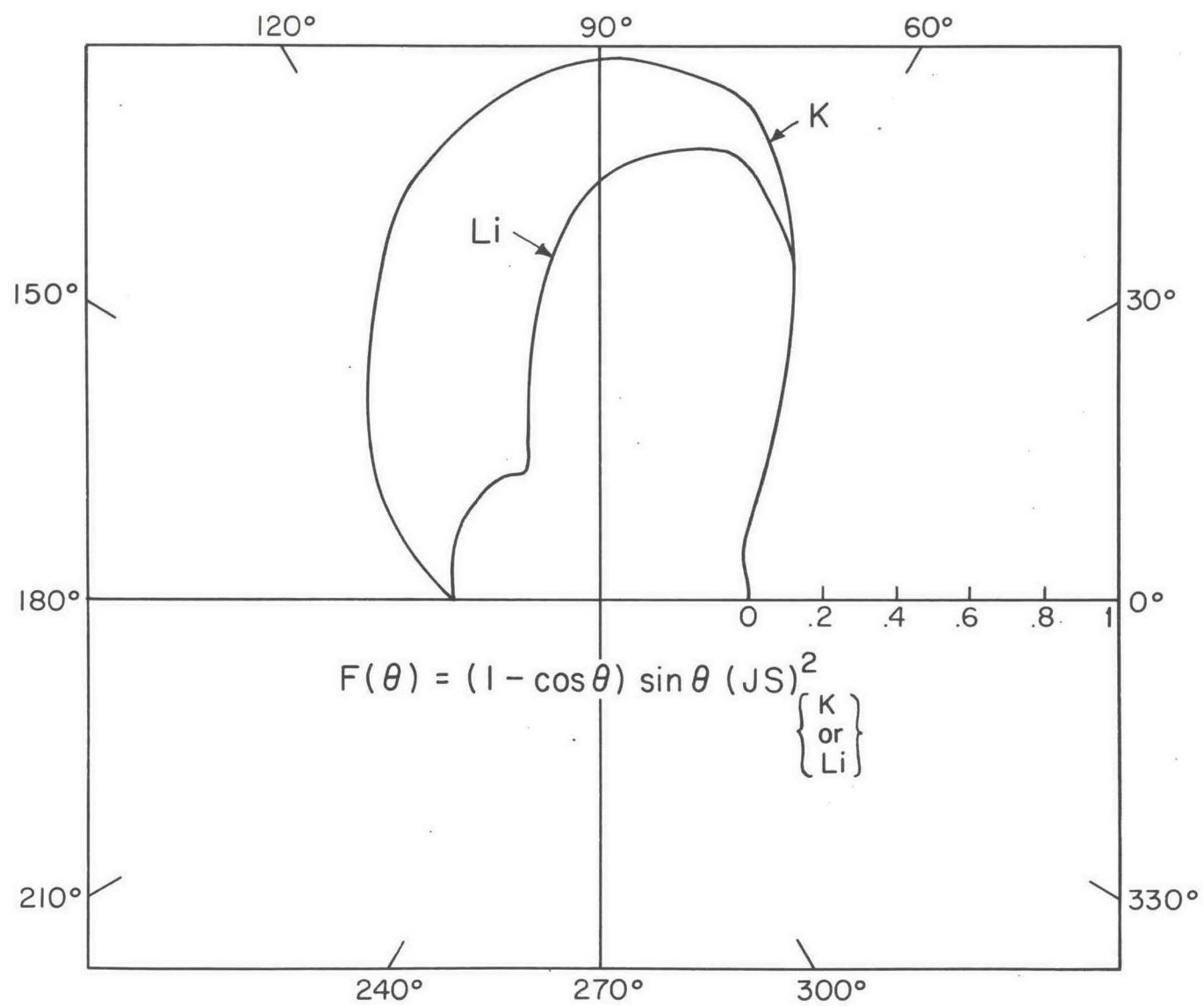


FIG. 4-3  $F(\theta)$  vs.  $\theta$  FOR POTASSIUM (K) AND LITHIUM (Li)

HP6

Values of  $\rho c^2_{q,p}$

Direction  
of polarization

Direction of propagation

	100	110	111
Longitudinal	$c_{11}$ = 4.2	$\frac{1}{2} [c_{11} + c_{12} + 2c_{44}]$ = 6.4	$\frac{1}{3} [c_{11} + 2c_{12} + 4c_{44}]$ = 7.1
Transverse 001	$c_{44}$ 2.6	$c_{44} = 2.6$	-
110	-	$\frac{c_{11} - c_{12}}{2} =$ .41	$\frac{c_{11} - c_{12} + c_{44}}{3} =$ 1.15

Numerical values are for potassium in units of dynes/cm<sup>2</sup> x 10<sup>-10</sup>, using values of  $c_{11}$ ,  $c_{12}$ ,  $c_{44}$  from Table 1-1.

Table 4 - 3

Velocity of Sound in Potassium

the particular reciprocal lattice vector  $\mathbf{K}$  used; the latter depends on the initial state  $\mathbf{k}$ .

Figure 4-2 shows a cross section of the Brillouin zone for a b.c.c. lattice, taken in a 001 plane. The circles are cross sections of the Fermi surface and the dashed square is a zone for phonons, centered on the state  $\vec{\mathbf{k}}$ . The U.K. processes will be those for which the final state  $\mathbf{k}'$  lies on that portion of the Fermi sphere centered at 0 which is outside the dashed square. A typical U.K. process and the associated phonon vector  $\vec{\mathbf{q}}$  is shown. For fixed  $\theta$ , the length  $|\mathbf{q}|$  depends on the initial state  $\vec{\mathbf{k}}$ ; this is most clearly seen by taking  $\theta = 180^\circ$  and  $\vec{\mathbf{k}}$  first in the 100 and then in the 110 direction. For the latter direction  $|\mathbf{q}|$  is about 1/4 as large as for  $\mathbf{k}$  in the 100.

Normal processes must use longitudinal phonons, at least for those directions in which a separation into longitudinal and transverse modes is possible, because the term  $\hat{\mathbf{e}}_{\mathbf{q},p} \cdot \hat{\mathbf{s}}$  becomes  $\hat{\mathbf{e}}_{\mathbf{q},p} \cdot \hat{\mathbf{q}}$  for a normal process and this is zero for transverse modes. On the other hand, for an U.K. process  $\vec{\mathbf{s}}$  is not usually parallel to  $\vec{\mathbf{q}}$  and transverse phonons may participate; in fact the low value of the velocity of sound for transverse phonons will act as a weighting factor which emphasizes those U.K. processes which use transverse phonons.

One source of anisotropy in  $\tau$  is then the  $\mathbf{k}$  dependence of the contribution of  $1/q^2$  to the integral for  $\tau(\vec{\mathbf{k}})$ . This source occurs in any b.c.c. metal; for the case of the alkali metals the anisotropy of the velocity of sound must also be considered.

We now wish to make some estimate of the anisotropy of  $\tau(\vec{\mathbf{k}})$ . The correct way to obtain  $\tau(\vec{\mathbf{k}})$  would be to choose a direction  $\vec{\mathbf{k}}$  and compute  $q$ ,  $c_{\hat{\mathbf{q}},p}^2$ , and  $e_{\hat{\mathbf{q}},p}$  for a large number of points  $\mathbf{k}'$  on a Fermi sphere and evaluate Eq. (IV-37). This would be a major computational task. A simpler but considerably less accurate procedure would be to consider only scattering in two dimensions and evaluate the  $\theta$  integral in Eq. (IV-37) for fixed  $\phi$ . Some of the loss of accuracy comes from the fact that for some  $\mathbf{k}$  directions the  $\theta$  integral depends strongly on the value of  $\phi$  chosen. For example, if one chose  $\mathbf{k}$  in the 110 direction and replaced the Brillouin zone for phonons

by a sphere of equal volume, there is  $\phi$  symmetry in the sense that the  $|\vec{q}|$  for fixed  $\theta$  is independent of  $\phi$ , although  $c_{\hat{q},p}$  and  $\hat{e}_{\hat{q},p} \cdot \hat{s}$  are not; on the other hand, for  $k$  in a 111 direction this is not true. In a repeated zone scheme the nearest neighbor Fermi spheres do not have their centers on a 111 axis and consequently the section of these spheres cut by the plane containing  $k$  (111) and  $k'$  depends on  $\phi$ . This makes it difficult to estimate  $\tau(111)$  by doing only the  $\theta$  integration.

We decided to estimate the anisotropy in  $\tau(\vec{k})$  by evaluating

$$I(\vec{k}) = \int_0^{2\pi} \frac{(1 - \cos \theta) |\sin \theta| [(JS)\theta]^2 d\theta}{|\vec{q}|^2} \quad (\text{IV-40})$$

for  $\vec{k}$  in the 100, 110, and 111 directions. This is a very crude procedure, which not only replaces the three dimensional integration in Eq. (IV-37) by a two dimensional one, but also considers the velocity of sound, the polarization factor  $\hat{e}_{\hat{q},p} \cdot \hat{s}$ , and the density of states as constants. Although we could have approximated  $c_{\hat{q},p}^2$  in Eq. (IV-37) by using the velocity of sound in the principal direction closest to that of  $\vec{q}$ , we felt this procedure ran the risk of weighting the integral by the sound velocity for an unrepresentative phonon; it would also give a factor  $\frac{1}{c_{\hat{q},p}}$  that was discontinuous in  $\theta$ .

We obtained the values of  $(JS)^2$  given by Bailyn [13]; in Table IV-4 we list his values of  $u^3 (JS)^2$  vs.  $u = \frac{\sin \theta}{2}$  for potassium and lithium. The square of the matrix element for potassium has values less than those for rubidium and cesium and greater than those for sodium; the general behavior of  $(JS)^2$  vs.  $u$  is similar for all these four metals and we chose potassium as representative of them. Lithium is unlike the other alkalis in that  $(JS)^2$  goes through a zero near  $\theta = 120^\circ$ . In Fig. 4-3 we have plotted

$$F(\theta) = (JS)^2 (1 - \cos \theta) \sin \theta \quad (\text{IV-41})$$

for  $\theta$  from 0 to  $180^\circ$  in a polar plot, using Bailyn's values for the potassium and lithium matrix elements. For  $\theta$  from  $180^\circ$  to  $360^\circ$  the absolute value of  $\sin \theta$  should be used.  $F(\theta)$  peaks rather sharply near  $75^\circ$  for lithium; this

HP6

$u$ $= \sin \frac{\theta}{2}$	$\theta$ degrees	$(1 - \cos \theta)$ $\times \sin \theta$	$u^3(JS)^2$ for K	$u^3(JS)^2$ for Li	$F(\theta)$ for K	$F(\theta)$ for Li
.00	0	0	0	0	.00	.00
.10	11.5	.004	0	0	.00	.00
.20	23	.03	.005	.005	.02	.02
.30	35	.10	.035	.035	.13	.13
.40	47	.23	.090	.090	.32	.32
.50	60	.43	.190	.190	.65	.65
.60	74	.70	.315	.265	1.02	.86
.65	81	.83	.345	.275	1.04	.83
.70	89	.98	.375	.265	1.07	.76
.75	97	1.11	.393	.220	1.03	.58
.80	106	1.22	.400	.125	.95	.30
.85	116	1.30	.385	.025	.82	.05
.90	128	1.28	.340	.010	.60	.02
.95	144	1.07	.305	.025	.38	.03
.97	152	.88	.300	.033	.29	.03
.98	157	.70	.296	.035	.23	.03
.99	164	.54	.293	.040	.17	.02
1.00	180	.00	.290	.042	.00	.00

Table 4-4

Scattering Functions for K and Li

Using Baily's Values of  $u^3(JS)^2$

will select a smaller range of phonon wave vectors and sound velocities than the  $F(\theta)$  for potassium and will probably give more anisotropy in  $\tau$ .

In Tables 4-5, 4-6, and 4-7 we list  $qa/2\pi$  as a function of  $\theta$  for various initial  $k$ . The values were obtained by measuring on a diagram such as that in Fig. 4-2. We also tabulate  $(\frac{2\pi}{qa})^2$  and  $F(\theta)(\frac{2\pi}{qa})^2$ ; the latter is proportional to the integrand in Eq. (IV-40). We used  $F(\theta)$  evaluated with both the potassium and lithium matrix elements. The integrand of Eq. (IV-40) was plotted as a function of  $\theta$  and  $I(\vec{k})$  evaluated graphically. The results are shown in Table IV-8; we have also evaluated the integral  $I(\vec{k})$  counting U.K. processes only. This takes account of the large velocity of sound for the longitudinal phonons used in normal processes by not counting these processes at all.

As was pointed out before, the integration for  $k$  in the 111 direction is unrepresentative because the possible scattering processes depend strongly on the angle  $\phi$ , that is on the particular great circle on the Fermi sphere for which we have chosen to do the  $\theta$  integration. Because of this strong  $\phi$  dependence no two-dimensional integration will give a very meaningful estimate of  $\tau(111)$ ; on the other hand, Eq. (IV-40) can give a meaningful estimate for  $\tau(100)$  and  $\tau(110)$  because of the weak  $\phi$  dependence.

The results of the integration using the K matrix element show a difference of about 20% in the values of  $I(\vec{k})$  for the 110 and 100 directions counting both N and U.K. processes; if only the U. K. processes are counted the values differ by nearly 70%. The lithium matrix element gives a difference of about 20% between  $I(100)$  and  $I(110)$  for N and U.K. processes and a 60% difference if only the U.K. processes are counted.

We have also tabulated  $1-.3Y_6$  for the three principal directions. This gives the dependence of  $\tau(\vec{k})$  on the sixth-order Kubic harmonic with  $C_1 = -.3$ . We should point out that we have no way of knowing what  $C$  is; there is no reason for  $C$  and  $C_1$  to be simply related in the way  $A$  and  $A_1$  were for certain shapes of the  $E$  vs.  $k$  curves. In addition, even though the influence of  $C$  on  $n^*$  may be small because of the smaller size of the coefficients arising from the fourth-order Kubic harmonic its influence on

$\tau$  is not. It is interesting to note that both matrix elements give  $\tau(110) > \tau(100)$ , as would be the case if  $\tau$  were proportional to  $1 - .3Y_6$ .

We conclude that if the matrix elements obtained by Bailyn are correct, then the geometry of the U.K. processes alone is sufficient to produce appreciable anisotropies in  $\tau$  for both potassium and lithium. We have seen that the velocity of sound is highly anisotropic in the alkalis and may produce further anisotropy in  $\tau$ ; like the geometrical factor  $(1/|q|^2)$  it is most significant in the umklapp region.

The highly anisotropic  $\vec{\tau}(k)$  for lithium is in line with the large deviation of  $n^*$  from unity for this metal noted in Table 1-1; however, it is not clear why the same deviation does not occur in the case of potassium where the anisotropy is also large. The form of  $F(\theta)$  for lithium also suggests a possible explanation for the strong temperature dependence of  $n^*$  shown in Fig. 3-15. Although  $F(\theta)$  peaks at  $75^\circ$ , scattering processes at  $\theta = 90^\circ$  are still quite heavily weighted. The wave vectors for  $\theta = 90^\circ$  and  $k$  in the 110 are quite large ( $qa/2\pi = .88$ ; see Table 4-5); as the temperature is lowered some of these phonons are no longer excited and the scattering should be changed severely. The high Debye temperature,  $\theta_D = 430^\circ\text{K}$ , suggests that there should actually be "freezing out" of phonons at nitrogen temperature even though we are interested in the Debye temperature for transverse phonons which will be lower than the specific heat  $\theta_D$ . However, there is also the possibility that the change in  $n^*$  may be connected with the martensitic transition occurring near  $77^\circ\text{K}$ .

The small changes in  $n^*$  with temperature for sodium and potassium may also be due to the beginning of the "freezing out" of some phonons. However, the scattering function  $F(\theta)$  is much less sharply peaked in the case of potassium than in the case of lithium and so the total scattering is much less sensitive to the freezing out of large  $q$  phonons. In addition, the Debye temperatures are lower for these metals. Both factors should decrease the temperature effect in sodium and potassium.

HP6

$\theta$	$\frac{qa}{2\pi}$	$\left(\frac{2\pi}{qa}\right)^2$	$F(\theta) \left(\frac{2\pi}{qa}\right)^2$ for potassium	$F(\theta) \left(\frac{2\pi}{qa}\right)^2$ for lithium
15	.15	44.4	.00	.00
30	.30	11.1	.89	.89
45	.45	4.9	1.37	1.37
60	.60	2.8	1.82	1.82
75	.75	1.8	1.84	1.55
90	.88	1.3	1.39	.99
105	.88	1.3	1.27	.42
120	.73	1.9	1.40	.02
135	.55	3.3	1.58	.10
150	.41	5.9	1.83	.18
165	.25	16.0	2.24	.32
175	.20	25.0	1.00	.25
180	.18	31.0	.00	.00

U. K. processes start at  $\theta \approx 95^\circ$

$\theta$  is measured in 100 plane

Table 4-5

Scattering Functions for  $\vec{k}$  in 110 Direction

HP6

$\theta$	$\frac{qa}{2\pi}$	$(\frac{2\pi}{qa})^2$	$F(\theta)(\frac{2\pi}{qa})^2$ for potassium	$F(\theta)(\frac{2\pi}{qa})^2$ for lithium
15	.15	44.4	.00	.00
30	.30	11.1	.89	.89
45	.45	4.9	1.37	1.37
60	.60	2.8	1.82	1.82
75	.75	1.8	1.84	1.55
90	.57	3.1	3.32	2.36
95	.50	4.0	4.26	2.56
105	.47	4.5	4.41	1.44
120	.48	4.3	3.18	.04
135	.58	2.9	1.39	.09
150	.73	1.9	.59	.06
165	.79	1.6	.06	.02
180	.75	1.8	.00	.00

U.K. processes start at  $\theta \approx 70^\circ$

$\theta$  is measured in 100 plane

Table 4-6

Scattering Functions for  $\vec{k}$  in 100 Directions

$\theta$	$\frac{qa}{2\pi}$	$(\frac{2\pi}{qa})^2$	$F(\theta) (\frac{2\pi}{qa})^2$	$F(\theta) (\frac{2\pi}{qa})^2$
			for potassium	for lithium
15	.15	44.4	.00	.00
30	.30	11.1	.89	.89
45	.45	4.9	1.37	1.37
60	.60	2.8	1.82	1.82
75	.70	2.0	2.04	1.72
90	.58	3.0	3.21	2.28
105	.44	5.2	5.09	1.66
120	.35	8.2	6.06	.08
135	.40	6.2	2.98	.18
150	.50	4.0	1.24	.12
165	.65	2.4	.34	.02
180	.80	1.6	.00	.00

U.K. processes start at  $\theta \approx 73^\circ$

$\theta$  is measured in 110 plane;

positive  $\theta$  go to 100 axis

-60	.60	2.8	1.82	1.82
-75	.75	1.8	1.84	1.55
-90	.88	1.3	1.39	.99

No U.K. processes for  $\theta$  between  $-90^\circ$  and  $-180^\circ$

Table 4-7

Scattering Functions for  $\vec{k}$  in 111 Direction

Quantity	Direction of $\vec{k}$		
	110	111	100
$1 - .3 Y_6$	1.5	.5	.7
Using potassium matrix element			
$I(\vec{k})$ N and U.K. processes - arbitrary units	46	48	57
$[I(\vec{k})]^{-1} \times 100$ [proportional to $\tau(\vec{k})$ ]	2.2	2.1	1.8
$I(\vec{k})$ U.K. processes only	26	34	44
$[I(\vec{k})]^{-1} \times 100$ U.K. only	3.8	2.9	2.3
Using Li matrix element			
$I(\vec{k})$ N and U.K. processes - arbitrary units	58	62	71
$[I(\vec{k})]^{-1} \times 100$	1.7	1.6	1.4
$I(\vec{k})$ U.K. processes only	25	28	40
$[I(\vec{k})]^{-1} \times 100$ U.K. only	4.0	3.6	2.5

Table 4-8

 $I(\vec{k})$  for Various Conditions

E. Conclusions

The observed pressure effects in the alkalis require the assumption of an anisotropic scattering time,  $\tau(\vec{k})$ , in order to explain how relatively small increases in the warping parameters which describe the Fermi surface cause  $n^*$  to decrease. The assumption of an anisotropy in  $\tau(\vec{k})$  is required both by the sign of the pressure effect, and, in the case of sodium and lithium, by its magnitude. The anisotropy in the shape of the Fermi surface is small, except possibly in the case of cesium, while the anisotropy in  $\tau$  is large.

The anisotropy in  $\tau$  comes from: (1) the fact that  $1/|q|^2$  occurs as a  $k$  dependent weighting factor in the expression for  $\tau$  and (2) the fact that  $1/c^2 \hat{q}_{q,p}$  occurs as a highly anisotropic weighting factor in the same expression. A very crude calculation shows that the first factor alone can cause considerable anisotropy in  $\tau$ .

IV. References

1. A. H. Wilson, The Theory of Metals, Cambridge Univ. Press, p. 226 (1953).
2. J. R. A. Cooper and S. Raimes, *Phil. Mag.* 4, 145 (1959).
3. J. R. A. Cooper and S. Raimes, *Phil. Mag.* 4, 1149 (1959).
4. F. C. von der Lage and H. A. Bethe, *Phys. Rev.* 71, 612 (1947).
5. F. Ham, Proceedings of the Fermi Surface Conference, New York, pg. 9 (1960).
6. J. R. A. Cooper - private communication.
7. F. J. Studer and W. D. Williams, *Phys. Rev.* 47, 291 (1935).
8. A. V. Ettingshausen and W. Nernst, *Ann. d. Physik* [3], 29, 343 (1886).
9. N. F. Mott and H. Jones, Theory of the Properties of Metals and Alloys, Dover, New York, p. 259 (1958).
10. Reference [9] p. 251.
11. M. Baily, *Phys. Rev.* 120, 381 (1960).
12. J. M. Ziman, Electrons and Phonons, Oxford Univ. Press, Oxford, England, p. 181 (1960).
13. Jules de Launay, Solid State Physics, Vol. II, Academic Press, New York, p. 267 (1956).

Appendix I

We wish to relate the coefficients  $B, B_1$ , in Eq. (IV-4) to  $A$  and  $A_1$  in Eq. (IV-1). For small warping we may express the energy in the form

$$E = \frac{\hbar^2 k_o^2}{m^*} \left[ \frac{1}{2} (k/k_o)^2 + r (k/k_o)^4 Y_4(\theta, \phi) + s (k/k_o)^6 Y_6(\theta, \phi) \right] \quad (A-1)$$

which is just Eq. (I-4) with  $s = rt$ .

Furthermore

$$\left( \frac{\partial E}{\partial k} \right)_{E_F} = \frac{\hbar^2 k_o^2}{m^*} \left[ \left( \frac{k}{k_o} \right) + 4r \left( \frac{k}{k_o} \right)^3 Y_4(\theta, \phi) + 6s \left( \frac{k}{k_o} \right)^5 Y_6(\theta, \phi) \right] \quad (A-2)$$

where the derivative is evaluated at the Fermi energy.

Now we know that

$$\left( \frac{\partial E}{\partial k} \right)_{E_F} \left( \frac{\partial k}{\partial E} \right)_{E_F} = 1 \quad (A-3)$$

in any direction in  $k$  space. Equation (IV-4) gives  $\left( \frac{\partial k}{\partial E} \right)_{E_F}$ .

We use the subscripts 1, 2, 3 to indicate the [100], [110], and [111] directions: the Kubic harmonics and  $\left( \frac{k}{k_o} \right)$  are evaluated in these directions. For example

$$k_1 = \left( \frac{k}{k_o} \right)_1 = (1 + A + A_1) \quad (A-4)$$

using  $Y_4 [100] = Y_6 [100] = 1$  in Eq. (IV-1).

Let us introduce the notation

$$\left[ \left( \frac{k}{k_o} \right)_i + 4r \left( \frac{k}{k_o} \right)_i^3 Y_4(i) + 6s \left( \frac{k}{k_o} \right)_i^5 Y_6(i) \right] = a_i(A, A_1, r, s) \quad (A-5)$$

where  $i$  runs from 1 to 3.

Substituting Eqs. (A-2), (A-5) and (IV-2) into Eq. (A-3) we obtain

$$(1 + B + B_1) a_1 = \left( 1 - \frac{B}{4} - \frac{13}{8} B_1 \right) a_2 = \left( 1 - \frac{2B}{3} + \frac{16}{9} B_1 \right) a_3 \quad (A-6)$$

From this we obtain two linear equations for B and B<sub>1</sub> whose solution is

$$B = \frac{\begin{vmatrix} (a_2 - a_1) \left(a_1 + \frac{13a_2}{8}\right) \\ (a_3 - a_1) \left(a_1 - \frac{16a_3}{9}\right) \end{vmatrix}}{\begin{vmatrix} \left(a_1 + \frac{a_2}{4}\right) \left(a_1 + \frac{13a_2}{8}\right) \\ \left(a_1 + \frac{2a_3}{3}\right) \left(a_1 - \frac{16a_3}{9}\right) \end{vmatrix}}$$

$$B_1 = \frac{\begin{vmatrix} \left(a_1 + \frac{a_2}{4}\right) (a_2 - a_1) \\ \left(a_1 + \frac{2a_3}{3}\right) (a_3 - a_1) \end{vmatrix}}{\begin{vmatrix} \left(a_1 + \frac{a_2}{4}\right) \left(a_1 + \frac{13a_2}{8}\right) \\ \left(a_1 + \frac{2a_3}{3}\right) \left(a_1 - \frac{16a_3}{9}\right) \end{vmatrix}}$$

The  $a_i$  depend on r and s of Eq. (A-1); we now obtain these. We substitute

$$\left(\frac{k}{k_0}\right) = 1 + A Y_4(\theta, \phi) + A_1 Y_6(\theta, \phi) = k_i \quad (\text{IV-1})$$

into the expression for the energy, Eq. (A-1). The energy must be constant on the Fermi surface. By requiring the energy in the three principal directions to be the same, we obtain

$$\begin{aligned} \frac{1}{2} k_1^2 + r k_1^4 + s k_1^6 &= \frac{1}{2} k_2^2 - \frac{1}{4} r k_2^4 - \frac{13}{8} s k_2^6 = \\ \frac{1}{2} k_3^2 - \frac{2}{3} r k_3^4 + \frac{16}{9} s k_3^6 &. \end{aligned} \quad (\text{A-7})$$

This yields 2 linear equations for  $r$  and  $s$  in terms of  $A$  and  $A_1$ .  
The solutions are:

$$r = -\frac{1}{2}$$

$$\begin{array}{l} \left| \begin{array}{cc} k_1^2 - k_2^2 & k_1^6 + 1.62 k_2^6 \\ k_1^2 - k_3^2 & k_1^6 - 1.78 k_3^6 \end{array} \right| \\ \hline \left| \begin{array}{cc} k_1^4 + \frac{k_2^4}{4} & k_1^6 + 1.62 k_2^6 \\ k_1^4 + .67 k_3^4 & k_1^6 - 1.78 k_3^6 \end{array} \right| \end{array}$$

and

$$s = -\frac{1}{2}$$

$$\begin{array}{l} \left| \begin{array}{cc} k_1^4 + \frac{k_2^4}{4} & k_1^2 - k_2^2 \\ k_1^4 + .67 k_3^4 & k_1^2 - k_3^2 \end{array} \right| \\ \hline \left| \begin{array}{cc} k_1^4 + \frac{k_2^4}{4} & k_1^6 + 1.62 k_2^6 \\ k_1^4 + .67 k_3^4 & k_1^6 - 1.78 k_3^6 \end{array} \right| \end{array}$$

We can now compute  $B$  and  $B_1$  as a function of  $A$  and  $A_1$ .

Acknowledgments

The financial support of the Office of Naval Research and the fellowships given me by the National Science Foundation, the Standard Oil Company of California, and the Union Carbide Company, are gratefully acknowledged.

I should like to thank Professor P. W. Bridgman for some of the equipment used in this work and for several helpful discussions.

The skill and helpfulness of Mr. James Inglis, who did most of the machine work, were invaluable. I would like to thank Mr. Charles Chase for packing the high pressure terminal plugs and Mr. Robert Longo for his help in preparing the alkali samples.

I would like to thank the drafting and photoshop staffs for preparing the figures.

I am grateful to Dr. Frank Ham for providing me with his results prior to publication and for several discussions. I am indebted to my colleagues, Dr. Manuel Cardona, Dr. Melvin Holland, Mr. Webster Howard, Dr. Marshall Nathan, Dr. Arthur Smith and Dr. Douglas Warschauer for many helpful discussions and suggestions.

Dean Harvey Brooks was somehow always able to find time to make suggestions and provide theoretical guidance. His critical reading of the manuscript was invaluable.

My greatest debt is to Professor William Paul to whom I owe much of my scientific education. He found time to discuss at length the many problems that arose in the course of this work and to read the manuscript in its entirety. Finally, he was a source of encouragement at those times when it was sorely needed.

1. Department of Defense

Assistant Secretary of Defense  
for Research and Development  
Information Office Library Branch  
Pentagon Building (2)  
Washington 25, D. C.

Armed Services  
Technical Information Agency  
Arlington Hall Station  
Attn: TIPCR (5)  
Arlington 12, Virginia

2. Department of the Navy

Chief, Bureau of Weapons  
Technical Library  
Navy Department  
Washington 25, D. C.

Chief, Bureau of Ships  
Code 300, Technical Library  
Navy Department  
Washington 25, D. C.

Chief of Naval Research  
Office of Naval Research (3)  
Attn: Physics Branch (Code 421)  
Washington 25, D. C.

Director  
Naval Research Laboratory  
Technical Information Officer  
Code 2021 (2 copies)  
Code 2000 (6 copies)  
Washington 25, D. C.

Commanding Officer  
Office of Naval Research  
Branch Office (2)  
495 Summer Street  
Boston 10, Massachusetts  
(Boston area only)

Commanding Officer  
Office of Naval Research  
Branch Office  
346 Broadway  
New York 13, New York

Commanding Officer  
U. S. Naval Ordnance Laboratory  
Corona, California

Contract Administrator  
Southeastern Area  
Office of Naval Research  
George Washington University  
2110 G Street, N. W.  
Washington 7, D. C.

Commanding Officer  
Office of Naval Research  
Branch Office  
86 East Randolph Street  
Chicago 1, Illinois

Commanding Officer  
Office of Naval Research  
Branch Office  
1000 Geary Street  
San Francisco 9, California

Commanding Officer  
ONR Branch Office  
1030 East Green Street  
Pasadena 1, California

Commanding Officer  
Office of Naval Research  
London Branch Office  
Navy # 100  
Fleet Post Office (2)  
New York, New York

Librarian  
U. S. Naval Post Graduate School  
Monterey, California

U. S. Naval Electronics Laboratory  
San Diego 52, California

Commanding Officer  
U. S. Naval War College  
Newport, Rhode Island

Director  
Research Department  
Naval Ordnance Laboratory  
White Oak, Maryland

Commanding Officer  
Physics Division  
Naval Ordnance Test Station  
Inyokern  
China Lake, California

3. Department of the Air Force

Commanding General  
Wright Air Development Center  
Wright-Patterson Air Force Base  
Dayton, Ohio

Commanding General  
Air Research and  
Development Command (2)  
Attn: Office of Scientific Research  
Washington 25, D. C.

Commander  
Air Force Cambridge Research Cntr.  
230 Albany Street  
Cambridge, Massachusetts  
Attn: CRHCP-1

4. Department of the Army

Commanding Officer  
Engineering Research and  
Development Laboratories  
Fort Belvoir, Virginia  
Attn: Technical Intelligence Branch

Office of Ordnance Research  
Box CM, Duke Station (2)  
Durham, North Carolina

Dr. J. L. Martin  
Watertown Arsenal  
Watertown 72, Massachusetts

Signal Corps Engineering Laboratory  
Fort Monmouth, New Jersey  
Attn: Technical Information Officer

5. Department of Commerce

Office of Technical Services  
Technical Reports Section  
Department of Commerce  
Washington 25, D. C.

Director  
National Bureau of Standards  
Washington 25, D. C.

6. Other Agencies

U. S. Atomic Energy Commission  
Washington 25, D. C.

Advanced Research Projects Agency  
The Pentagon  
Room 3E 157  
Washington 25, D. C.

National Aeronautics and  
Space Administration  
1520 H Street, Northwest  
Washington 25, D. C.

National Research Council  
Division of Physical Sciences  
National Academy of Sciences  
Washington 25, D. C.

Director  
National Science Foundation  
Washington 25, D. C.

U. S. Atomic Energy Commission  
Technical Information Service  
P. O. Box 62  
Oak Ridge, Tennessee

AFSWC, SWRP  
Kirkland Air Force Base  
New Mexico

Defense Atomic Support Agency  
Sandia Base  
New Mexico

7. Non-Governmental Agencies(a) Domestic

Professor A. W. Lawson  
Institute for the Study of Metals  
University of Chicago  
Chicago 36, Illinois

Professor R. W. Hoffmann  
Case Institute of Technology  
Cleveland, Ohio

Professor S. Mrozowski  
Department of Physics  
University of Buffalo  
Buffalo, New York

Dr. Linus Pauling  
California Institute of Technology  
Pasadena  
California

Professor Frederick Seitz  
Department of Physics  
University of Illinois  
Urbana, Illinois

Professor H. B. Callen  
University of Pennsylvania  
Philadelphia, Pennsylvania

Professor G. Kittel  
University of California  
Berkeley, California

Professor C. S. Smith  
Institute for the Study of Metals  
University of Chicago  
Chicago 37, Illinois

Professor John C. Slater  
Department of Physics  
Mass. Institute of Technology  
Cambridge 39, Massachusetts

Dr. R. Smoluchowski  
Carnegie Institute of Technology  
Pittsburgh, Pennsylvania

Dr. George A. Morton  
Radio Corporation of America  
David Sarnoff Research Center  
Princeton, New Jersey

Dr. H. P. R. Frederikse  
National Bureau of Standards  
Washington 25, D. C.

Lincoln Laboratory  
Box 73  
Lexington, Massachusetts  
Attn: Dr. B. Lax  
Dr. D. T. Stevenson

Professor N. Cabrera  
Physics Department  
University of Virginia  
Charlottesville, Virginia

Professor R. L. Sproull  
Department of Physics  
Rockerfeller Hall  
Cornell University  
Ithaca, New York

Dr. W. W. Tyler  
General Electric Laboratory  
The Knolls  
Schenectady, New York

Dr. J. S. Toll  
Dr. R. Ferrell  
Dr. E. Montroll  
Department of Physics  
University of Maryland  
College Park, Maryland

Dr. Ernst Weber  
Polytechnic Institute of Brooklyn  
99 Livingston Street  
Brooklyn 2, New York

Dr. A. C. Beer  
Battelle Memorial Institute  
505 Kings Avenue  
Columbus, Ohio

Professor A. W. Ewald  
Northwestern University  
Physics Department  
Evanston, Illinois

Dr. M. Lax  
Bell Telephone Laboratories  
Murray Hill, New Jersey

Professor J. S. Koehler  
University of Illinois  
Urbana, Illinois

Dr. M. I. Nathan  
I. B. M. Laboratories  
Poughkeepsie, New York

Professor H. Y. Fan  
Physics Department  
Purdue University  
Lafayette, Indiana

Dr. C. Herring  
Dr. J. Burton  
Bell Telephone Laboratories  
Murray Hill, New Jersey

Dr. F. Herman  
R. C. A. Laboratories  
Princeton, New Jersey

Dr. R. H. Parmenter  
R. C. A. Laboratories  
Princeton, New Jersey

Professor K. F. Herzfeld  
Department of Physics  
Catholic University  
Washington, D. C.

Professor John Bardeen  
Physics Department  
University of Illinois  
Urbana, Illinois

Professor Julius Taylor  
Morgan State College  
Baltimore 12, Maryland

Professor H. G. Drickamer  
Chemistry Department  
University of Illinois  
Urbana, Illinois

Professor A. B. Scott  
Oregon State College  
Corvallis, Oregon

Professor R. J. Maurer  
Department of Physics  
University of Illinois  
Urbana, Illinois

Professor E. T. Jaynes  
Stanford University  
Stanford, California

Dr. L. Marton  
National Bureau of Standards  
Washington 25, D. C.

Professor A. R. Von Hippel  
Mass. Institute of Technology  
Laboratory for Insulation Research  
Cambridge 39, Massachusetts

Professor W. Kohn  
Physics Department  
University of California  
La Jolla, California

Professor G. L. Pearson  
Physics Department  
Stanford University  
Palo Alto, California

Professor Elias Burstein  
Physics Department  
University of Pennsylvania  
Philadelphia, Pennsylvania

Dr. D. M. Warschauer  
Raytheon Manufacturing Company  
Research Division  
Waltham, Massachusetts

Professor J. Callaway  
Physics Department  
University of California  
Riverside, California

Dr. R. O. Carlson  
General Electric Laboratory  
The Knolls  
Schenectady, New York

Professor J. Krumhansl  
Physics Department  
Cornell University  
Ithaca, New York

Dr. M. G. Holland  
Raytheon Manufacturing Company  
Research Division  
Waltham, Massachusetts

Dr. Thomas Deutsch  
Raytheon Manufacturing Company  
Research Division  
Waltham, Massachusetts

Professor A. C. Smith  
Mass. Institute of Technology  
10-193  
Cambridge 39, Massachusetts

Dr. Henry Ehrenreich  
General Electric Research Company  
The Knolls  
Schenectady, New York

Dr. L. M. Roth  
Lincoln Laboratory  
P. O. Box 73  
Lexington 73, Massachusetts

Dr. H. Fritsche  
Physics Department  
University of Chicago  
Chicago, Illinois

Dr. E. O. Kane  
Hughes Products  
Newport Beach, California

Dr. F. J. Morin  
Bell Telephone Laboratories  
Murray Hill, New Jersey

Dr. A. Sagar  
Westinghouse Research Labs  
Pittsburgh, Pennsylvania

Dr. R. W. Keyes  
I. B. M. Research Laboratory  
Poughkeepsie, New York

Dr. E. M. Conwell  
General Telephone and Electronics  
Laboratories, Incorporated  
Bayside, New York

Dr. R. Braunstein  
RCA Research Laboratories  
Princeton, New Jersey

Dr. C. S. Smith  
Physics Department  
Case Institute of Technology  
Cleveland, Ohio

Dr. J. C. Phillips  
Physics Department  
Institute of Metals  
University of Chicago  
Chicago, Illinois

7. Non-Governmental Agencies

(b) Foreign

Dr. Manuel Cardona  
RCA Ltd.  
Hardturmstrasse 169  
Zurich, Switzerland

Professor P. Aigrain  
Ecole Normale Supérieure  
Paris, France

Dr. R. A. Smith  
Radar Royal Establishment  
Great Malvern, England

Dr. B. Vodar  
CNRS  
Bellevue, Paris, France

Dr. A. F. Gibson  
Radar Royal Establishment  
Great Malvern, England

Dr. T. S. Moss  
RAE  
Farnborough, England

Dr. C. Hilsum  
SERL  
Baldock  
Hertfordshire, England

Dr. H. Welker  
Siemens-Schuckertwerke  
Erlangen  
Germany

Dr. C. J. M. Rooymans  
Philips Research Laboratories  
Eindhoven  
Netherlands

Dr. H. J. G. Meyer  
Philips Research Laboratories  
Eindhoven  
Netherlands

\*One copy unless otherwise indicated.